Aus dem Zentrum für Innere Medizin der Universität zu Köln
Klinik und Poliklinik für Innere Medizin I
Direktor: Universitätsprofessor Dr. med. M. Hallek

Deciphering metastatic signaling cascades in small cell lung cancer

Inaugural-Dissertation zur Erlangung der Doktorwürde
der Medizinischen Fakultät
der Universität zu Köln

vorgelegt von
Charlotte Isabelle Orschel

promoviert am 04. Dezember 2025

Gedruckt mit Genehmigung der Medizinischen Fakultät der Universität zu Köln
2025

Dekan: Universitätsprofessor Dr. med. G. R. Fink
1. Gutachterin: Professorin Dr. nat. med. L. Meder
2. Gutachterin: Universitätsprofessorin Dr. rer. nat. R. Stripecke

Erklärung

Ich erkläre hiermit, dass ich die vorliegende Dissertationsschrift ohne unzulässige Hilfe Dritter und ohne Benutzung anderer als der angegebenen Hilfsmittel angefertigt habe; die aus fremden Quellen direkt oder indirekt übernommenen Gedanken sind als solche kenntlich gemacht.
Bei der Auswahl und Auswertung des Materials sowie bei der Herstellung des Manuskriptes habe ich Unterstützungsleistungen von folgenden Personen erhalten:
Frau Prof. Dr. Lydia Meder
Herr Prof. Dr. Dr. Roland T. Ullrich

Weitere Personen waren an der Erstellung der vorliegenden Arbeit nicht beteiligt. Insbesondere habe ich nicht die Hilfe einer Promotionsberaterin/eines Promotionsberaters in Anspruch genommen. Dritte haben von mir weder unmittelbar noch mittelbar geldwerte Leistungen für Arbeiten erhalten, die im Zusammenhang mit dem Inhalt der vorgelegten Dissertationsschrift stehen.

Die Dissertationsschrift wurde von mir bisher weder im Inland noch im Ausland in gleicher oder ähnlicher Form einer anderen Prüfungsbehörde vorgelegt.

Die in dieser Arbeit angegebenen Experimente sind nach entsprechender Anleitung unter Frau Prof. Dr. Lydia Meder und Herrn Prof. Dr. Dr. Roland T. Ullrich von mir selbst ausgeführt worden. Die Auswertung der hierbei entstandenen Daten führte ich nach entsprechender Anleitung durch Frau Prof. Dr. Lydia Meder eigenständig durch. Dabei standen die folgenden Software-Programme Excel®, Kaluza®, GraphPad Prism® bei der Analyse und Darstellung im Vordergrund. Die genutzten RNA-Analysen wurden mit Hilfe von Herrn Dr. Johannes Brägelmann erstellt. Die vorgelegten Western Blots, sowie die durchgeführten CRISPR Knockouts von CD29 (ITGB1) und B2M sind auf die Arbeit von Frau Mirjam Koker, B.Sc. zurückzuführen. Das Sammeln von Patienten Proben erfolgte in Kooperation mit dem Institut der Pathologie der Uniklinik Köln insbesondere mit Frau Dr. Marie-Lisa Eich.

Diese Arbeit ist teilweise in Anlehnung und Zusammenarbeit mit der Publikation mit dem Titel „Blocking the angiopoietin-2–dependent integrin β-1 signaling axis abrogates small cell lung cancer invasion and metastasis." von Meder et al. 2024 (https://doi.org/10.1172/jci.insight.166402) entstanden. Weitere in der Publikation gelistete Mitautoren waren an der Entstehung dieser Arbeit über diesen Weg mittelbar beteiligt. In dieser Arbeit werden Inhalte, die aus der Publikation Meder et al. mit freundlicher Genehmigung übernommen wurden, entsprechend zitiert.

Diese Arbeit ist zusätzlich in Kooperation mit der noch unveröffentlichten Publikation mit dem vorläufigen Titel „ERBB2 signaling drives immune cell evasion and resistance against immunotherapy in small cell lung cancer " von Meder et al. (Ersteinreichung am 13.11.2024 bei „Nature Communications“, in Revision seit dem 15.01.2025, Manuskript NCOMMS-24-74632-T) entstanden. Weitere in der Publikation gelistete Mitautoren waren an der Entstehung dieser Arbeit über diesen Weg mittelbar beteiligt. In dieser Arbeit werden Inhalte, die aus der noch unveröffentlichten Publikation Meder et al. mit freundlicher Genehmigung übernommen wurden, entsprechend zitiert und als „*under revision in Nature Communications since 15th January 2025 under review again since 4th August 2025*“ gekennzeichnet. Das schriftliche Einverständnis von Frau Prof. Dr. Lydia Meder über die Vorabveröffentlichung von Teilergebnissen in dieser Arbeit liegt vor.

Erklärung zur guten wissenschaftlichen Praxis:

Ich erkläre hiermit, dass ich die Ordnung zur Sicherung guter wissenschaftlicher Praxis und zum Umgang mit wissenschaftlichem Fehlverhalten (Amtliche Mitteilung der Universität zu Köln AM 132/2020) der Universität zu Köln gelesen habe und verpflichte mich hiermit, die dort genannten Vorgaben bei allen wissenschaftlichen Tätigkeiten zu beachten und umzusetzen.

Köln, den 22.02.2025

Unterschrift: .....

Acknowledgement

I would like to thank my supervisor Prof. Dr. Lydia Meder for giving me the opportunity to be a part of this amazing project. Her outstanding dedication to experimental work has inspired me all the way through and it was a privilege to work with her. Secondly, I would like to thank Prof. Dr. Dr. Roland T. Ullrich for always having open ears for my questions, for his advice and support.

Furthermore, I would like to thank Dr. Cyrielle Bouchez, Dr. David Stahl, Dr. Carolin Selenz, Dr. Phillip Gödel and Dr. Tabea Gewalt for giving useful advice at the lab meeting's discussion; Mirjam Koker for execution of the western blots; Dr. Johannes Brägelmann for RNA-sequencing analysis; Dr. Marie-Lisa Eich for collaboration at pathology; Alexandra Florin for the immunohistochemistry, and Marieke Nill for assistance with lab work.

TABLE OF CONTENTS

Abbreviations

AB	Antibody
ABL	Abelson murine leukemia viral oncogene homolog 1
ANG-1	Angiopoietin-1
ANG-2	Angiopoietin-2
B2M	Beta-2 microglobulin
CT	Computer tomography
DC	Dendritic cells
ECM	Extracellular matrix
EGFR	Epidermal growth factor receptor
EMT	Epithelial-mesenchymal transition
ES	Extensive stage
ESCC	Esophageal squamous cell carcinoma
FACS	Fluorescence-activated cell sorting
FAK	Focal adhesion kinase
FasL	Fas ligand
FFPE	Formalin-fixed paraffin-embedded
FN	Fibronectin
ICAM-1	Intercellular adhesion molecule-1
IFNγ	Interferon gamma
IHC	Immunohistochemistry
IL-10	Interleukin 10
i.p.	Intraperitoneal
IRF	Interferon regulatory factor
iv.	Intravenous
KO	Knockout
LS	Limited stage
mAbs	Monoclonal antibodies
MAPK	Mitogen-activated protein kinase
MFI	Mean fluorescence intensity
MHC	Major histocompatibility complex
MRI	Magnetic resonance imaging
NSCLC	Non-small cell lung cancer
NSG	NOD scid gamma
OV	Overview
PBS	Phosphate buffered saline
PD-1	Programmed cell death protein 1

PD-L1	Programmed death ligand 1
PFA	Paraformaldehyde
PI3K	Phosphoinositid-3 kinase
RB1	Retinoblastoma 1
RNA-Seq	RNA-sequencing
ROI	Region of interest
RT	Room temperature
sc.	Subcutaneous
SCLC	Small-cell lung cancer
STAT	Signal transducer and activator of transcription
STING	Stimulator of interferon genes
TAM	Tumor associated macrophage
TBK1	TANK-binding kinase 1
TBST	Tris-buffered saline with tween
TIE	Tyrosine kinase with immunoglobulin-like and EGF-like domains
TP53	Tumor protein p53
TRAIL	TNF-related apoptosis-inducing ligand
VEGF	Vascular endothelial growth factor
VEGFR	VEGF receptor
WT	Wild type

1. Zusammenfassung

Das kleinzellige Lungenkarzinom (SCLC) zählt nach wie vor zu den tödlichsten Krebserkrankungen. Die frühe Metastasierung und die schnelle Entwicklung von Resistenzen gegenüber klassischen Therapien stellen eine besondere Herausforderung dar. Da es vor allem im fortgeschrittenen Stadium kaum wirksame Behandlungsoptionen gibt, ist es von besonderer Bedeutung, die Mechanismen zu ergründen, die für die aggressive Natur, die hohe Migrationsfähigkeit und das Umgehen des Immunsystems des SCLCs verantwortlich sind.

In meiner Dissertation fokussiere ich mich auf den CD29-abhängigen Signalweg und die MHC-I-abhängige Regulation im Tumormikromilieu und erörtere deren Beteiligung an Prozessen der Metastasenbildung und Immunresistenz.

Zunächst zeigte ein breites Screening von SCLC-Probenpaaren aus Primärtumor und Lebermetastasen, menschlichen und murinen Ursprungs, eine erhöhte CD29 Expression im Metastasengewebe. Um die genaue Funktion von CD29 zu verstehen, wurden Knockout-(KO)-SCLC Klone mithilfe von CRISPR erzeugt. Diese Klone wurden auf zellulärer und funktioneller Ebene mit der ursprünglichen, aus Lebermetastasen gewonnenen Zelllinie verglichen. Dazu wurden die Verfahren des Scratch Assays und der Boyden Chamber angewandt, um das Migrations- bzw. Invasionsverhalten des CD29 KO zu analysieren. Zusätzlich wurden *in vivo*-Experimente durchgeführt, bei denen CD29 KO und Wildtyp SCLC Tumorzellen in immunkompetente und immundefiziente Mäuse injiziert wurden, um die Metastasenbildung zu untersuchen.

Die Ergebnisse zeigten, dass der CD29 KO das Migrationsvermögen der Tumorzellen hemmte, insbesondere unter Stimulation mit Fibronektin und Angiopoietin-2 (ANG-2). *In vivo* konnten die CD29 KO Tumorzellen im Gegensatz zum Wildtyp keine Lebermetastasen bilden, was durch immunhistochemische Analysen und Durchflusszytometrie bestätigt wurde. Insgesamt zeigt sich, dass CD29 eine entscheidende Rolle bei der Metastasenbildung des SCLCs spielt, was durch einen Knockout unterdrückt werden kann.

Im weiteren Verlauf, konzentriert sich meine Dissertation auf MHC-I und dessen Rolle bei der Umgehung der Immunabwehr und Metastasenbildung. Bei der Analyse der gepaarten SCLC-Patientenproben zeigte sich eine reduzierte MHC-I Expression in den Lebermetastasen. Zur Untersuchung der Auswirkungen eines MHC-I Verlusts auf die Wechselwirkungen zwischen Tumor und Immunsystem wurden MHC-I defiziente Klone (MHC-I KO) durch gezielten Knockout des β2-Mikroglobulin-Gens (*B2M*) erzeugt. *In vivo* zeigte sich, dass die MHC-I KO-Tumore deutlich aggressiver wuchsen. Dabei wurde eine verstärkte Aktivierung des angeborenen Immunsystems in den Lebermetastasen und eine reduzierte T-Zell-Antwort im Pleuraerguss beobachtet. Allerdings zeigte sich keine ausgeprägte Lebermetastasierung. Ein Vergleich zwischen Primärtumoren und Metastasen ergab eine verstärkte Phosphorylierung von ERBB2 in den SCLC Metastasen. Erste *in vitro* Experimente mit einem ERBB2 Inhibitor

zeigten eine Hemmung zentraler nachgeschalteter Signalwege und die Aktivierung immunstimulierender Signale durch *TBK1*. In unserem autochthonen SCLC Mausmodell erzielte die kombinierte Blockade von PD-1 und ERBB2 eine signifikante Verlängerung des Gesamtüberlebens, sowie des progressionsfreien Überlebens. Zusammenfassend stellt diese Dissertation die entscheidende Bedeutung der CD29-ANG-2-Signalkaskade für die Metastasenbildung von SCLC sowie die immunologischen Folgen des MHC-I Verlusts dar, und erörtert darauf basierend mögliche Therapieansätze.

Summary

Down to the present-day small cell lung cancer (SCLC) remains one of the deadliest cancer entities. Due to its early metastasis formation and wide therapy resistance, SCLC occupies a special place within cancer research. Given the limited treatment options, particularly in advanced stages, it is vital to examine how certain signaling cascades contribute to the aggressive phenotype, immune evasion and high migration potential of SCLC.

My dissertation mainly focuses on the CD29-dependent signaling pathway and MHC-I-dependent regulation of the tumor micro-milieu and discusses their involvement in processes of metastasis formation and immune evasion mechanisms of SCLC.

In our initial screening, we observed elevated CD29 expression in liver metastases in both human and murine samples. Therefore, CD29 Knockout (KO) clones were generated using CRISPR to test the characteristics on functional and cellular level in comparison to the original liver metastasis-derived cell line. To evaluate migration behavior, the different clones and the wild type were subjected to a series of cell migration and cell–cell interaction tests (Scratch Assay, Boyden Chamber). To elucidate the functional role of CD29 in metastasis formation, the CD29 KO clones were also tested in an *in vivo* setting. *In vivo*, tumors were induced via orthotopic and intravenous injection of the respective tumor cells into immunocompetent and immune deficient mouse models. A fluorescence-activated cell sorting (FACS) readout of tumor and metastasis tissue provided insights into immune cell involvement and tumor expression markers. Additionally, immunohistochemistry (IHC) was applied to assess tumor cells and desmoplastic reactions *ex vivo*. *In vitro* migration assays demonstrated that CD29 KO abrogates fibronectin- and angiopoietin-2 (ANG-2) stimulated migration. *In vivo* experiments further revealed that, in contrast to the wild type SCLC cells, CD29 KO clones did not form liver metastasis, which was confirmed by flow cytometry and IHC. Altogether, CD29 is a potent driver of metastasis in SCLC, which can be abrogated by knockout.

Furthermore, my dissertation explores MHC-I and its role in SCLC immune evasion and metastasis formation. In a patient sample screen, we found a downregulation of MHC-I in SCLC liver metastases. To investigate the impact of MHC-I loss on tumor-immune interactions, MHC-I-deficient clones (MHC-I KO) were generated by targeted knockout of the β2 microglobulin (*B2M)* gene. The MHC-I KO was tested *in vivo* by orthotopic and intravenous injection and presented a more aggressive, fast-growing phenotype. In MHC-I KO tumors, we found an enhanced reaction of the innate immune system in the liver metastases and a decreased T cell answer in the pleural effusion. A comparison between primary tumors and metastases revealed increased phosphorylation of ERBB2 in SCLC metastases. Initial *in vitro* experiments with an ERBB2 inhibitor demonstrated suppression of key downstream signaling pathways and induction of immune activating signals via TBK1. Notably, in our autochthonous

SCLC mouse model, combined blockade of PD-1 and ERBB2 resulted in a significant extension of both overall and progression-free survival.

Overall, this study states the importance of the CD29-ANG-2 signaling axis in SCLC metastasis formation and portrays the immune evading effects caused by MHC-I loss. Based on these findings, potential therapeutic approaches are discussed and tested in preclinical setting

2. Introduction

2.1. Small cell lung cancer

Small-cell lung carcinoma (SCLC) is a highly malignant and aggressive subtype of lung cancer and makes up approximately 13-15% of all lung cancer cases diagnosed (1). One specialty is that it shows endocrine activity, which can lead to paraneoplastic syndromes (2). Although frequently initially sensitive to chemo- and radiotherapy, resistances and thereby further progress develop quickly. Therefore, the prognosis is still very poor with a 5-year survival rate of less than 7% (3). A major reason for patients' morbidity and mortality is an exceptional tendency to metastatic spread (4). The lymphatic and hematogenous disseminations typically happen rapidly and enable metastasis formation in the brain, liver, bones or adrenal glands (Fig. 1A) (4,5). Clinically, SCLC is typically classified into limited-stage (LS-SCLC) and extensive-stage (ES-SCLC) disease. The limited stage is restricted to one side of the lung and adjoining lymph nodes. The extensive stage disease is the more common and describes the spread beyond a single area, i.e., the state of metastatic disease (6). At the time of the initial diagnosis, the majority of patients (80-85%) are ascribed to an ES-SCLC (1). Because of the mostly inoperable situation, these patients are often treated in palliative care. In this stage of diagnosis, the median overall survival is around 9-10 months (7). Although diagnosed at an earlier stage, the LS-SCLC also just has median ranges of survival of only 15-20 months (8).

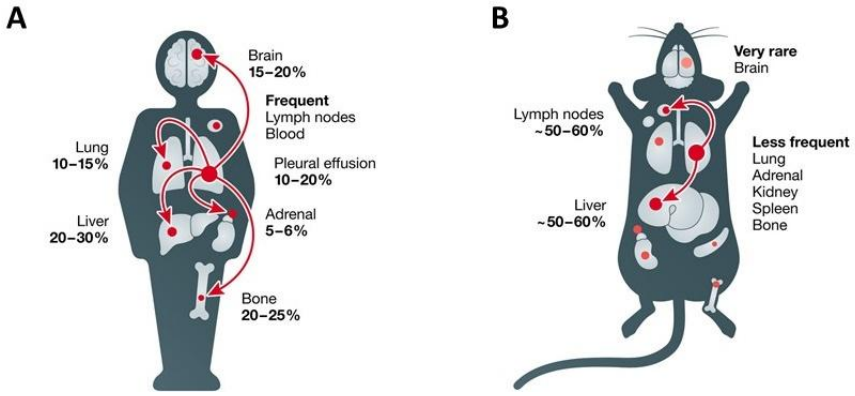

Fig. 1: Sites of metastasis (A) SCLC metastasis formation in patients **(B)**, and in genetically engineered mouse model (4).

Pathophysiologically, SCLC often arises out of specialized pulmonary epithelial cells, which carry genomic aberrations. Mutations can be hereditary or develop due to various environmental circumstances, most notably smoking, which is one of the leading causes for SCLC (9). Typical genetic alterations involve the tumor suppressor genes retinoblastoma 1 (*RB1*) and tumor protein 53 (*TP53*), resulting in uncontrolled cell proliferation due to impaired apoptotic mechanisms (10). This finding lays the foundation for the "autochthonous mouse model" for SCLC. In this model, cancer is induced by letting mice inhale adenoviral vectors

expressing Cre-recombinase, which leads to conditional inactivation of *Rb1* and *Trp53* (11). The tumor formation takes approximately 6 months. Mice develop aggressive tumors with characteristics similar to SCLC and often form extrapulmonary metastasis e.g. in the liver or lymph nodes (Fig. 1B) (4,11).

Current chemotherapy for SCLC consists of platinum and etoposide, which interfere with the process of DNA replication. These agents have already been in use since the 1980s and are ever since first- and second-line standard treatments for SCLC (12). However, this rather unspecific therapy approach is also associated with numerous side effects and mostly shows short-term effects only (12). The second mainstay of therapy is radiation of chest and lymph nodes (13). However, carries the risk of life-threatening pulmonary fibrosis (14). A major challenge remains that currently there is no favorable therapy for relapsed SCLC (15). Overall, the current treatment landscape for SCLC remains unsatisfactory, highlighting the urgent need for novel therapeutic strategies.

2.2. Current state of research (2025)

The key to successful treatment most likely lies in specific molecular targeting and to treat patient's heterogeneity, respectively. Aiming at tyrosine kinase signaling already has been tested in SCLC patients. For example, Imatinib, targeting the abelson murine leukemia viral oncogene homolog 1 (ABL), and Gefitinib, targeting the epidermal growth factor receptor (EGFR), were tested but yielded underwhelming results (16,17). In contrast, immune checkpoint therapy has already been implemented in the therapy regime of patients in ES disease, who showed no remission upon platinum-based chemotherapy and where another line of treatment failed. Recently, the PD-L1 inhibitor atezolizumab has established after the IMpower133 trial revealed a significant improvement in overall survival in combination with standard carboplatin plus etoposide compared to placebo (18).

However, the follow-up study by Horn and colleagues revealed that the formation of metastases remains a major limiting factor increasing the hazard ratio of death (19). Therefore, future therapeutic strategies must focus not only on initial tumor control but also on preventing metastatic spread and targeting established lesions. Recent research has indicated that chromatin remodeling is a driver of metastatic progression in SCLC. The upregulation of the transcription factor NFIB has been shown to promote neuronal gene expression programs (20). However, a recent study has shown that NFIB is not required for metastasis formation (21). Further, proto-oncogene MYC is associated with increased metastatic potential by driving phenotypic plasticity, suppressing neuroendocrine differentiation, and promoting invasive behavior (22,23). Recent comparative transcriptomic analysis of primary tumors from non-metastatic and metastatic SCLC patients also revealed ASCL1–FOXA2 transcriptional axis as a driver of multiorgan metastasis in SCLC by inducing fetal neuroendocrine gene expression

programs (24). Despite these findings, the molecular mechanisms promoting invasion and dissemination especially the interaction between tumor cells and the metastatic niche, are still not fully understood and their clinical relevance remains to be elucidated.

Beside the critical point of metastasis formation several studies have also revealed reduced immunogenicity as a limiting factor of response to immunotherapy. Analysis of the CASPIAN phase III trial (NCT03043872), in which the combination of CTLA-4 and PD-L1 blockade tested demonstrated the importance of efficient antigen processing and a functional adaptive immune response for effective immunotherapy in SCLC (25). Also, RNA sequencing of SCLC cohort in CheckMate-032 (NCT01928394) identified MHC-I as a critical determinant of tumor response to immune checkpoint inhibitors (26). In SCLC various mechanisms of MHC-I downregulation have been described. One factor influencing SCLC immunogenicity is the tumor cell neuroendocrine phenotype. Notch signaling for example can promote the transition into a non-neuroendocrine phenotype with higher MHC-I expression (27). Also, epigenetic repression of antigen presentation by EZH2 and LSD1 has been described. Epigenetic therapies for example with valemetostat, a dual EZH1/2 inhibitor revealed increased MHC-I expression in chemotherapy pretreated SCLC patients (28). Similarly, the LSD1 inhibitor bomedemstat improved the efficacy of PD-1 checkpoint blockade in a syngeneic SCLC mouse by inhibition of tumor growth and increased $CD8^+$ T cell efficiently (29). However, the full regulatory landscape governing MHC-I expression in SCLC is still not fully understood.

2.3. Metastasis formation

Quick metastasis formation is a characteristic feature of SCLC and comprises a highly complex process with a considerable number of steps (30). For detailed information on metastasis development, the reader is referred to the review article by Zij and colleagues (31). In brief, the initial step for metastasis is the breakthrough of the basal lamina and the evasion of single cells or collectives into the extracellular stroma. The cancer cells undergo the epithelial-mesenchymal transition (EMT), which allows them to migrate from the primary side. The surrounding extracellular matrix (ECM) undergoes changes due to the influence of the cancer cells (Fig. 2C). It gains rigidity and enters the process of degeneration for example, through the secretion of metalloproteases. In addition, supplying vascularization plays an important role. It is permeable and fragile and thereby enables the exit of further plasma proteins, which promote angiogenesis. Through the leakage of the vessels, cancer cells also have access to the blood circulation, where immune cells and shear forces await them. Surviving tumor cells roll by E-selectin binding. Firm binding is ensured by intercellular adhesion molecule-1 (ICAM-1). The exit from the bloodstream is prepared by the pre-established metastatic niche, which serves factors for settling (31). This aforementioned process is subject to various regulating

molecular cascades (Fig. 2), which among others can be found downstream to cell surface receptors (4,31).

Another important aspect of tumor proliferation and metastasis formation is the extracellular matrix. Around the neoplasm itself and around metastases, often a reaction called desmoplasia can be found. The cancer cells engage in continuous crosstalk with ECM components and infiltrating immune cells (Fig. 2C) (4). Clinically, it was shown that a strong desmoplastic response in gastric cancer is associated with a lower survival rate (32). One reason might be that it hinders immune cells i.e., T cells from entering the tumor (33).

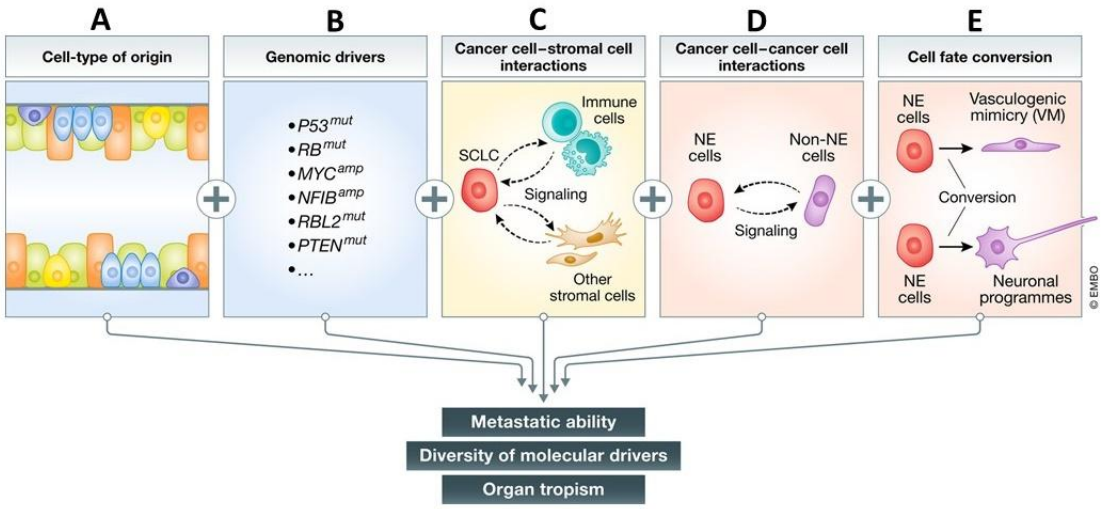

Fig. 2: Metastasis formation in SCLC **(A)** SCLC deriving from epithelial cells carrying mutations. **(B)** Extensive genetic heterogeneity within SCLC. **(C)** Interactions between tumor cells, immune cells, and stromal components. **(D)** Reciprocal impact of neuroendocrine and non-neuroendocrine cells. **(E)** Distinct developmental programs of neuroendocrine cells (4).

On a molecular level, desmoplasia is characterized by an increase in extracellular matrix components such as for example fibronectin or hyaluronic acid. Fibronectin binds to integrins on the surface of tumor cells. It thereby promotes cell migration and enables metastasis formation (34). Further, fibronectin is also responsible for inducing the formation of a pre-metastatic niche (35). Hence, understanding the highly complex interaction between cancer cells and the surrounding ECM is vital for research of SCLC metastasis formation (Fig. 2C).

2.4. CD29 and its role in metastasis formation

Already in 1991, Feldman and colleagues identified CD29, also called Integrin β-1, expressed on the surface of human SCLC cells (36). Also recently, CD29 and its role in cancers pathophysiology is debated briskly (37,38). CD29 is a glycoprotein localized on the cell surface. Integrins consist of α and β subunits, that externally bind to specific ECM components.

Internally, CD29 is linked to the actin cytoskeleton (27,28). Thereby, it depicts a linkage between the inside and the outside of the cell and enables bidirectional communication (39). It has various functions and is for instance involved in physiological processes such as cell survival, cell cycle and migration i.e., of immune cells (39,40). However, integrins have become of importance in cancer research as they are suspected to promote tumor cell survival, proliferation as well as migration processes in the context of metastatic spread (41). Integrin expression also influences clinical parameters. In this context, CD29 expression on SCLC tumor cells is associated with poor prognosis (42,43) and chemotherapy resistance (44). Therefore, CD29 is an interesting target in treating and understanding SCLC and its metastatic characteristics.

2.4.1. CD29 and its ligand fibronectin

CD29 consists of three repeating parts, which provide various binding sides for other integrins, collagen and other extracellular molecules (45). One of the numerous ligands of CD29-dependent signaling is fibronectin (46). Fibronectin exists in a soluble and insoluble form (47). The latter is expressed by different cells, in particular fibroblasts, which are known as drivers of desmoplastic reaction (47,48). Enhanced expression of fibronectin nurtures early tumor progression (49) and is associated with a poor prognosis in different cancer entities for example in gastric cancer (50). In renal cell carcinoma and colorectal carcinoma, fibronectin levels in the blood can serve as a prognostic factor (51,52). Later stages are associated with higher levels of fibronectin (51,52). Hence, fibronectin is a pivotal ligand responsible for CD29-dependent signaling, which should be considered in research of CD29-dependent metastatic spread.

2.4.2. CD29 and its ligand angiopoietin-2

Another of the numerous ligands of CD29 is angiopoietin-2 (ANG-2) (53). ANG-2 is a proangiogenic factor and belongs to the family of vascular growth factors. Therefore, it is classically ascribed to the process of angiogenesis. Angiopoietin-1 (ANG-1) and ANG-2 are involved in a close interplay with the vascular endothelial growth factor (VEGF). Their receptors, such as tyrosine kinases with immunoglobulin-like and EGF-like domains 1 (TIE1) and 2 (TIE2), are located on endothelial cells (54). Besides its physiological functions, ANG-2 has gained increasing importance in the field of cancer research. ANG-2 expression plays a role in the formation of leaky tumor vasculature (55). Beyond its role in angiogenesis ANG-2 enhances tumor metastasis formation in lung cancer by promoting epithelial-mesenchymal transition (EMT) (56). Blocking ANG-2 led to a downregulation of EMT markers such as

Vimentin, Twist, and Snail (56). This observation is vital, as EMT is a decisive point in the formation of metastasis.

2.5. Immune micro-milieu

The immune micro-milieu is pivotal for the anti-tumor response. Therefore, one has to take a closer look at the involved immune cells, which interact with the tumor cells. Main players in the immune micro-milieu are macrophages. Physiologically, they take up pathogens or cancer cells nonspecifically by phagocytosis and thereby constitute a central component of the innate immune system (57). In the context of cancer, a certain type of macrophage emerges. The so-called tumor-associated macrophages (TAMs) appear during constant inflammation. Instead of cytotoxic potential, they acquire a M2-like macrophage signature. Physiologically, M2-like macrophages are involved in tissue repair (57,58). In contrast to M1-like macrophages, they secrete anti-inflammatory signals as interleukin 10 (IL-10) or promote tumor growth by epidermal growth factor secretion (58). In breast cancer, for example an increased number of TAMs is associated with poorer prognosis (59).

Another factor contributing to an anti-inflammatory milieu is the programmed cell death protein 1 (PD-1) and the programmed death ligand 1 (PD-L1) pathway, which form an immune checkpoint and prominent target of modern immunotherapy (60). The expression the immune checkpoint PD-L1 on the surface of the cancer cells hinders T cell attack (61). Therefore, tumor-infiltrating lymphocytes cannot exert a proper anti-tumor response. Lately, Gordon and colleagues also found macrophages to express PD-1, restricting phagocytosis and nonspecific anti-tumor activity of macrophages (62). The cancer cells further foster the immunosuppressive milieu by driving activated T cells into apoptosis releasing exosome death ligands as Fas ligand (FasL) and TNF-related apoptosis-inducing ligand (TRAIL) (63). In summary, the immune micro-milieu comprises several players contributing to the immune escape of the tumor cells.

2.6. MHC-I and its role in cancer

The previously described complex interactions of tumor cells and immune cells in the tumor micro-milieu can be summarized as cancer immunoediting and are decisive for therapy outcome. Dunn and colleagues coined the term of cancer immunoediting by dividing it into “The Three Es” - elimination, equilibrium, and escape(64). The phase of elimination involves the recruitment of the innate and acquired immune system. The equilibrium phase is decisive as persistent tumor cells typically develop mutations, which lead to decreased immunogenicity. This survival benefit leads to the selection of the tumor cells with decreased antigen presentation (64). The phase of escape is characterized by reduced antigenicity of tumor cells

and the formation of a suppressive tumor micro-milieu, which consequently facilitates immune evasion and subsequent proliferation (64) .

One major mechanism of the described immune escape is the loss of antigen presenting major histocompatibility complex class I (MHC-I). MHC-I is a protein complex, which is presented on nearly every body cell except for red blood cells (65). It serves the presentation of endogenous or non-self-polypeptides to the T cell receptors (TCRs) of $CD8^+$ T-lymphocytes and is therefore a central component of the adaptive immune system (65). Structurally, MHC-I can be subdivided into four protein subunits namely α1, α2, and α3 and β2 microglobulin. In mice, the *B2M* gene for β2 microglobulin can be deleted, which leads to a loss of MHC-I presentation (66).

Common mechanisms of MHC-I loss on tumor cells are inactivating alterations in encoding genes or decreased transcription of pathway genes (67). Clinically, it was described that patients with impaired MHC-I presentation on tumor cells tend to be refractory (68). As MHC-I is essential for $CD8^+$ anti-tumor response, the question is, how to counteract the downregulation of MHC-I. One mechanism to enhance MHC-I expression is the stimulation of interferon gamma (IFNγ) release by infiltrating T cells. The consequent activation of the JAK-STAT pathway leads to an increased MHC-I presence on the surface of the tumor cells. This enables the recognition of neoantigens by $CD8^+$ T cells and the following elimination by excretion of granzymes and perforins (69). To effectively counteract MHC-I loss, it is important to understand pathways with MHC-I regulatory potential and their activation.

2.7. ERBB2 alteration and its effects on MHC-I presentation

One player with increasing importance in the study of cancer immune escape mechanisms is ERBB2. ERBB2, also known as HER2, is an epidermal growth factor receptor and part of the ERBB family. Other members are EGFR, ERBB3 and ERBB4 (70). These receptors can be typically subdivided into an intracellular, extracellular and transmembrane domain. Remarkably, there is no specific ligand of ERBB2 known (70). Activation of ERBB2 occurs through homodimerization or heterodimerization with other receptors, such as EGFR (71). ERBB2 is joint with downstream signaling cascades, which are interconnected (Fig. 3) (72). Downstream signaling pathways include the mitogen-activated protein kinase (MAPK) and the phosphoinositide 3-kinase phospholipase C kinase (PI3K) pathway (Fig. 3) (70,73). These pathways drive increased cell proliferation (72).

Clinically, ERBB2 has established as a target of treatment and as a negative prognostic factor in the field of breast cancer (74). Here ERBB2 positive tumors have shown a decreased response upon modern immunotherapy (75).

Beyond its prominent role in the field of breast cancer, ERBB2 is also expressed in around 13% of SCLC cases diagnosed (76). In SCLC, ERBB2 amplification is associated with a

shorter median survival (77). Furthermore, ERBB2 shows an upregulation with upcoming chemo resistance, which is one of the major challenges in SCLC treatment (78).

ERBB2 also contributes to the establishment of an immunosuppressive microenvironment (70). ERBB2 overexpressing cell lines for example show an increase in the production of negative immune modulators as IL-10, TGFβ and VEGF (70). Additionally, both EGFR and ERBB2 inhibit IFNγ signaling. ERBB2 for example suppresses the stimulator of interferon genes (STING) pathway (70,79). Moreover, the downstream PI3K–AKT pathway is activated, which leads to a loss of phosphorylation of TANK-binding kinase 1 (TBK1). Another pathway responsible for MHC downregulation is the MAPK pathway (80). Together the PI3K–AKT and MAPK pathways inhibit the interferon signaling (Fig. 3). The interferon regulatory factor 3 (IRF3), which is a transcriptional factor of MHC, is downregulated (Fig. 3) (70). It was found that when the MAPK is blocked an increase in MHC class I and MHC class II can be observed (81), providing evidence that upstream ERBB2 signaling may regulate MHC-I.

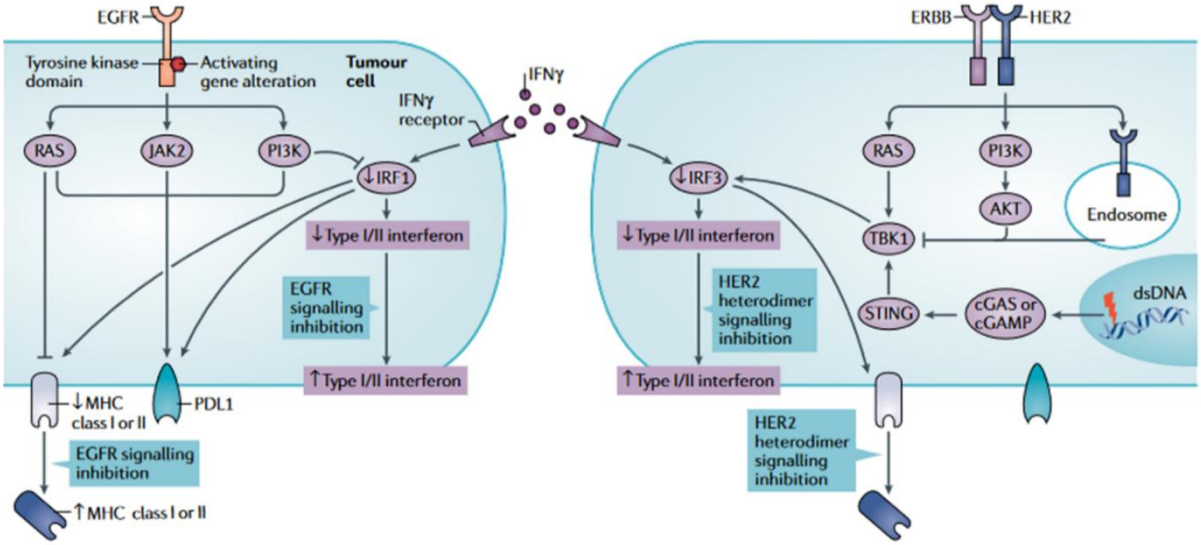

Fig. 3: ERBB2 signaling downregulates the presentation of MHC-I The activation of ERBB2 signaling via homo- or heterodimerization leads to the activation of the downstream PI3K-Akt and MAPK pathway. This affects TBK1 by a loss of phosphorylation. Moreover, it attenuates STING, which causes a downregulation of IRF3, which is a transcriptional factor for MHC-I (60).

2.8. Study Aims

SCLC is characterized by early metastatic spread and poor immunogenicity, both of which contribute to its dismal prognosis and limited response to immunotherapy (4,19). Despite advances in understanding SCLC biology, the molecular mechanisms underlying metastatic progression and immune evasion remain still not fully understood.

1) The aim of this study is to identify key molecular drivers of metastasis in SCLC. Specifically, we aim to characterize signaling pathways and key regulators that promote invasive behavior and promote the process of intra- and extravasation.

2) The second objective is to elucidate the regulatory mechanisms controlling antigen presentation as a mechanism of immune escape in SCLC and their influence on metastasis formation.

2.9. Hypothesis

We hypothesize that heterogeneity within primary SCLC gives rise to distinct cellular subpopulations characterized by specific gene expression programs with enhanced capacity to extravasate and colonize distant metastatic regions. Integrins have been described in processes of migration in cancer context and their interaction with extracellular matrix could portray a target to prevent process of metastasis formation (41).

Furthermore, we hypothesize that under selective pressure from therapy and immune surveillance, MHC-I deficient subpopulations are selected, contributing to immune evasion and metastasis formation. The loss of MHC-I expression is potentially mediated by actively regulated mechanisms that may be reversible, opening new approaches for therapeutic sensitization to immunotherapy.

To test these hypotheses, we screen matched patient samples by IHC to identify proteins differentially expressed in metastatic lesions. Based on our hypothesis we expect differential expression of integrins and antigen presentation associated proteins. The functional role is assessed by CRISPR/Cas9-mediated knockout in SCLC cell lines. These genetically modified clones are evaluated in *in vitro* migration and invasion assays. The role of the identified proteins will be examined in *in vivo* metastasis models, allowing us to study their contribution to tumor extravasation and intravasation processes as well as their interaction with tumor microenvironment and immune landscape. In parallel, we investigate the role of antigen presentation via MHC-I in SCLC tumor control and metastasis. Potentially regulatory genes will be tested therapeutically.

To test these hypotheses, we formulated the following research questions:

1. What is the functional contribution of the integrin CD29 and its ligands to the migratory and invasive phenotype of SCLC cells?
2. How does reduced MHC-I antigen presentation influence immune evasion and metastatic progression in SCLC?
3. Can pharmacological targeting of signaling pathways restore MHC-I expression and thereby counteract immune escape?

3. Materials and Methods

3.1. Materials

3.1.1. Mice

For this study male and female C57BL/6J mice and NOD scid gamma mice (NSG) were used. In addition, experiments were carried out using the genetically engineered SCLC mouse model driven by conditional deletion of the tumor suppressor genes *Rb1* and *Trp53* (11). All animal procedures followed the German Laws of Animal Protection after obtaining the approval of the local animal care committee governmental authority (2020.A219, 2020.A026, 2021.A328).

3.1.2. Cell lines

Table 1: List of origin and sources of cell lines.

Material	Source	Origin
157.8	*RB1, TP53 KO* model	mouse
240.1	*RB1, TP53 KO* model	mouse
240.5	*RB1, TP53 KO* model	mouse
100.H7	*RB1, TP53 KO* model	mouse
Glc-1	Department of Translational Genomics (Prof. Dr. Thomas)	human
Glc-8	Department of Translational Genomics (Prof. Dr. Thomas)	human
H69	Department of Translational Genomics (Prof. Dr. Thomas)	human
H82	Department of Translational Genomics (Prof. Dr. Thomas)	human
H735	Department of Translational Genomics (Prof. Dr. Thomas)	human
H1688	Department of Translational Genomics (Prof. Dr. Thomas)	human

3.1.3. Reagents and kits

Table 2: List of laboratory reagents and kits with corresponding suppliers.

Material	Producer
ACK Lysing Buffer	Lonza Group AG, Basel, Switzerland
ANG-2	Adipogen Life Sciences, Inc., San Diego, USA
Crystal violet	Sigma-Aldrich, St. Louis, USA
DPBS 1x, Gibco®	Thermo Fisher Scientific Inc., Waltham, USA
FBS Gold	PAN Biotech, Aidenbach, Germany
Fibronectin	STEMCELL Technologies, Vancouver, Canada
Lexogen QuantSeq Kit	Lexogen, Vienna, Austria
NuPAGE Bis-Tris Gels 4-12%	Life Technologies, Thermo Fisher Scientific Inc., Waltham, USA
NuPAGE™ LDS Sample Buffer (4X)	Life Technologies, Thermo Fisher Scientific Inc., Waltham, USA
Paraformaldehyde 4%	Carl Roth GmbH + Co. KG, Karlsruhe, Germany
Pierce BCA Protein Assay Kit	Thermo Fisher Scientific Inc., Waltham, USA
RNeasy Mini Kit	Qiagen N.v., Venlo, Netherlands

RPMI Medium 1640 + GlutaMAX Gibco®	Thermo Fisher Scientific Inc., Waltham, USA
Trypan Blue Stain 0.4% Gibco®	Thermo Fisher Scientific Inc., Waltham, USA
Trypsin-EDTA Gibco®	Thermo Fisher Scientific Inc., Waltham, USA

3.1.4. Software

Table 3: List of software and suppliers.

Material	Producer
GraphPad Prism Version 8	GraphPad Software, San Diego, USA
ImageJ v1.48	National Institutes of Health, Bethesda, USA
Kaluza Flow Cytometry Analyzing software	Beckman Coulter, Brea, USA
Microsoft Excel 2018	Microsoft Inc., Redmond, USA
Microsoft PowerPoint 2018	Microsoft Inc., Redmond, USA
Microsoft Word 2018	Microsoft Inc., Redmond, USA
NDP view 2.0	Hamamatsu Photonics, Hamamatsu, Japan

3.1.5. Technical equipment

Table 4: Technical equipment and corresponding suppliers.

Material	Producer
Axiovert 40 C Microscope	Carl Zeiss AG, Oberkochen, Germany
CO_2 Incubator	Binder GmbH, Tuttlingen, Germany
Eppendorf Centrifuge 5417 R	Eppendorf SE, Hamburg, Germany
Eppendorf Centrifuge 5702	Eppendorf SE, Hamburg, Germany
Illumina HiSeq 4000	Illumina, San Diego, USA
LabVision Autostainer 480S	Thermo Scientific, Waltham, USA
LaTheta mCT,	Hitachi Alcoa Medical, Ltd, Tokyo, Japan
NanoZoomer S360 digital slide scanner	Hamamatsu Photonics, Hamamatsu, Japan
Nikon Eclipse TS100	Nikon, Tokyo, Japan
Phillips Achieva 3.0 T	Philips, Amsterdam, Netherlands
Stuart Digital water bath SWB6D	Antylia Scientific, Vernon Hills, USA
Vortex Mixer VTX 3000 L	LMS Consult GmbH & Co. KG, Brigachtal, Germany

3.1.6. Laboratory equipment

Table 5: Laboratory equipment and corresponding suppliers.

Material	Producer
Boyden Chamber	Greiner Bio One GMBH, Leipzig, Germany
Caliper	FINO, Bad Bocklet, Germany
Cell culture flasks, filter screw cap (T25, T75, T175)	Greiner Bio One GMBH, Leipzig, Germany
Cell Strainer 40 µm	Sarstedt AG & Co. KG, Nümbrecht, Germany
Cellstar™ 6-well plate	Greiner Bio One GMBH, Leipzig, Germany
CytoOne 12-, 24- well plate	Starlab, Hamburg, Germany
30G needle	B. Braun, Melsungen, Germany
Neubauer chamber	Paul Marienfeld GmbH, Lauda-Königshofen, Germany
Safe-Lock Tubes (1.5 ml, 2 ml, 5 ml)	Eppendorf SE, Hamburg, Germany

Serological Pipettes (5 ml, 10 ml, 25 ml)	Greiner Bio One GMBH, Leipzig, Germany
XCell II™ Blot Module	Invitrogen, Thermo Fisher Scientific Inc., Waltham, USA

3.1.7. Drugs

Table 6: Administered drugs and corresponding suppliers.

Material	Producer
Dexpanthenol-ointment (Bepanthen®)	Bayer AG, Leverkusen, Germany
Isoflurane 100 %	Piramal, Mumbai, India
Ketaset, Ketamin injections solution (100 mg/ml)	Zoetis Inc., Parsippany-Troy Hills, USA
Kodan Tinktur forte	Schülke & Mayr GmbH, Norderstedt, Germany
Mubritinib	Selleckchem, Houston, USA
Rompun, Xylazine Injection solution (2%)	Bayer AG, Leverkusen, Germany

3.1.8. Antibodies FACS

Table 7: Fluorochrome-conjugated antibodies used for flow cytometry with corresponding suppliers.

Cytochrome	Antibody	Producer	Host	Dilution
Alexa Fluor	CD25	BioLegend, San Diego,USA	rat	1:200
Alexa Fluor	I-A/I-E	BioLegend, San Diego,USA	rat	1:200
Alexa Fluor	Ly-6G	BioLegend, San Diego,USA	rat	1:200
APC	CD56	R&D Systems Minneapolis, USA	rat	1:200
APC	CD86	BioLegend, San Diego,USA	rat	1:200
APC	CD274 (PD-L1)	BioLegend, San Diego,USA	rat	1:200
APC	CD279 (PD-1)	BioLegend, San Diego,USA	rat	1:200
APC	IgG1	BioLegend, San Diego,USA	mouse	1:200
APC/Cyanine7	CD45	BioLegend, San Diego,USA	rat	1:200
APC/Cyanine7	IgG2b	BioLegend, San Diego,USA	rat	1:200
FITC	CD47	BioLegend, San Diego,USA	rat	1:200
FITC	CD80	BioLegend, San Diego,USA	armenian hamster	1:200
FITC	IgG1	BioLegend, San Diego,USA	mouse	1:200
FITC	NK-1.1	BioLegend,San Diego,USA	rat	1:200
Pacific Blue	CD8a	BioLegend, San Diego,USA	rat	1:200
Pacific Blue	CD29	BioLegend, San Diego,USA	armenian hamster	1:200
Pacific Blue	H-2Kb	BioLegend, San Diego,USA	mouse	1:200
PE	CD202b	BioLegend, San Diego,USA	rat	1:200
PE	ErbB2/ERBB2	R&D Systems, Minneapolis, USA	rat	1:200
PE	IgG2a	BioLegend, San Diego,USA	rat	1:200
PE-Cyanine 7	Axl	eBioscience, San Diego, USA	rat	1:200
PE-Cyanine7	CD11b	BioLegend, San Diego,USA	rat	1:200
PE-Cyanine7	CD107a	BioLegend, San Diego,USA	rat	1:200
PE-Cyanine7	CD274 (PD-L1)	BioLegend, San Diego,USA	rat	1:200
PE-Cyanine7	IgG2bK	BioLegend, San Diego,USA	rat	1:200
PE/Dazzle	CD31	BioLegend, San Diego,USA	rat	1:200
PE/Dazzle	CD4	BioLegend, San Diego,USA	rat	1:200
PE/Dazzle	CD11c	BioLegend, San Diego,USA	american hamster	1:200
PE/Dazzle	IgG1	BioLegend, San Diego,USA	mouse	1:200
PerCP/Cyanine5.5	H-2Kb/H-2Db	BioLegend, San Diego,USA	mouse	1:200

PerCP/Cyanine5.5	I-A/I-E	BioLegend, San Diego,USA	rat	1:200
PerCP/Cyanine5.5	IgG1	BioLegend, San Diego,USA	rat	1:200
PerCP/Cyanine5.5	CD366 (Tim-3)	BioLegend, San Diego,USA	rat	1:200

3.1.9. Antibodies Western Blot

Table 8: Western Blot antibodies and corresponding suppliers.

Antibody	Producer	Dilution
Anti-mouse-HRP	Millipore, Billerica, USA	1:3,000
Anti-rabbit-HRP	Millipore, Billerica, USA	1:3,000
β-actin	MP Biomedicals, Irvine, USA	1:3,000
FAK	Cell Signaling, Danvers, USA	1:1,000
p-FAK Tyr397	Cell Signaling, Danvers, USA	1:1,000
p-SRC Tyr416	Cell Signaling, Danvers, USA	1:500
SRC	Cell Signaling, Danvers, USA	1:1,000
Vimentin	Abcam, Cambridge, UK	1:500

3.1.10. Antibodies immunohistochemistry

Table 9: Immunohistochemistry antibodies and corresponding suppliers.

Antibody	Producer	Host	Dilution
CD45	BD Pharmingen, Franklin Lakes, USA	rat	1:500
CD56	Zytomed, Berlin, Germany	rabbit	1:1,000

3.2. Methods

3.2.1. Cell biological methods

3.2.1.1 Cell culture

The cell lines are listed in Table 1. The cell lines were cultured in 250 ml, 75 cm^2 and 550 ml, 175 cm^2 cell culture flasks (Greiner Bio One GMBH, Germany) under conditions of 5% CO2 and 37 °C. Unless stated otherwise, the cell culture media RPMI medium 1640 (Thermo Fisher Scientific Inc., USA) was supplemented with 10% FBS (PAN-Biotech, Germany), 50 U/ml Penicillin and 50 µg/ml Streptomycin. For subculture, cells were detached from the plate floor by trypsinization (Thermo Fisher Scientific Inc., USA). Cells were split two times per week at a dilution of 1:3-1:15 depending on the proliferation rate of the specific cell line. All cell culture work was performed under sterile conditions.

3.2.1.2 Scratch Assay

Fibronectin (STEMCELL Technologies, Canada) was used in different concentrations (1 µg/cm^2, 10 µg/cm^2). Via previously conducted pilot testing we found the best results obtained for a fibronectin concentration of 10 µg/cm^2 and thus used it for all subsequent experiments. Fibronectin was used to cover the ground of a 12-well plate (Greiner Bio One GMBH, Germany). The well plate was moved in circular motion to assure an even spread of fibronectin on the ground surface. Subsequently, the well plate was incubated for 60 min. Afterwards, each well was washed with 400 µl phosphate buffered saline (PBS). Tumor cells were harvested with trypsin (Thermo Fisher Scientific Inc., USA) and counted with the Neubauer Chamber (Paul Marienfeld GmbH, Germany). Around 70,000 cells per well were diluted in 800 µl RPMI medium and were given 24 h to settle down. The tip of a 1000 µl pipette was used to make a vertical scratch. Hereby detached cells were removed by washing with 400 µl PBS. Fresh medium was applied. 8 h and 24 h after the drawn scratch photos were taken by microscope (Nikon Eclipse TS100, Nikon, Japan).

The scratch assay was further used for assessing the migrative reaction upon ANG-2 (Adipogen Life Sciences Inc., USA) stimulation. Instead of previous incubation, ANG-2 (500 ng/ml) was directly added to the cell suspension. The protocol continued with letting the cells settle down as described above. With the polygon tool of the ImageJ software (National Institutes of Health, USA), the initial area of scratch and the respective areas after 8 h and 24 h were measured. Since single invaded cells were difficult to count due to overlapping cells and cell processes, the threshold method was applied to analyze the area covered by scratch invading tumor cells. Finally, a ratio of the area of invasive tumor cells and of the original scratch size was calculated.

3.2.1.3 Boyden Chamber

The Boyden Chamber system (Greiner Bio One GMBH, Germany) was hung up into 24-well plate filled with 500 µl medium containing the respective chemoattractant underneath (Fig. 5). For the migration assay 30,000 cells were placed into the chamber above which is separated from the medium by a porous membrane of 8 µm pore size. The upper chamber was filled with serum-free medium (Fig. 5). The ground compartment was supplemented with RPMI medium 1640 containing 10% FBS and respectively with fibronectin (10 µg/cm^2) and ANG-2 (500 ng/ml) (Fig.4). The cells were incubated for 48 h. With a cotton swab, cells in the interior part of the insert were removed. Cells on the bottom of the membrane were fixated with 4% paraformaldehyde (PFA) (Carl Roth GmbH + Co.KG, Germany) for 20 min and stained with 1% crystal violet solution (Sigma-Aldrich, USA) for 5 min. The excess dye was washed away with PBS and the chamber was dried for 20 min at room temperature (RT). The stained cells

on the underside of the membrane were photographed by microscope (Nikon Eclipse TS100, Nikon, Japan). Five representative 4x magnification images were taken from the entire surface.

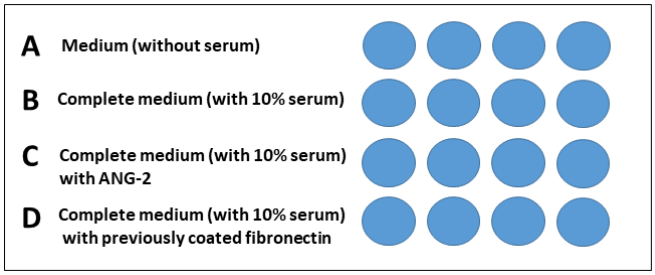

Fig. 4: **Different tested conditions in the Boyden Chamber (A)** Starving medium with 1% FBS. **(B)** Medium 10% with FBS. **(C)** Medium with ANG-2 (500 ng/ml). **(D)** Wells coated with 10 µg/cm^2 fibronectin.

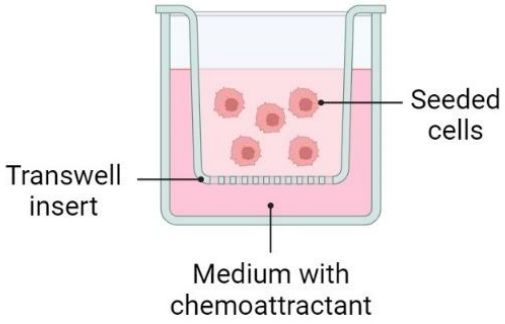

Fig. 5: Boyden Chamber setup Seeded cells migrate through porous membrane attracted by a chemoattractant underneath. Created with BioRender.com.

The color threshold method was applied to analyze the density/area covered by tumor cells or respectively the cells placed on the other side of the membrane in the Boyden Chamber. The tool selects the area of tumor cells by differences in color. With the color threshold tool of the ImageJ software, the minimum and maximum value of the crystal violet labelled area was chosen by hand and the area was measured. Subsequently, the mean value was calculated.

3.2.1.4 Flow cytometry

At first the tissue was harvested and pressed through a 40 µm cell strainer (Sarstedt AG & Co. KG, Germany) with 500 µl PBS. The cell suspension was collected using 500 µl PBS and collected in an Eppendorf tube. Subsequently, cell suspension was centrifuged for 4 min at 350 xg and the supernatant was discarded. To lyse red blood cells, 800-1000 µl ACK lysing Buffer (Lonza Group AG, Swiss) was added and incubated for 5-15 min at RT. Then the suspension was centrifuged for 4 min at 350 xg again. After discarding the supernatant cells were washed with 1000 µl PBS. The cells were incubated with the staining mix for 25 min at 4

°C. FACS antibodies listed in 3.1.8 were used for staining. For viability staining the Zombie Aqua Fixable Viability Kit (BioLegend, USA) was used. Subsequently, the cells were washed with 100 µl PBS. Diluted in 200 µl PBS cell suspension was transferred into FACS tubes with inlays. ABs were used in concentration 1:200.

3.2.2. Molecular biological methods

3.2.2.1 RNA isolation and sequencing

As described above (see 3.2.1.2) initially the respective chambers of a 6-well plate were coated with fibronectin (10 µg/cm^2). Approximately 300,000 WT cells per well were settled with 2.5 ml medium. The ANG-2 stimulated condition additionally contained ANG-2 in a concentration of 250 ng/ml. After 48 h the cells were harvested for RNA-sequencing (RNA-Seq) and the RNeasy Mini Kit (Qiagen N.v., Netherlands) was applied according to manufacturer's instruction. Total RNA was submitted to the CCG, a core facility specializing in high-throughput sequencing and molecular analysis. The RNA was submitted with a concentration of 200 ng/µL. 3' mRNA sequencing libraries were generated using the Lexogen QuantSeq kit (Lexogen, Austria) following the standard protocol. After validation and quantification cDNA libraries were pooled. The pools were quantified and subsequently sequenced with Illumina HiSeq 4000 (Illumina, USA) using a 2 × 100 bp protocol.

3.2.2.2 Western Blot

The cell lysates were generated by digesting the cells with lysing buffer. The BCA Protein Assay (Pierce, Thermo Fisher Scientific Inc., USA) was applied to define protein concentrations. For separating the protein samples by SDS-PAGE the cell lysates were incubated with 4× NuPage® LDS buffer and sample reducing agent (10×) (Thermo Fisher Scientific Inc., USA) for 10 min at 80 °C. The samples were placed on NuPAGE Bis-Tris Gels 4-12% (Thermo Fisher Scientific Inc., USA) for around 90 min at 130 V. The proteins were transferred to a nitrocellulose membrane (Amersham Hybond-C Extra) using the wet transfer apparatus XCell II™ Blot Module (Thermo Fisher Scientific Inc., USA). After blocking with Blocking Buffer (4% milk in TBST) the respective primary antibody (AB) was added and left to incubate overnight for approximately 14 h. Primary Antibodies: Vimentin (Abcam, 1:500, EPR3776), p-Fak Tyr397 (Cell Signaling, 1:1000, polyclonal, 3283), FAK (Cell Signaling, 1:1000, D2R2E), p-SRC Tyr416 (Cell Signaling, 1:500, polyclonal, 2101), SRC (Cell Signaling, 1:1000, 36D10), β-actin (MP Biomedicals, 1:3000, C4).

Tris-buffered saline with Tween (TBST) was used to wash the membrane. Ensuingly, secondary HRP-conjugated antibody 1:3000 in TBST was added for 1 h at RT (anti-rabbit-HRP and anti-mouse-HRP antibodies; both from Millipore, USA). With ECL western blot

detection System (GE Healthcare, Germany) ECL Hyperfilm was developed. Using 300 µg protein the RTK assay (R&D Systems, USA) was conducted.

3.2.3. *In vivo* methods

3.2.3.1 Animal Welfare and the 3Rs Principle

In accordance with the 3Rs principle (reduce, refine and replace) all animal experiments were designed and conducted with an emphasis on minimizing animal use and distress in accordance to Federation of European Laboratory Animal Science Associations (FELASA) guidelines (82,83). Prior to initiating our *in vivo* studies, we substantiated our hypothesis *in vitro* to establish a solid rationale for subsequent animal testing. The principle reduce was addressed by planning the minimal number of animal to achieve reliable results per group determined by statistical power calculations using G*Power 3.1 (84). The actual number of animals included in the analysis varied across experimental arms (Table 10, 11). This variation was primarily due to unrelated illness determined during regular scoring of the animals. Scoring was performed on a daily basis upon mild suffering according the approved score sheets. The final group sizes are reported below (Table 10,11).

For refinement, *in vivo* imaging via microCT and MRI was employed to enable longitudinal monitoring of tumor progression and minimize suffering during the determination of tumor growth. Particularly, application of these in vivo methods reduces the amount of required animals, since several time points can be assessed in the same mouse. Furthermore, animals showing signs of reduced food intake or weight loss were provided with nutritional support such as soaked chow. In case, the weight loss would reach 20 % and more compared to the time point o measurable target lesion the experiment will be directly abrogated due to severe suffering, which is not tolerated.

The overall burden of conducted *in vivo* experiments is expected as low to moderate due to continuous monitoring guided by the score sheets (Appendix 8.3). Upon reaching defined human endpoints or detection of major progredient lesions by imaging, animals will be euthanized in accordance with animal welfare regulations by cervical dislocation.

3.2.3.2 Mouse cohorts

Table 10: Orthotopically or intravenously injected mice cohorts

Genotype cell line	Administration route	Mouse model	Animal number
mRBP_157.8_WT	Orthotopic	C57BL/6J	7
mRBP_157.8_WT	Orthotopic	NSG	6
mRBP_157.8_CD29_KO	Orthotopic	C57BL/6J	3
mRBP_157.8_CD29_KO	Orthotopic	NSG	10

mRBP_157.8_WT	Intravenous	C57BL/6J	3
mRBP_157.8_CD29_KO	Intravenous	C57BL/6J	4
mRBP_100.H7_WT	Orthotopic	C57BL/6J	7
mRBP_100.H7_MHCI-KO	Orthotopic	C57BL/6J	6
mRBP_100.H7_WT	Intravenous	C57BL/6J	3
mRBP_100.H7_MHCI-KO	Intravenous	C57BL/6J	5
Total			**54**

3.2.3.3 Treatment cohorts

Table 11: Autochthonous SCLC mice therapy cohorts

Treatment cohorts	**Mouse model**	**Animal number**
Vehicle	Rb1/Trp53-deleted SCLC mice	9
ERBB2 inhibitor (mubritinib)	Rb1/Trp53-deleted SCLC mice	6
Anti-PD-1	Rb1/Trp53-deleted SCLC mice	16
Anti-PD-1 + ERBB2 inhibitor (mubritinib)	Rb1/Trp53-deleted SCLC mice	11
Total:		

3.2.3.4 Subcutaneous tumor cell injection

Mice were anesthetized with isoflurane (O_2: 30%; N_2O: 70%; isoflurane 4%) (Piramal, India). Surgical tolerance was tested by interdigital reflex. A heating pad ensured a constant body temperature of 37 °C. To prevent drying-out, the eyes were protected with eye ointment (Bayer, Germany). Subsequently $5x10^6$ tumor cells in a volume of 0.1 ml/per 10 g body weight per mouse were injected subcutaneously (sc.) in both femoral sides with a maximum volume of 0.1 ml per side. Mice were randomly assigned to different cell lines. After the procedure, mice were allowed to regain consciousness in their warmed cages. Tumor development and animal conditions were assessed daily. Detailed tumor measurement was conducted weekly by caliper (FINO, Germany).

3.2.3.5 Orthotopic tumor cell injection

Previously mice received anesthesia by intraperitoneal injection of xylazine (Bayer AG, Germany)/ketamine (Zoetis Inc., USA) (10/100 mg/kg/KGW; max. injection volume 0.1 ml/10 g mouse). Surgical tolerance was tested by interdigital reflex. Eyes were protected by eye ointment and mice were warmed by a heating pad. To guarantee a safe injection the mouse was laid on its left side and injected into the right thorax. Before the procedure the injection side was disinfected and shaved. A 32 G needle (Braun, Germany) was applied to bring in 80

µl of approximately 5x10^6 tumor cells diluted in PBS. The scapula served as an orientation point leading to the 4th or 5th intercostal space. The needle was inserted in a position of 90°

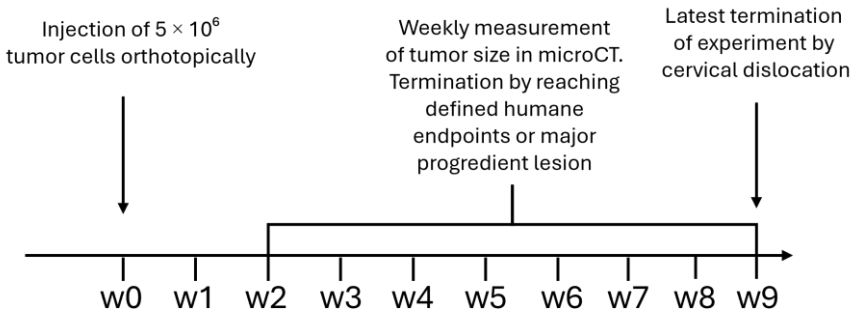

Fig. 6: Experimental setup orthotopic injection Initial tumor injection into the lung and following continuous tumor monitoring. Termination of experiment with reaching of human endpoint or tumor outgrowth.

angular degrees. After the procedure, mice were allowed to regain consciousness in their warmed cages. Animal conditions were assessed daily. Tumor growth was followed by serial *in vivo* imaging using microCT.

3.2.3.6 Intravenous tumor cell injection

The mice were mechanically restrained. The tail was disinfected by antiseptic spray (Schülke & Mayr GmbH, Germany). A distant tail vein section was selected for intravenous (iv.) injection. Approximately 1x10^6 tumor cells in a volume of 80 µl PBS were injected by a 30 G needle (Braun, Germany). After the procedure, mice were allowed to regain consciousness in their warmed cages. Animal conditions were assessed daily. Tumor growth was followed by serial *in vivo* imaging using Magnetic resonance imaging (MRI).

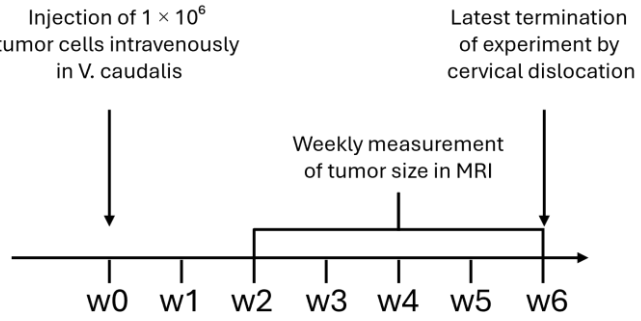

Fig. 7: Experimental setup intravenous injection Initial tumor injection into the V. caudalis and continuous tumor monitoring by MRI. Termination of experiment with reaching of human endpoint or tumor outgrowth.

3.2.3.7 Autochtonous mouse model and therapy cohorts

Genetically engineered SCLC mouse model based on the conditional inactivation of the tumor suppressor genes Rb1 and Trp53 were used (11,85,86) Mice were bred on a C57BL/6 background and included in experiments at minimal age of 6 weeks and with a minimum body weight of 20 g. Tumor induction was achieved via inhalation of Adeno-Cre virus, which was delivered under anesthesia (xylazine/ketamine at 10/100 mg/kg body weight, max. 0.1 ml/10 g), which was administered intraperitoneally. The viral vectors were sourced from the University of Iowa Viral Vector Core. Tumor formation was regularly monitored using micro- (µCT; LaTheta mCT, Hitachi Aloka). Therapy began only after the identification of at least one measurable pulmonary lesion with a diameter of ≥1 mm. Mice were randomized into four treatment arms with balanced baseline tumor sizes across groups. Interventions were administered every three days: vehicle (PBS), anti–PD-1 monotherapy (clone RMP1-14; 10 mg/kg, i.p.), ERBB2 inhibitor monotherapy (mubritinib 10 mg/kg, orally) and combination therapy with anti–PD-1 and ERBB2 inhibitor (mubritinib). Tumor development and treatment response were assessed weekly using serial µCT scans under isoflurane anesthesia. Tumor progression and regression were classified according to mouse-adapted RECIST v1.1 criteria, using a slice thickness of 0.3 mm.

3.2.3.8 *In vivo* imaging

For imaging the small animal microCT (LaTheta mCT, Hitachi Alcoa Medical, Japan) or the Ingenia 3.0 Tesla (T) MR system (Philips, Germany) was used. In the clinical setting the CT is preferred to detect tumor growth in the lung, MRI was only applied upon the need to detect liver metastases. A CT scan was run for 8 min, and an MRI scan for 15 min. Tumor growth was assessed using mouse adapted RECIST criteria, as previously described (85). Mice were narcotized with isoflurane. Each mouse was continuously observed during measurement. In case of early awakening the measurement was stopped immediately. After the scan the mice were placed on a heating pad and further controlled. After regaining consciousness, they were transported back to the animal housing facility.

3.2.3.9 Animal euthanasia

All mice were euthanized by cervical dislocation.

3.2.3.10 Tissue processing

After removal of a part of the tumor tissue for FACS analysis the lung, liver, kidneys and adrenal glands, as well as the brain were fixated with 4% PBS-buffered PFA (Carl Roth GmbH + Co.KG, Germany) overnight. Three-micrometer tissue sections were deparaffinized and IHC

was performed using the LabVision Autostainer-480S (Thermo Scientific, USA) staining with H&E, primary antibodies against CD56 (Zytomed, Germany) and CD45 (BD Pharmingen, USA). For later analysis, parts of lung and liver were frozen in liquid nitrogen and immediately placed at -80 °C.

3.2.4. Statistical analysis

To analyze the statistics of the experiments, Microsoft Excel (Microsoft Inc., USA) and the GraphPad Prism software (6.0 GraphPad Software, USA) were applied. Initially, the normal distribution was checked with the D'Agostino Pearson normality test for $n \geq 8$, the Shapiro-Wilk normality test. In the t-test, the means of two samples were compared, provided that the values follow normal distribution (parametric test). If not stated otherwise error bars indicated standard error of the mean (SEM). The *p*-value was set at 0.05 for statistical significance.

4. Results

4.1. CD29-dependent metastasis formation

4.1.1. Elevated CD29 and vimentin expression in patients' SCLC liver metastases

EMT is one of the major mechanisms of metastasis formation, frequently indicated by vimentin expression as a biomarker for mesenchymal differentiation (87). Thus, we analyzed publicly available RNA-Seq datasets from large SCLC patient sample cohorts (88) and SCLC cell lines (89) (Fig. 8A, B). It was revealed that in SCLC patients the expression of CD29 significantly correlates with the expression of the EMT marker vimentin (r= 0.5266; Fig. 8A). This could also be confirmed in the case of a large set of SCLC cell lines (r= 0.6224, Fig. 8B). The mesenchymal cells display a high expression of vimentin associated with an increasing expression of CD29 (Fig. 8B). Analyzing human cell lines, unveiled that with progression of the disease the CD29 expression increases (Fig. 8C). The cell line derived from a primary tumor displays the lowest CD29 expression. In the pleural effusion cell lines, the CD29 expression is elevated in comparison. The SCLC liver metastasis cell line shows the highest CD29 expression (Fig. 8C).

To investigate this phenomenon at a protein level in SCLC patients, we initially received an exclusive patient sample cohort (*n*=6) of matched lung and liver tissue (Fig. 8D). A histological comparison of the lung tumor and the liver metastases revealed a significant higher CD29 (Fig. 8F) and vimentin (Fig. 8G) expression in the respective liver metastases. In summary, in SCLC patients CD29 is increased in liver metastases compared to primary tumors and goes along with the EMT marker vimentin (86).

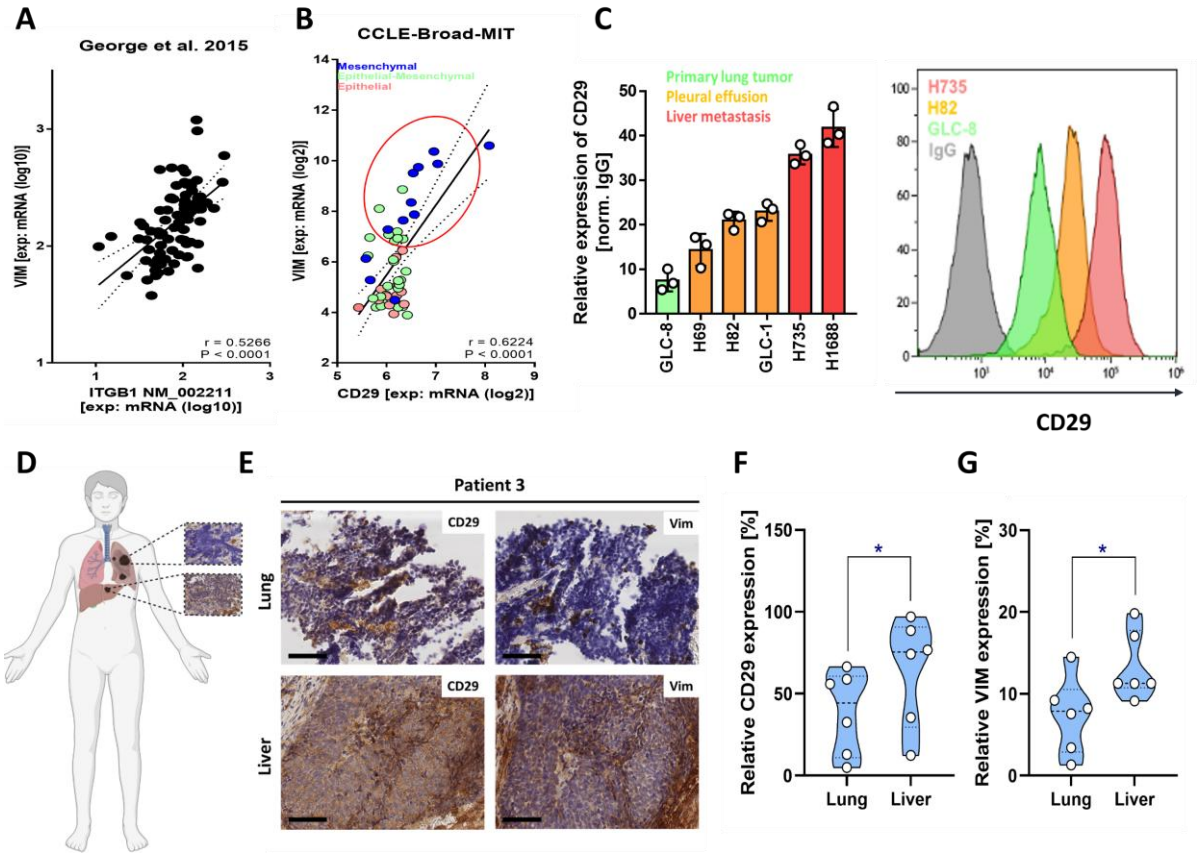

Fig. 8: **Increased CD29 and vimentin expression in SCLC liver metastasis**

(A) Correlation graph of CD29 and vimentin expression in publicly available RNA-Seq data of SCLC patient tissue. **(B)** Correlation graph of CD29 and vimentin expression in publicly available RNA-Seq data of patient SCLC cell lines. **(C)** CD29 expression in human SCLC cell lines derived from primary tumor, pleural effusion and liver metastasis, analyzed by flow cytometry. **(D)** Matched SCLC patient samples (*n*=6) obtained from primary lung tumor and matching liver metastasis. Created with BioRender.com. **(E)** IHC of patient´s matched lung and liver FFPE SCLC tissue samples stained for CD29 and vimentin. **(F, G)** Quantification of CD29 and vimentin expression in IHC samples using ImageJ, shown as relative expression in percent. Scale bar is 100 µm in E. Bar graphs represent mean ± SD. Violin plots (minimum to maximal values) show median, Q1 and Q3 (dashed lines) with individual values. * $p < 0.05$. Institute of Pathology, University Hospital Cologne, Germany performed by M.L. Eich. The analysis was conducted by C. Orschel. This figure contains data that is adapted from (86)

4.1.2. Liver metastases in the autochthonous SCLC mouse model show the highest CD29 expression

We further analyzed our autochthonous SCLC mouse model, in which *Rb1* and *Trp53* are Cre-mediated deleted biallelically, regarding metastatic characteristics. As in the clinical setting, a separation into limited and extensive stage disease is possible (Fig. 9A). We analyzed the expression of CD29 measured by mean fluorescence intensity (MFI) in murine SCLC lung, lung in metastatic disease and in liver metastases. The liver metastases exhibited the highest CD29 expression, but also the lung in the stage of metastatic disease shows a significantly elevated CD29 expression compared to the primary lung tumor in non-metastatic disease (Fig. 9B). Thus, also in the murine setting, the CD29 expression increases with progressing metastatic disease.

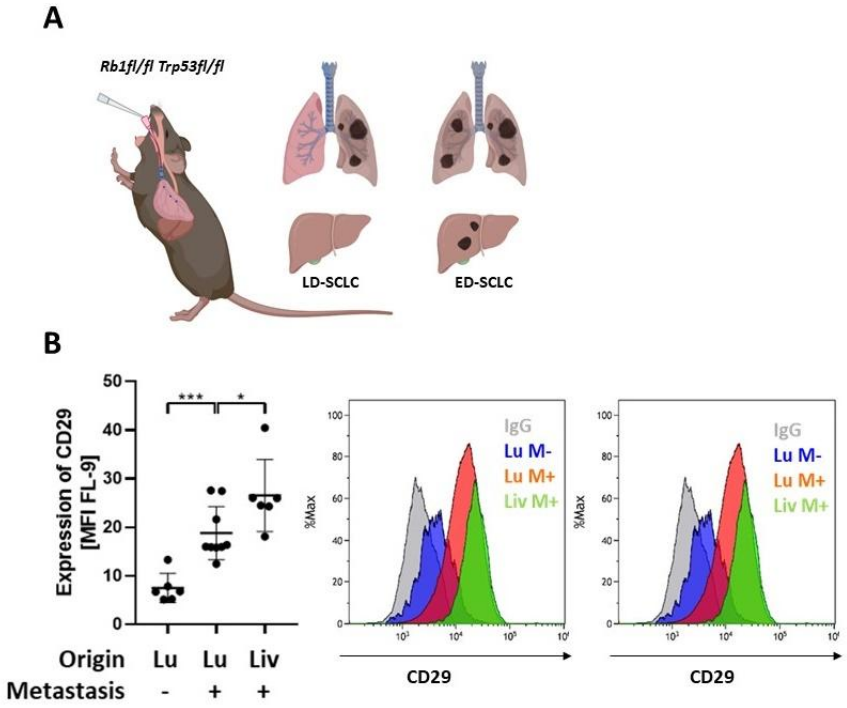

Fig. 9: Increased CD29 with disease progression (A) Autochthonous mouse model of SCLC. *Rb1* and *Trp53* are Cre-mediated biallelicly deleted by virus inhalation. Created with BioRender.com. **(B)** CD29 expression in cells isolated from primary lung tumor, lung tumor in metastatic disease and liver metastasis from autochthonous SCLC mouse model (mean fluorescence intensity, MFI). Horizontal lines in dot plots represent mean ± SD. * $p < 0.05$, *** $p < 0.001$. Lu – lung; Liv – liver; M – metastasis. The analysis was conducted by L. Meder. This figure contains data that is adapted from (86).

4.1.3. CD29 high-level expressing cell line shows migrative behavior upon fibronectin stimulation

In the next step, we aimed to unravel the role of CD29 in SCLC metastasis. Thus, CD29-dependent signaling was activated in tumor cells by fibronectin stimulation.

Tumor cell lines 240.1 and 240.5 were obtained from different primary lung tumor lesions from our autochthonous SCLC mouse model (Fig. 10A). Cells were taken into culture and were cultivated until a stable passage. Comparing 240.1 and 240.5, a significantly stronger CD29 expression on 240.5 (MFI) was detectable (Fig. 10B).

In a scratch assay, cell migration was assessed. Interestingly, cell line 240.5 showed a significant and dose-dependent migration into the scratch in reaction to fibronectin coating (1 mg/cm^2; 10 mg/cm^2) (Fig. 10C). Cell line 240.1 did not show a significantly altered migration behavior when comparing PBS and fibronectin coating (Fig. 10C). Taken together, CD29 expression correlates with enhanced migration capacity *in vitro*.

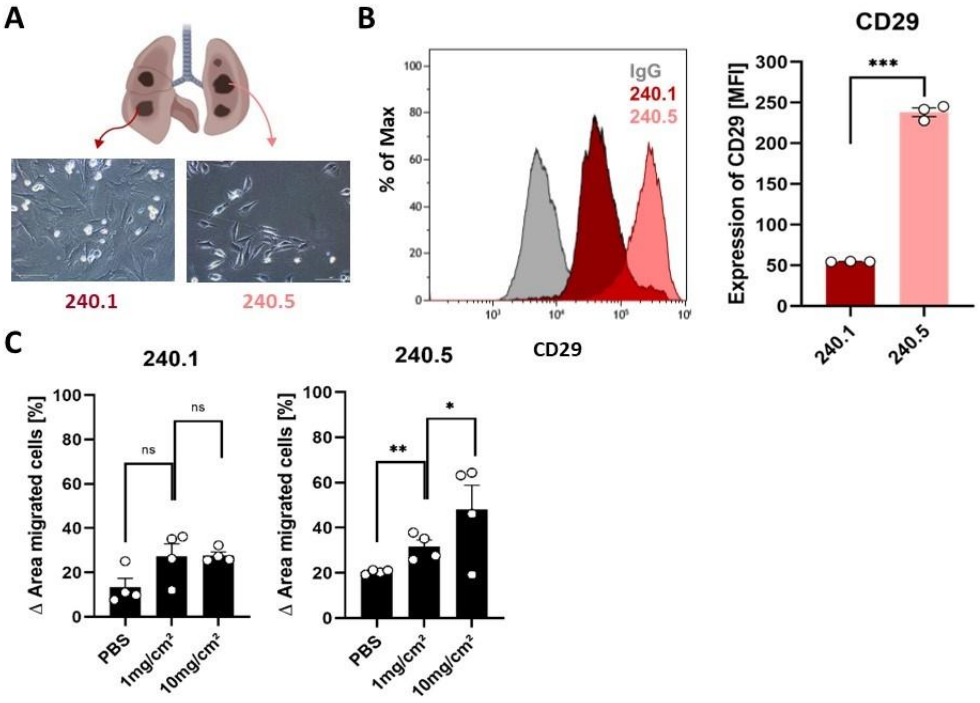

Fig. 10: CD29-expressing SCLC cell line presents stronger invasive reaction upon fibronectin stimulation (A) Tumor cell lines 240.1 and 240.5 generated out of different lung lesions in autochthonous SCLC mouse model. Created with BioRender.com. **(B)** Comparison of CD29 expression in the cultivated tumor cell lines 240.1 and 240.5 measured by FACS (mean fluorescence intensity, MFI). Scale bar is 500 µm in A. Bar graphs represent mean ± s.e.m. * $p < 0.05$, ** $p < 0.01$, *** $p < 0.001$. These experiments were conducted and analyzed by C. Orschel. This figure contains data that is adapted from (86).

4.1.4. CRISPR-Cas CD29 KO generation

To functionally elucidate the importance of CD29 in the process of migration we performed a CRISPR-Cas9 KO on the cell line 157.8. Four different clones were generated (Clone 2, 3, 6, 14) and checked on CD29 expression by FACS. All clones have lost CD29 expression (Fig. 11) in comparison to the WT.

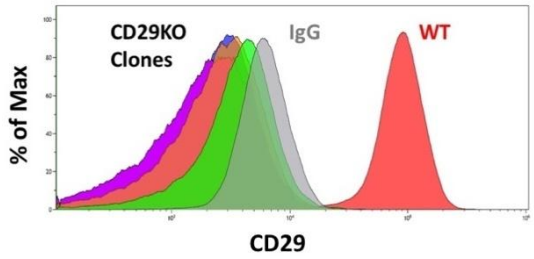

Fig. 11: CRISPR KO of CD29 CD29 expression in CD29 KO clones 2, 3, 6, and 14 compared to the WT and IgG control, measured by FACS. The CRISPR KO was performed by M. Koker. The FACS experiment was conducted and analyzed by C. Orschel.

4.1.5. CD29 KO abrogates fibronectin promoted migration

To check whether the CD29 KO has altered the migratory behavior in comparison to the WT, also here a scratch assay was performed. After 24 h of incubation, microscope images showed the overgrown scratch by the WT and the clearly visible scratch in the CD29 KO condition (Fig. 12A). After 8 h of incubation the WT, CD29 KO Clone 2 and 3 show a significant decrease in the scratch area (Fig. 12B). However, the WT exhibited a greater reduction in scratch area than Clone 2 (Fig. 12B). This is also the case for WT vs. Clone 3 after 24 h (Fig. 12C). The WT, Clone 6 and Clone 14 show no significant differences after 8 h (Fig. 12D). After 24 h the WT demonstrated a significantly higher decrease in scratch area than Clones 6 and 14 (Fig. 12E). In summary, these results show that all CD29 KO clones tested lost the capacity to close the scratch upon fibronectin stimulation as fast as the original WT did.

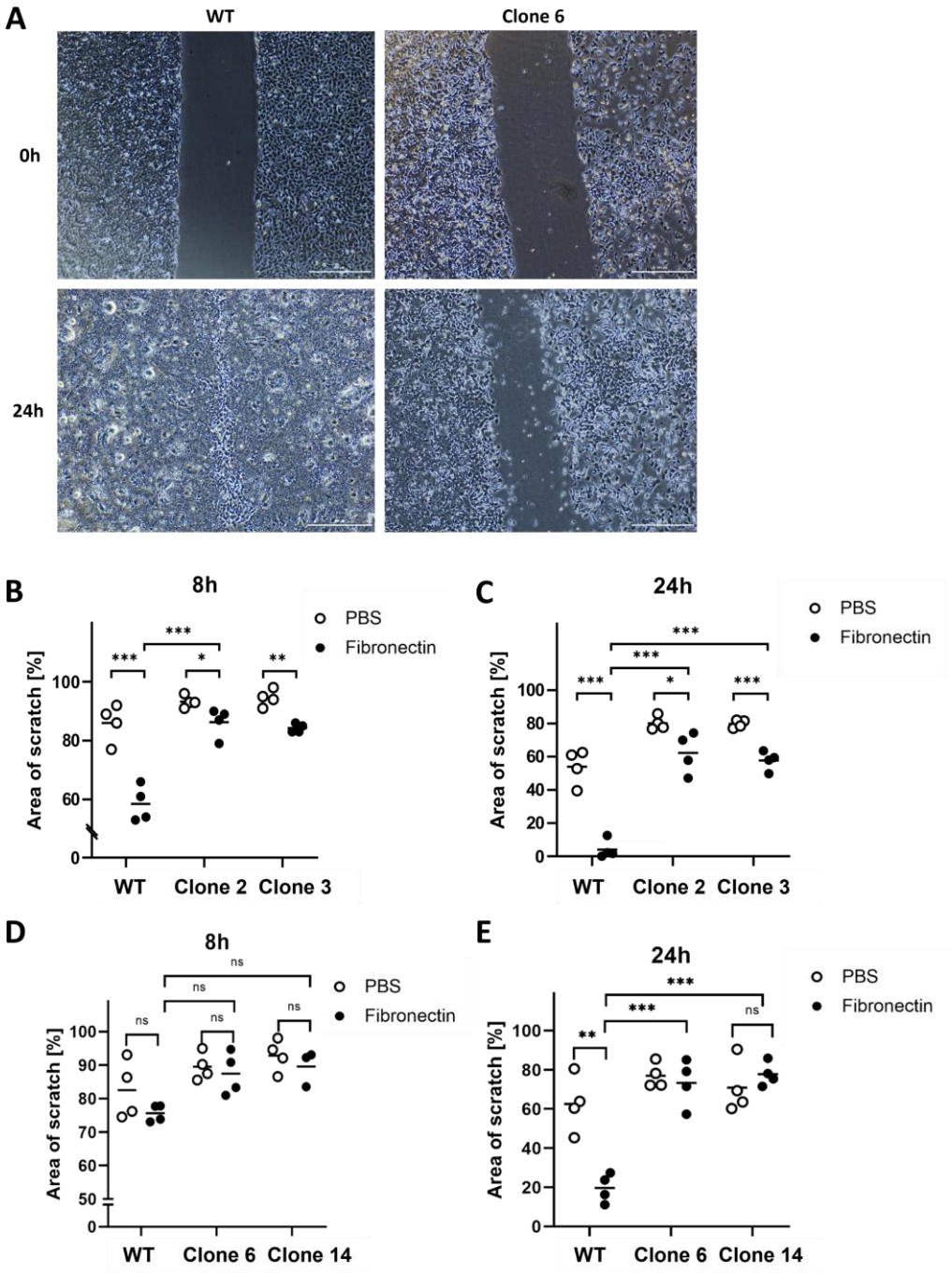

Fig. 12: CD29 KO clones show an abrogation of migratory behavior upon fibronectin stimulation (A) Scratch assay images at time point 0 h and after 24 h of the WT and CD29 KO Clone 6. **(B)** Area of the scratch in % of WT, Clone 2, and Clone 3 after 8 h of incubation under fibronectin stimulation. **(C)** Area of the scratch in % WT, Clone 2, and Clone 3 after 24 h of incubation under fibronectin stimulation. **(D)** Area of the scratch in % of WT, Clone 6, Clone 14 after 8 h of incubation under fibronectin stimulation. **(E)** Area of the scratch in % of WT, Clone 6 and Clone 14 after 24 h of incubation under fibronectin stimulation. Horizontal lines in dot plots represent the mean. * $p < 0.05$, ** $p < 0.01$, *** $p < 0.001$. These experiments were conducted and analyzed by C. Orschel. This figure contains data that is adapted from (86).

To confirm those results and to further check especially on invasion the Boyden Chamber assay was applied. Cells were placed in a chamber above and migrated through a porous filter (8 µm pore size) to the respective chemoattractant underneath, in this case fibronectin. The images on the left depict the cells (stained with trypan blue), which have reached the other side of the membrane after an incubation time of 48 h. The WT tumor cells cover a much higher area in the fibronectin stimulated setting (Fig. 13A). Also, the CD29 KO cells have migrated through. However, the medium and the fibronectin stimulated migration show no difference. The images on the right show the cells settled on the ground of the well (Fig. 13A). In the fibronectin stimulated condition the WT has formed a huge cell colony on the ground (Fig. 13A). Also Clone 2 forms single small populations on the ground (Fig. 13A). Regarding the fold change in covered area, the WT invasion was significantly increased upon fibronectin stimulation compared to CD29 KO Clone 2 (Fig. 13B).

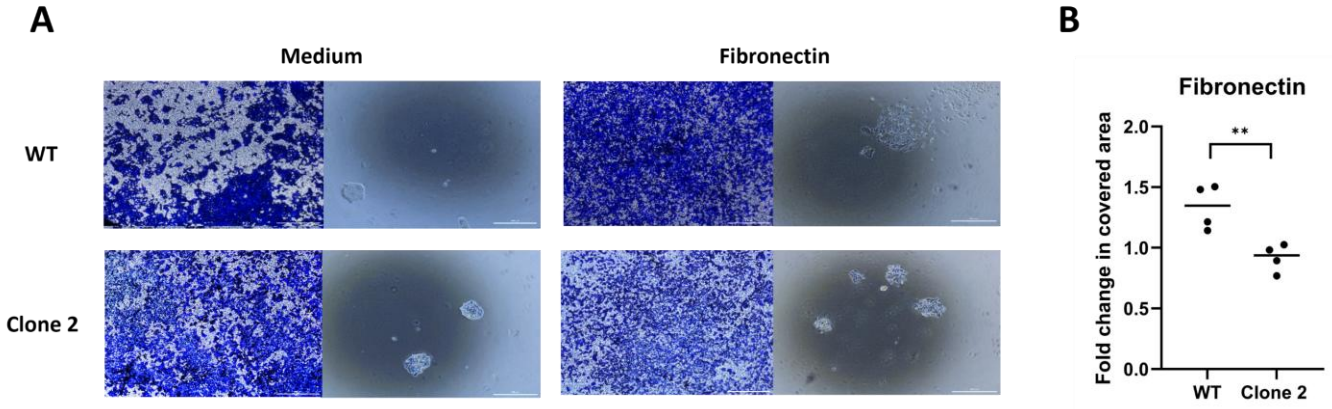

Fig. 13: CD29 KO abrogates invasion capacity upon fibronectin stimulation

(A) On the left, microscopic images show the membrane on the other side of the Boyden chamber. On the right, images show of the cells settled on the ground of the well. **(B)** Fold change in covered area. Scale bar is 500 µm in A. Horizontal lines in dot plots represent the mean. ** $p < 0.01$. These experiments were conducted and analyzed by C. Orschel.

4.1.6. CD29 deletion decreases ANG-2 stimulated migration

As ANG-2 is another important ligand to CD29 (90), we wanted to clarify how the CD29 KO affects the behavior of the tumor cells under ANG-2 stimulation (500 ng/ml) in comparison to the WT. After an incubation time of 24 h, the original scratch in the WT colonized well is visibly reduced (Fig. 14A). In contrast, the CD29 KO Clones 2 and 3 still show a clearly discernible scratch after 24 h (Fig. 14A). Measurements revealed that after 24 h the WT does not show a significant reaction to ANG-2 stimulation as there is no significant difference compared to the control (Fig. 14B). After 48 h, the WT shows a significant decrease in scratch size upon ANG-2 stimulation, whereas Clone 2 and Clone 3 show no significant reduction in comparison to the control (Fig. 14C). Moreover, the area of the remaining scratch in percent under ANG-2 stimulation of the WT is significantly smaller than the area of the remaining scratch of Clone 2 and Clone 3 (Fig. 14C).

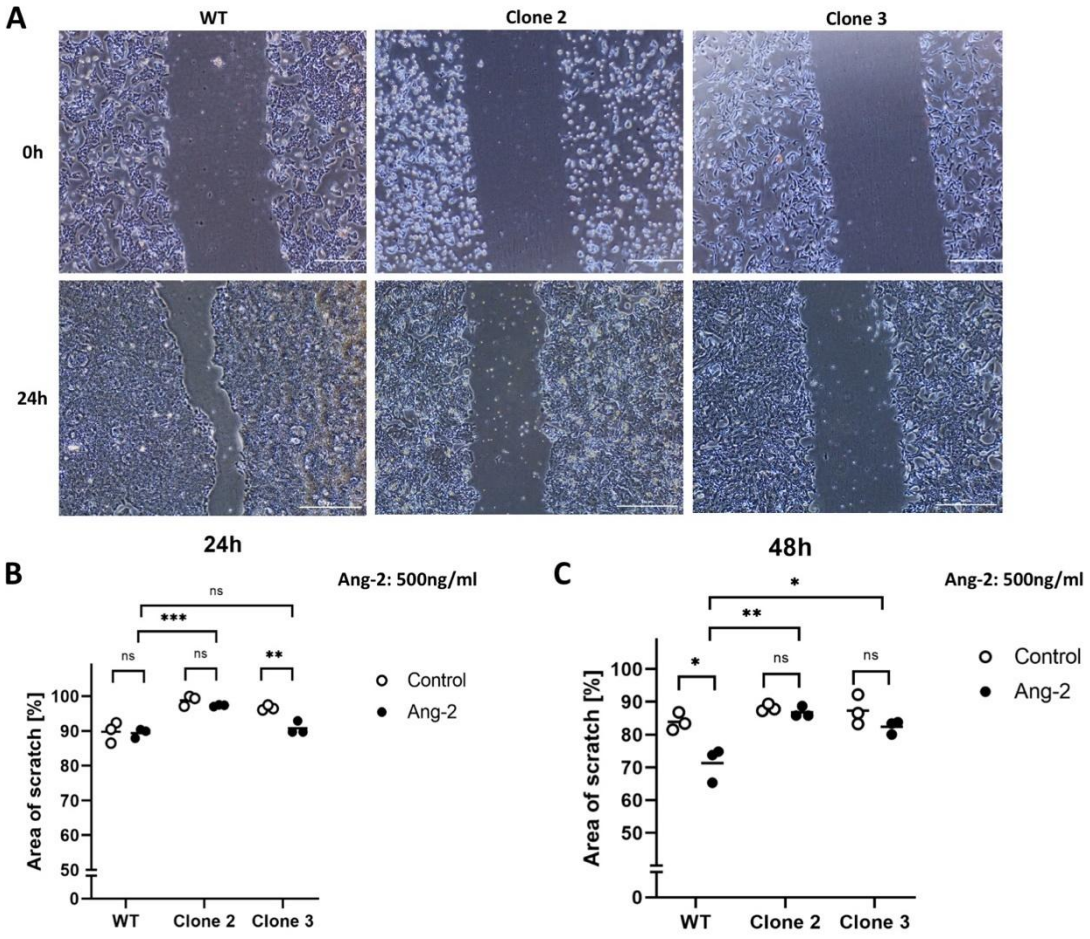

Fig. 14: CD29 KO abrogates ANG-2 stimulated migration (A) Scratch assay pictures at time point 0 h and after 24 h of the WT, Clone 2, and Clone 3 under ANG-2 stimulation. **(B)** Area of the scratch in % of WT, Clone 2, Clone 3 after 24 h of incubation under ANG-2 stimulation (500 ng/ml). **(C)** Area of the scratch in % of WT, Clone 2, Clone 3 after 48 h of incubation under ANG-2 stimulation (500 ng/ml). Horizontal lines in dot plots represent the mean. * $p < 0.05$, ** $p < 0.01$, *** $p < 0.001$. These experiments were conducted and analyzed by C. Orschel. This figure contains data that is adapted from (86).

To corroborate those results the Boyden Chamber was applied, and the underneath was supplemented with ANG-2. The photos on the left depict the cells, which have reached the other side of the porous membrane after an incubation time of 48 h (Fig.15). It is evident that the WT under ANG-2 stimulation passes through the membrane and colonizes a broader area compared to the unstimulated condition (Fig. 15A). The photos on the right depict the ground of the well and thereby portray the next step of migration. Under ANG-2 stimulation, the WT is able to form a huge colony of tumor cells on the ground of the well. Also, the CD29 KO cells migrate through the porous membrane and colonize the outer side of the membrane. However,

the medium and the ANG-2 stimulated well show no significant difference in colonization (Fig. 15A). The fold change in covered area with ANG-2 supplemented medium of Clone 2 is significantly decreased towards the WT (Fig. 15B) (86).

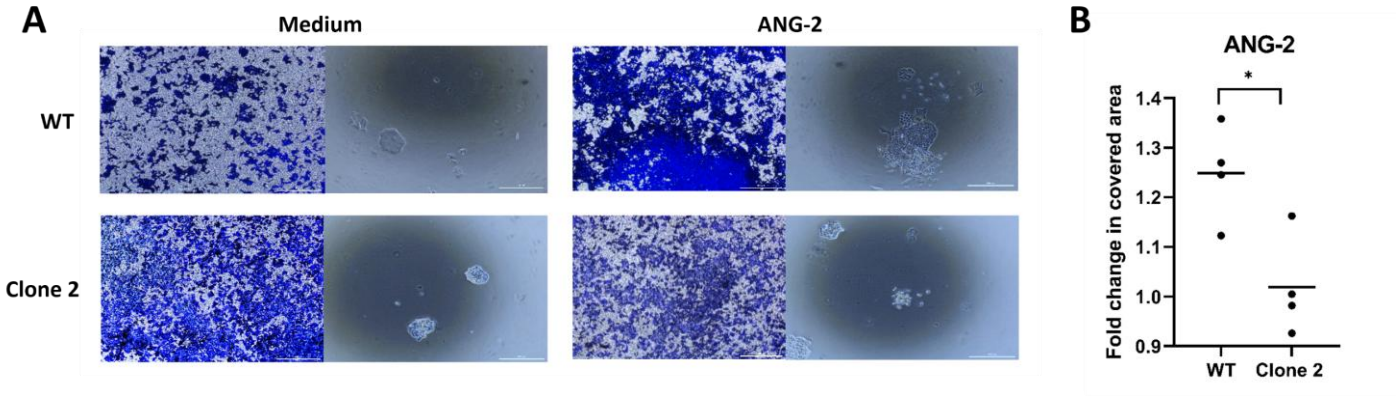

Fig. 15: CD29 KO shows no increased invasion upon ANG-2 stimulation (A) Photos of the Boyden Chamber membrane colonized with WT and Clone 2 after 48 h of incubation with medium and medium supplemented with ANG-2. **(B)** Fold change in coverage of the outer Boyden chamber membrane under ANG-2 stimulation. Scale bar is 500 µm in A. Horizontal lines represent mean. *$p < 0.05$. In this figure, the same images for the Clone 2 medium condition as in Fig. 11 are applied, as they represent the control condition in an experiment testing fibronectin and ANG-2 as chemoattractants in the Boyden chamber. These experiments were conducted and analyzed by C. Orschel. This figure contains data that is adapted from (86).

4.1.7. CD29/ANG-2 signaling activates FAK/SRC cascade

To exclude possible effects due to proliferation, we compared the proliferation rate of the WT to Clone 2 and 3. Up to 48 h, no significant differences in proliferation were observed comparing WT and clones. However, after 72 h, Clone 2 showed elevated cell proliferation compared to WT and Clone 3 (Fig. 16A). Next, we wanted to check whether ANG-2 or fibronectin have effects on the proliferation rate. ANG-2 and fibronectin stimulated WT tumor cells show no increased proliferation rate in comparison to untreated cells (Fig. 16B). Then, we analyzed intracellular signaling proteins, known to be involved in migration (91), namely the focal adhesion kinase (FAK) and the non-receptor tyrosine kinase SRC (short for Sarcoma). Indeed, after 20 min of ANG-2 stimulation there was an upregulation of phosphorylated SRC and FAK (Fig. 16C) (86).

4.1.8. CD29/ANG-2 signaling causes an upregulation of ADAM9

To examine how ANG-2 and fibronectin affect migration set genes, initially cells of the WT were seeded and stimulated with the respective agent (Fig. 16D). RNA was isolated and analyzed by RNA-Seq. Both fibronectin and ANG-2 showed similar migration gene expression profiles, marked by an upregulation of ADAM9 in comparison to the untreated WT (Fig. 16E) (86).

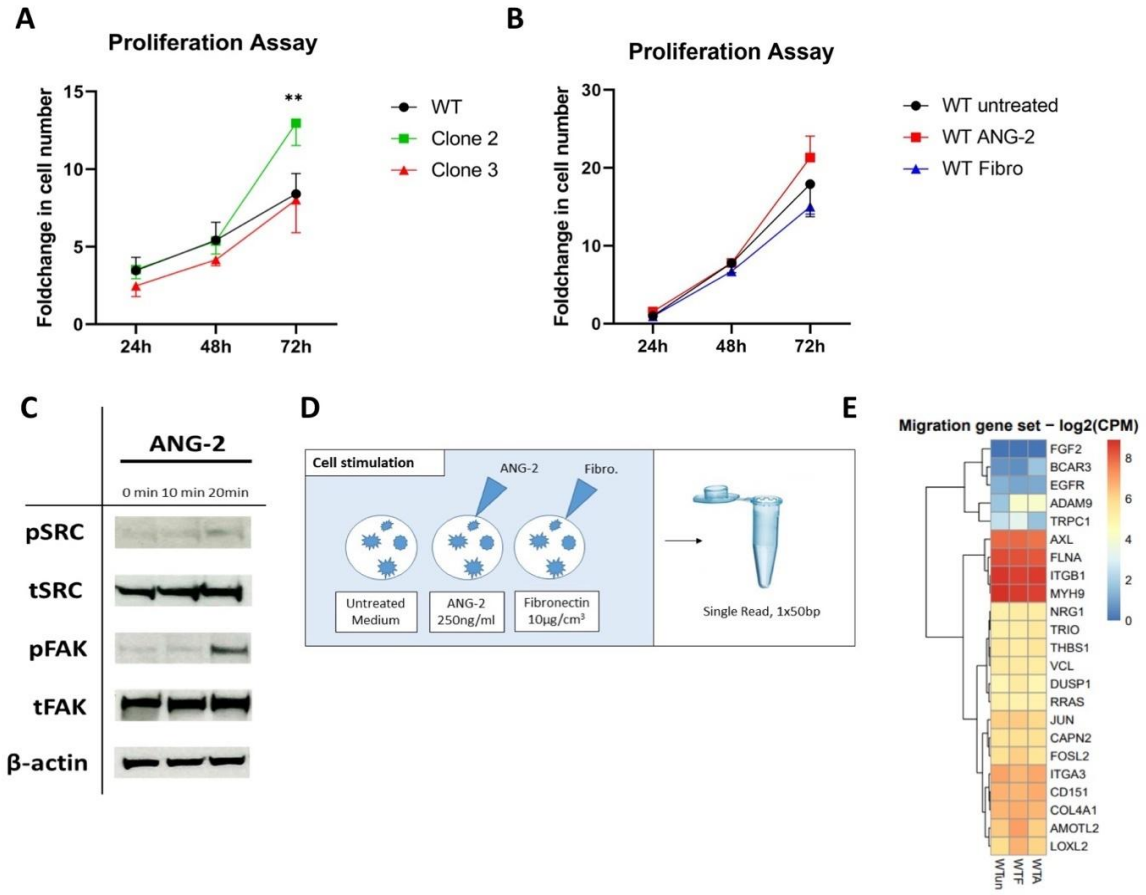

Fig. 16: ANG-2 stimulation activates the FAK/SRC signaling cascade and upregulates ADAM9 (A) Proliferation assay of WT, Clone 2, and 3 over 72 h measured by fold change in cell number. **(B)** Proliferation assay of WT untreated, stimulated by ANG-2 and by fibronectin measured by fold change in cell number. **(C)** Western blot of the FAK/SRC signaling cascade in WT after 10 min and 20 min of ANG-2 stimulation. **(D)** Experimental setup of RNA isolation of untreated WT and WT treated with ANG-2 or fibronectin. Created with Microsoft PowerPoint. **(E)** Expression of migration genes of the untreated WT and WT stimulated with ANG-2 or fibronectin. Line graphs represent the mean ± SD. ** $p < 0.01$. CMP – counts per million. These experiments were conducted and analyzed by L. Meder and C. Orschel. Western blot in C was provided by M. Koker. RNA sequencing analysis was provided by J. Brägelmann. This figure contains data that is adapted from (86).

4.1.9. CD29 KO clones can form subcutaneous and orthotopic lesions in NSG mice

After testing the CD29 KO clones behavior in an *in vitro* setting, we wanted to examine their characteristics *in vivo*. Initially, we chose immune-compromised NOD scid gamma (NSG) mice, where tumor cells (WT & CD29 KO clones) were brought in by sc. and orthotopic injection into the lung (Fig. 17, Fig.16). The orthotopically injected mice were then monitored regarding tumor initiation and progression by *in vivo* microCT. After injection, Clone 2 showed the fastest tumor growth with progressed disease on day 5 post injection (Fig. 17B). Clone 6 displayed a slow growing phenotype with CT visible tumor on day 54 (Fig. 17B). All clones formed metastases in the ribcage (Fig. 17B).

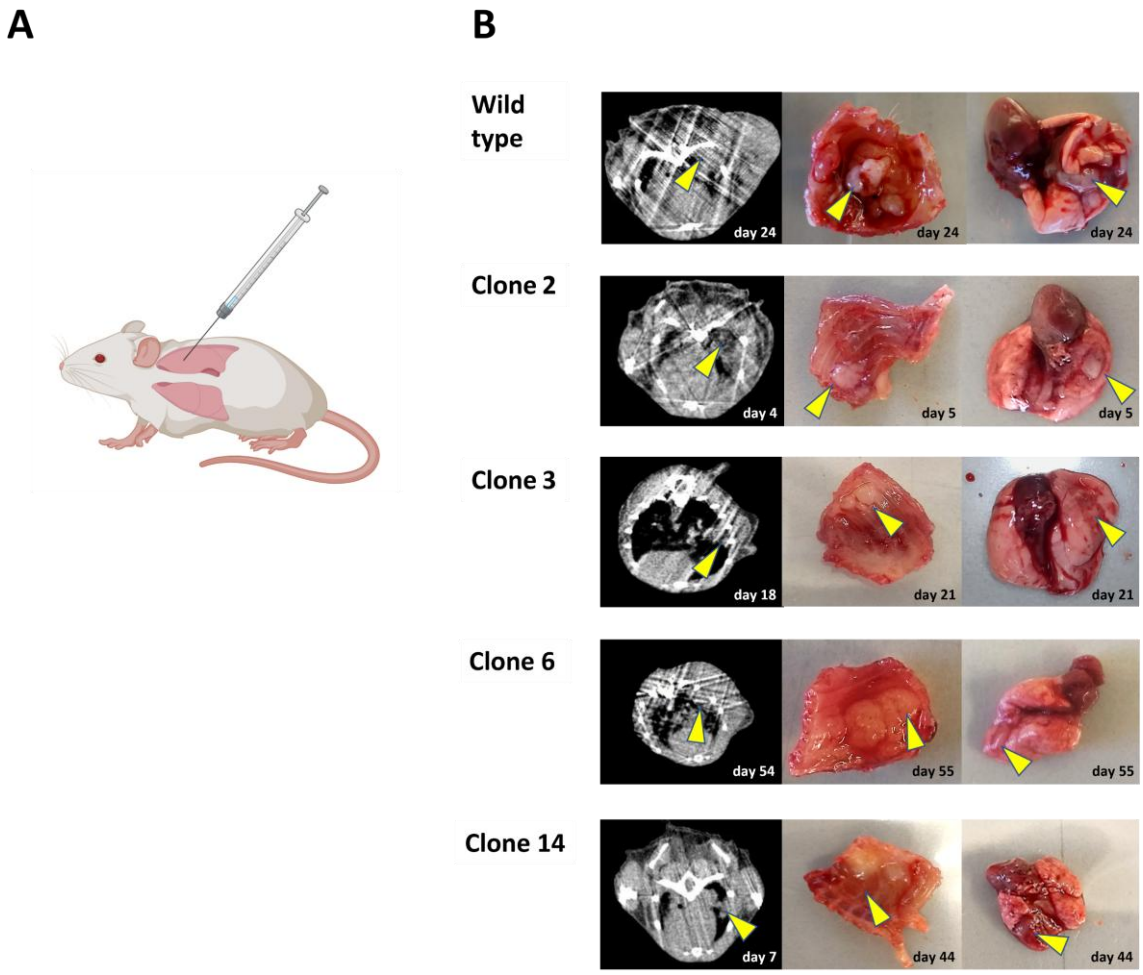

Fig. 17: CD29 KO clones form lung tumors after orthotopic injection (A) Schematic representation of orthotopic injection of NSG mouse. Created with BioRender.com. **(B)** CT lung images and macroscopic images of lung and ribcage of orthotopically injected mice. WT and CD29 KO clones (2, 3, 6, 14) with different time interval until tumor outgrowth. The experimental procedures and animal care were conducted by C. Orschel. This figure contains data that is adapted from (86).

4.1.10. CD29 KO abrogates metastasis formation in vivo

To confirm the presence of the macroscopic lung tumors of WT and the CD29 KO clones after orthotopic injection, we analyzed harvested tissues by immunohistochemistry (IHC) (Fig. 18). The stains show that the WT and all CD29 KO clones were able to form tumors positive for the neuroendocrine marker CD56 (N-CAM). The respective matched liver tissue is portrayed underneath and was analyzed for metastasis formation. While the WT forms tumor cell nests in the liver (Fig. 18A), none of the clones were able to form liver metastases (Fig 18B) (86). The staining with CD45 highlights the immune desert in the tumor tissue (Fig. 18).

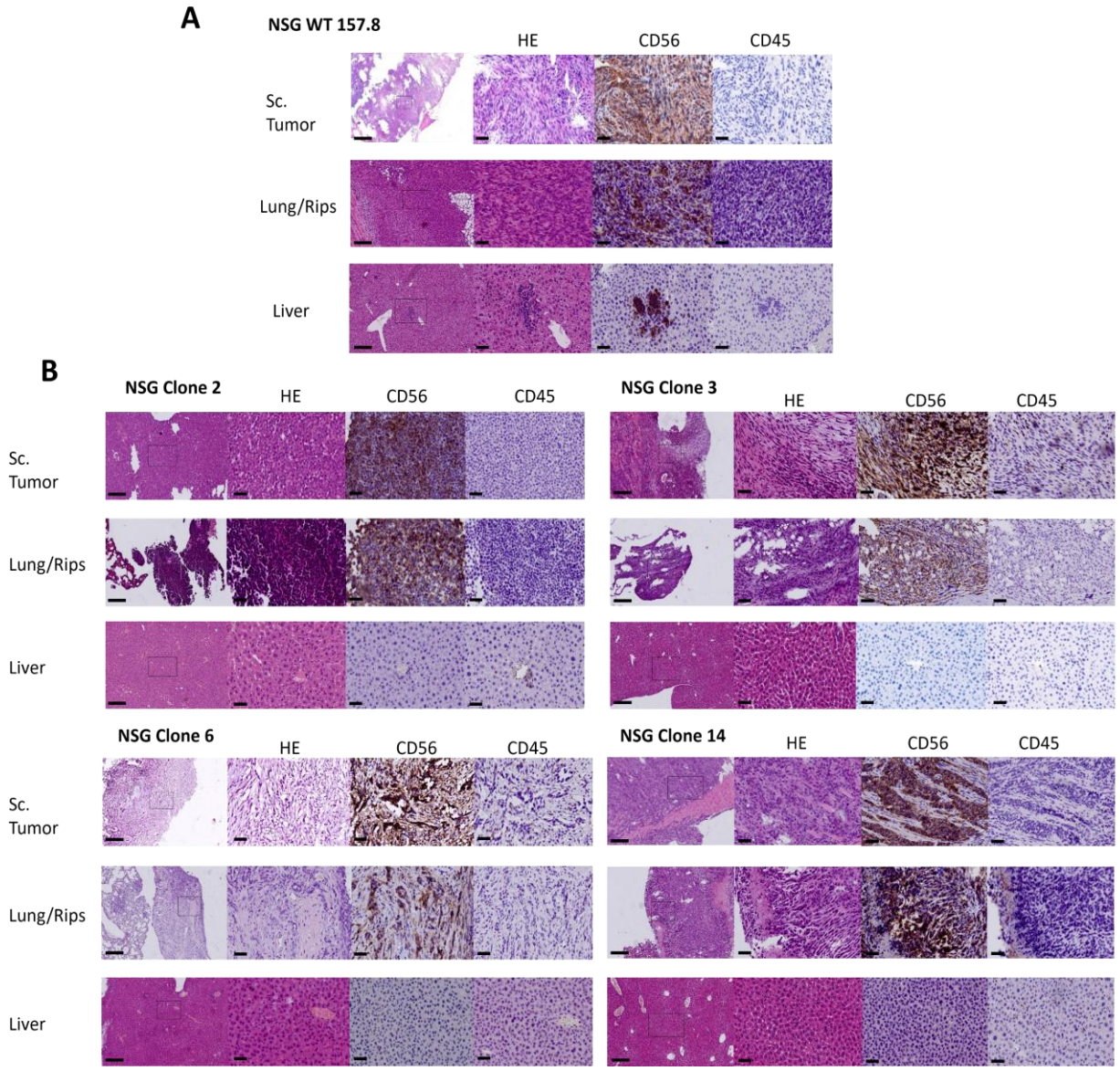

Fig. 18: CD29 KO clones show no liver metastasis formation in contrast to the WT cell line (A) IHC of FFPE tissue samples from subcutaneously and orthotopically WT-injected mice, stained with HE, CD56 (N-CAM) and CD45. Tissue samples originate from subcutaneous tumor (sc. injection), lung and matching liver tissues (orthotopic injection). **(B)** Histology samples of subcutaneously injected CD29 KO clones (2,3,6,14), followed by orthotopic injection induced CD29 KO lung tumors with matching liver samples stained with HE, CD56 (N-CAM) and CD45. Scale bar is 250 µm in overview and 50 µm in the following images in A, B. The experimental procedures and animal care were conducted by C. Orschel. IHC staining was done by A. Florin. This figure contains data that is adapted from (86).

4.1.11. Pleural infiltration of CD29 KO clones is decreased

NSG mice harbor an immunocompromised phenotype (92). However, they still have neutrophils and monocytes. DCs and macrophages are also present in their immune cell compartment, though with limited activation potential (92). After orthotopic injection of WT and CD29 KO clones we observed the infiltration in the rib cage (see 4.1.9) and the formation of pleural effusions. After centrifugation of the pleural effusion formed by the WT SCLC tumor cells, a large cell pellet was visible (Fig. 19A). When taken into culture, one can see a major difference in morphology towards the original cells (Fig. 19A). The pleural tumor cells tendentially showed a higher proliferation rate (Fig. 19B). Also the CD29 KO clones formed pleural effusions. However, the calculated tumor/immune cell ratio in pleural effusion was significantly decreased in comparison to the WT. Examining the immune cells in the pleural effusion, we found the dendritic cells (DCs) in the CD29 KO condition to be decreased (Fig. 19D). Additionally, the dendritic cells in the pleural effusion of the CDKO mice showed a lower expression of the activation marker CD80 (Fig. 19E). In summary, the CD29 KO clones infiltrate the pleura to a lesser extent compared to the WT (Fig. 19).

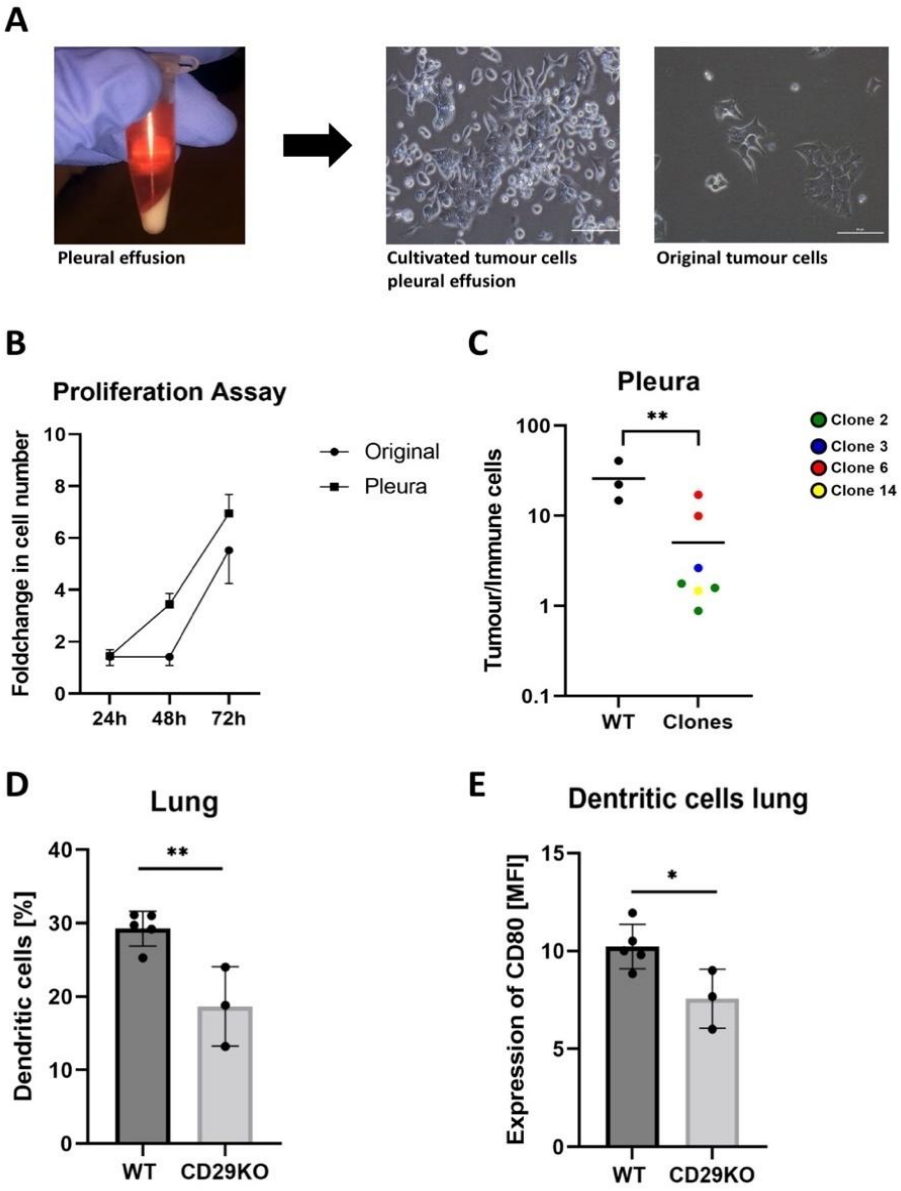

Fig. 19: Lower CD29 KO tumor cell infiltration in the pleura (A) Macroscopic image of pleural effusion after centrifugation. Microscopic image of tumor cells from pleural effusion taken into culture in comparison to the original injected tumor cell line. **(B)** Proliferation assay of cultivated pleura tumor cells and the original injected cell lines. **(C)** Tumor/Immune cell ratio in the pleural effusion of WT and CD29 KO-injected mice. **(D)** Percentage of dendritic cells in the lung of WT and CD29 KO. **(E)** Expression of the dendritic cell activation marker CD80 (MFI) on DCs in the lung. Scale bar is 100 µm in A. Line graphs represent and the bar graphs represent mean ± SD. Horizontal lines in dot plots represent the mean. * $p < 0.05$, ** $p < 0.01$. These experiments were conducted and analyzed by C. Orschel.

4.1.12. CD29 KO abrogates the process of intravasation and extravasation

In a next step, we aimed to investigate whether an intact immune system may affect liver metastasis potential of SCLC WT and CD29 KO.

For comparison, in the immune-compromised NSG mice orthotopically injected WT SCLC cells produced a tumor in 100% of cases (6/6) and formed liver metastasis in 83.3% of cases (5/6) (Table 12). The CD29 KO also develops a lung tumor to 100% (10/10) cases but instead forms no liver metastasis (0/10) (Table 12, Fig. 20A) (86).

Now, in the immunocompetent setting the WT did form a lung tumor and liver metastasis in 71.4 % of cases (5/7), respectively when orthotopically injected in BL6 mice (Table 13). Also, the CD29 KO was able to form a lung tumor in the presence of an intact immune system in 66.7% (2/3), but as in the immune-compromised mouse, did not develop liver tumors (0/3) (Table 13). Injected intravenously into BL6, the WT developed lung (3/3) and liver tumors (3/3) in 100% of cases. In contrast, CD29 KO cells failed to establish tumors at any site following intravenous injection (0/4) (Table 13, Fig. 20B) (86).

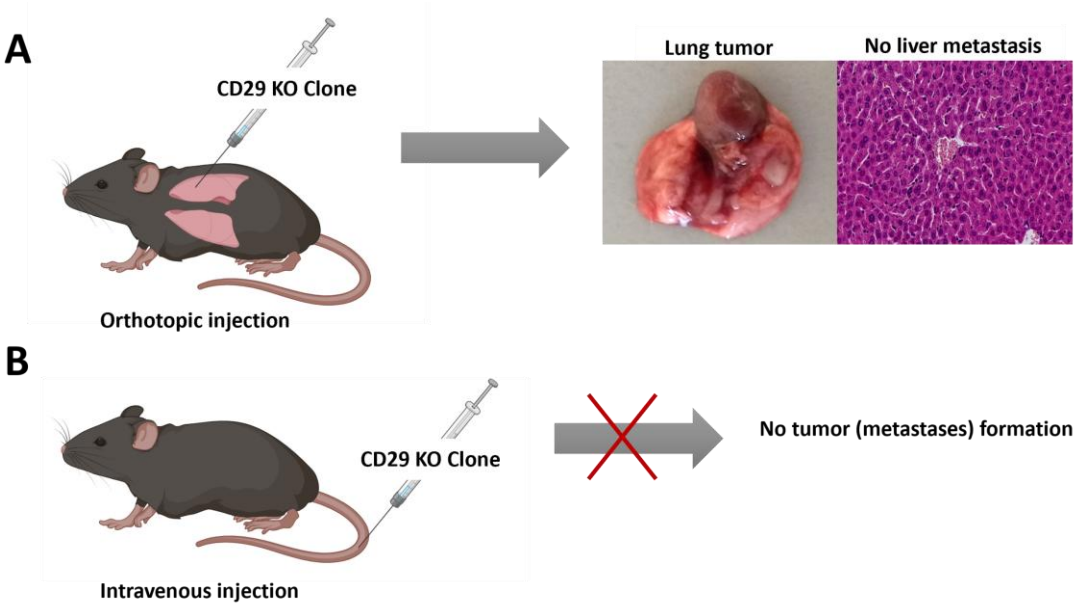

Fig. 20: CD29 KO clones lose their capacity to intra- and extravasate (A) Orthotopic injection of CD29 KO in BL6 mice. Macroscopic image of CD29 KO lung tumor. HE staining of respective liver tissue with no detectable metastases. Created with BioRender.com. **(B)** Intravenous injection of CD29 KO in BL6 mice with no detectable tumor formation in the lung and liver. Created with BioRender.com. The experimental procedures and animal care were conducted by C. Orschel. This figure contains data that is adapted from (86).

Table 12: Tumor formation of WT and CD29 KO after orthotopic injection in immune deficient setting. This table contains data that is adapted from (86).

NSG				
	WT		ITGB1 KO	
	Lung	Liver	Lung	Liver
Orthotopic	6/6	5/6	10/10	0/10

Table 13: Tumor formation of WT and CD29 KO with different injection methods in immunocompetent setting. This table contains data that is adapted from (86).

BL6				
	WT		ITGB1 KO	
	Lung	Liver	Lung	Liver
Orthotopic	5/7	5/7	2/3	0/3
Intravenous	3/3	3/3	0/4	0/4

4.2. Effects of MHC-I loss

4.2.1. Downregulation of MHC-I and activation of ERBB2 in SCLC liver metastases

In the initial screen of matched SCLC patient samples of lung and liver (n=6), a downregulation of MHC-I in the respective liver metastases could be observed (Fig. 21A) (*under revision in Nature Communications since 15th January 2025 under review again since 4th August 2025)*. The same pattern was observed in the murine setting comparing matched SCLC lung tumors and liver metastases by flow cytometry (Fig. 22A).

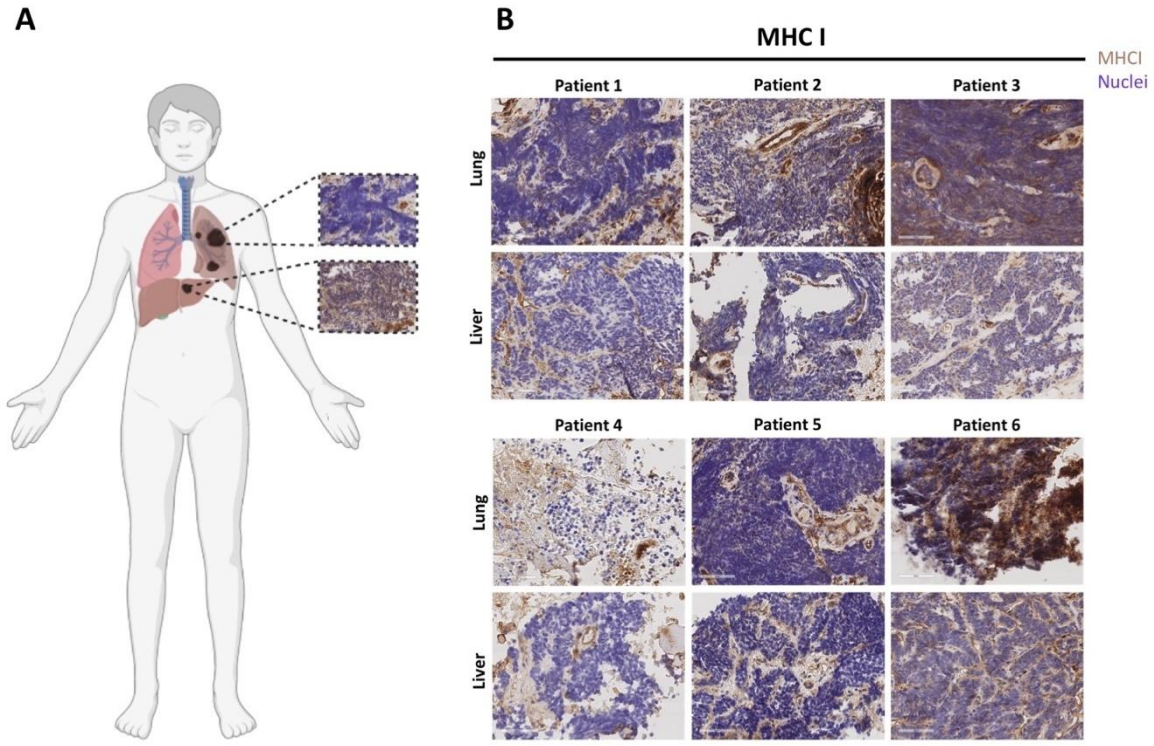

Fig. 21: Loss of MHC-I expression in matched patient liver metastases (A) Matched patient samples of the lung and the respective liver metastases (*n*=6). Created with BioRender.com. **(B)** Histological staining of MHC-I of matched lung and liver samples. Collection of patient samples was done in cooperation with Institute of Pathology, University Hospital Cologne, Germany performed by M.L. Eich. This figure contains unpublished data that is adapted from *under revision in Nature Communications since 15th January 2025, under review again since 4th August 2025*.

As there is evidence, that potentially targetable receptor tyrosine kinases (RTKs) are involved in MHC-I regulatory mechanisms (93), we performed an RTK array comparing tumor cells of murine SCLC lung tissue and liver metastases. The array revealed that the phosphorylation of

ERBB2 was increased in liver metastases (Fig. 22B, C) (*under revision in Nature Communications since 15th January 2025 under review again since 4th August 2025)*. ERBB2 also influences downstream signaling pathways (Fig. 3, Fig. 22D). The cell lines 157.8 and 240.5 were tested with different concentrations of the ERBB2 blocker mubritinib (100 nM, 1 µM). With time, in both cell lines mubritinib (1 µM) led to an upregulation of pTBK and a downregulation of pAKT (Fig. 22D) (*under revision in Nature Communications since 15th January 2025 under review again since 4th August 2025)*.

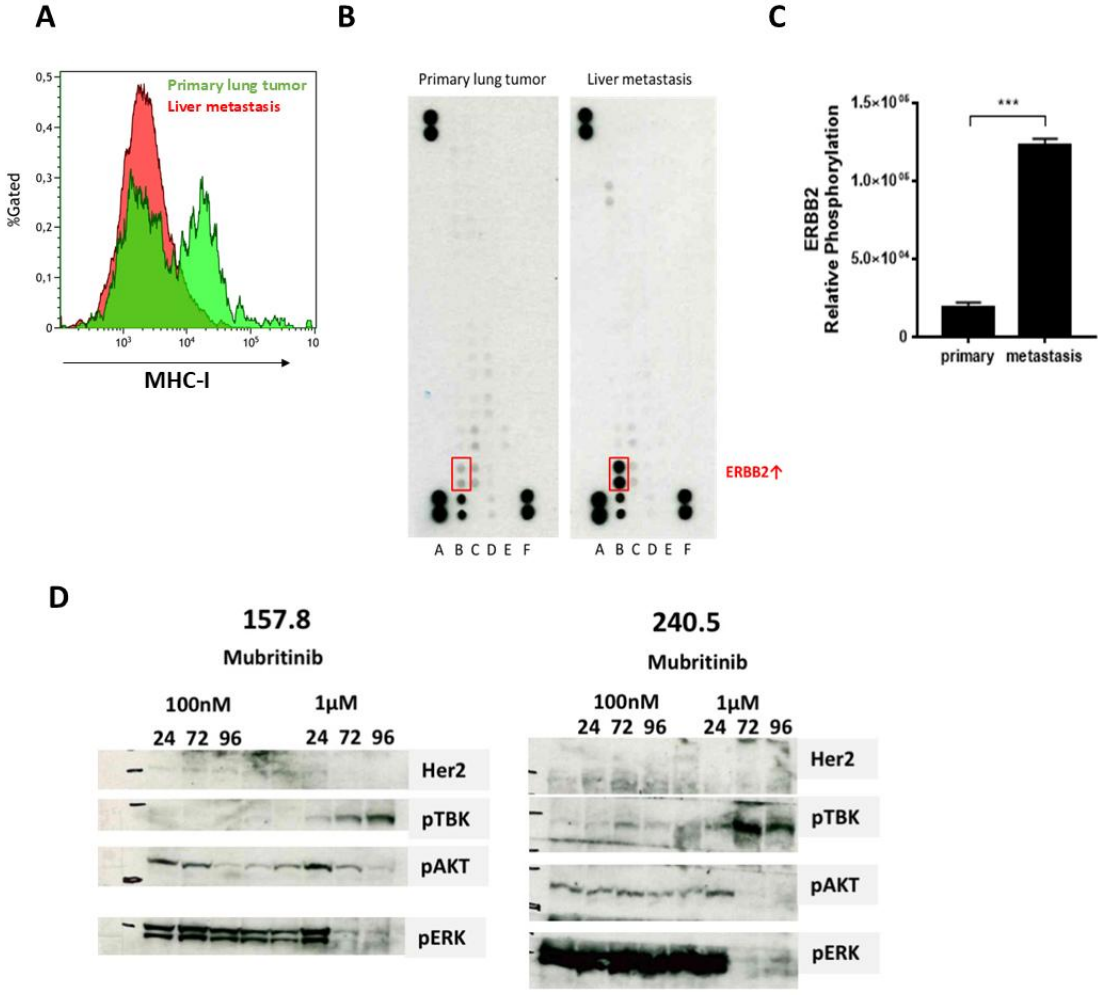

Fig. 22: Increased ERBB2 activity in SCLC liver metastasis (A) MHC-I expression in primary lung tumor and matched liver metastasis measured by FACS. **(B)** RTK array of ERBB2 expression in primary lung tumor and liver metastasis. **(C)** Relative ERBB2 phosphorylation in primary tumor and metastasis. **(D)** Western blots of ERBB2 downstream cascade under 100 nM and 1 µM mubritinib treatment of liver metastasis cell line 158.8 and primary tumor cell line 240.5 after 24 h, 72 h, and 96 h. Bar graphs represent mean ± s.e.m. *** $p < 0.001$. Western blots in D were provided by M. Koker. The analysis was conducted by L. Meder (B, C) and C. Orschel (A). This figure contains unpublished data that is adapted from *under revision in Nature Communications since 15th January 2025 under review again since 4th August 2025*.

4.2.2. CRISPR-Cas B2M KO generation

We used an in suspension growing SCLC cell line, 100.H7, derived from a primary lung tumor and performed a B2M CRISPR-Cas9 KO to analyze the consequences of a MHC-I loss *in vivo*. The original cell line showed an upregulation of MHC-I expression upon extensive IFNγ stimulation (40 ng/ml). Simultaneously, there was an upregulation of PD-L1, used as a control (Fig. 23). The CRISPR B2M KO did not show MHC-I expression upon IFNγ stimulation (40 ng/ml), but an increased expression of the control PD-L1 (*under revision in Nature Communications since 15th January 2025 under review again since 4th August 2025)*. Therefore, the generated B2M KO clones are hereinafter referred to as MHC-I KO.

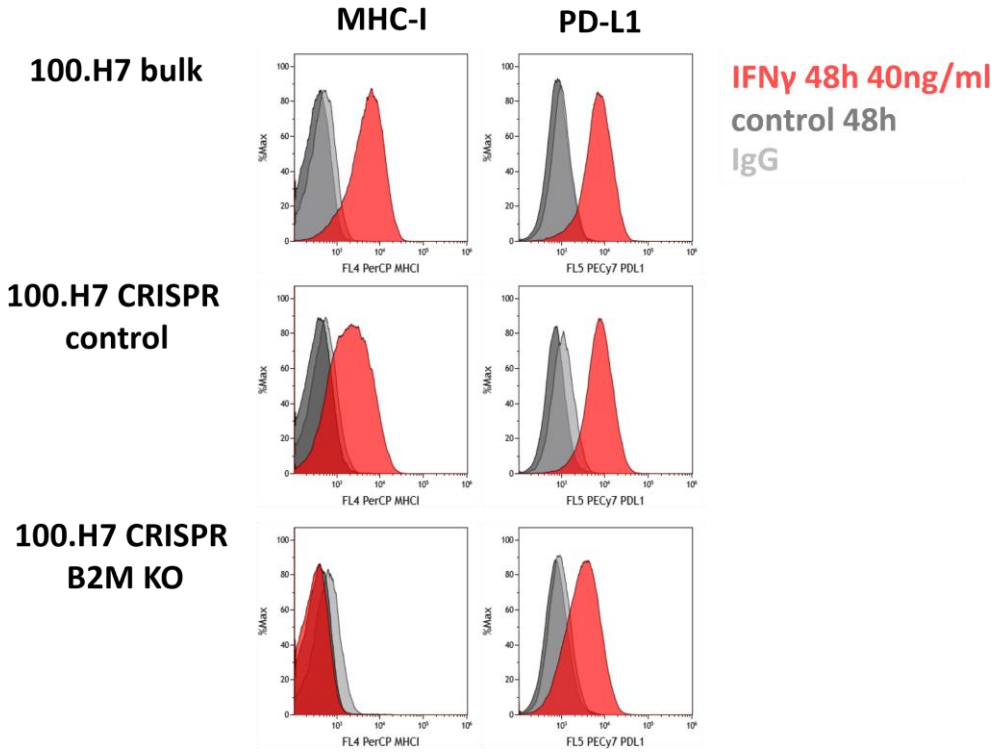

Fig. 23: CRISPR KO of B2M leads to a loss of MHC-I expression FACS readout of the original 100.H7 cell line and the CRISPR B2M KO concerning the expression of MHC-I and the expression of PD-L1 as a control. The analysis was conducted by L. Meder and C. Orschel. This figure contains unpublished data that is adapted from *under revision in Nature Communications since 15th January 2025 under review again since 4th August 2025*.

4.2.3. IFNγ stimulation leads to MHC-II expression of the MHC-I KO

To further characterize the B2M KO SCLC cells, we checked MHC-II, ERBB2, and AXL expression. MHC-II is of particular interest, as growing evidence shows, that MHC-II expression on tumors was associated with improved survival and increased response to immunotherapy (94). This suggests that MHC-II plays a role in cancer antigen presentation, besides its physiological functions on antigen-presenting cells (94). ERBB2 and AXL are interesting markers as we see both phosphorylated in the RTK array.

Stimulating the WT with IFNγ (40 ng/ml) for 24 h led to an upregulation of MHC-I (Fig. 24A) and MHC-II (Fig. 24B). As expected, the MHC-I KO did not exhibit MHC-I expression under IFNγ stimulation (Fig. 24E). However, there was still an upregulation of MHC-II (Fig. 24F). Testing several markers, we found that the original WT cell line also demonstrated an upregulation of the receptor tyrosine kinase AXL upon IFNγ stimulation (Fig. 24C). The AXL expression of the MHC-I KO did not increase after IFNγ stimulation (Fig. 24G). Both the WT and the MHC-I KO displayed no significant differences in ERBB2 expression upon IFNγ stimulation (Fig. 24D, 24H).

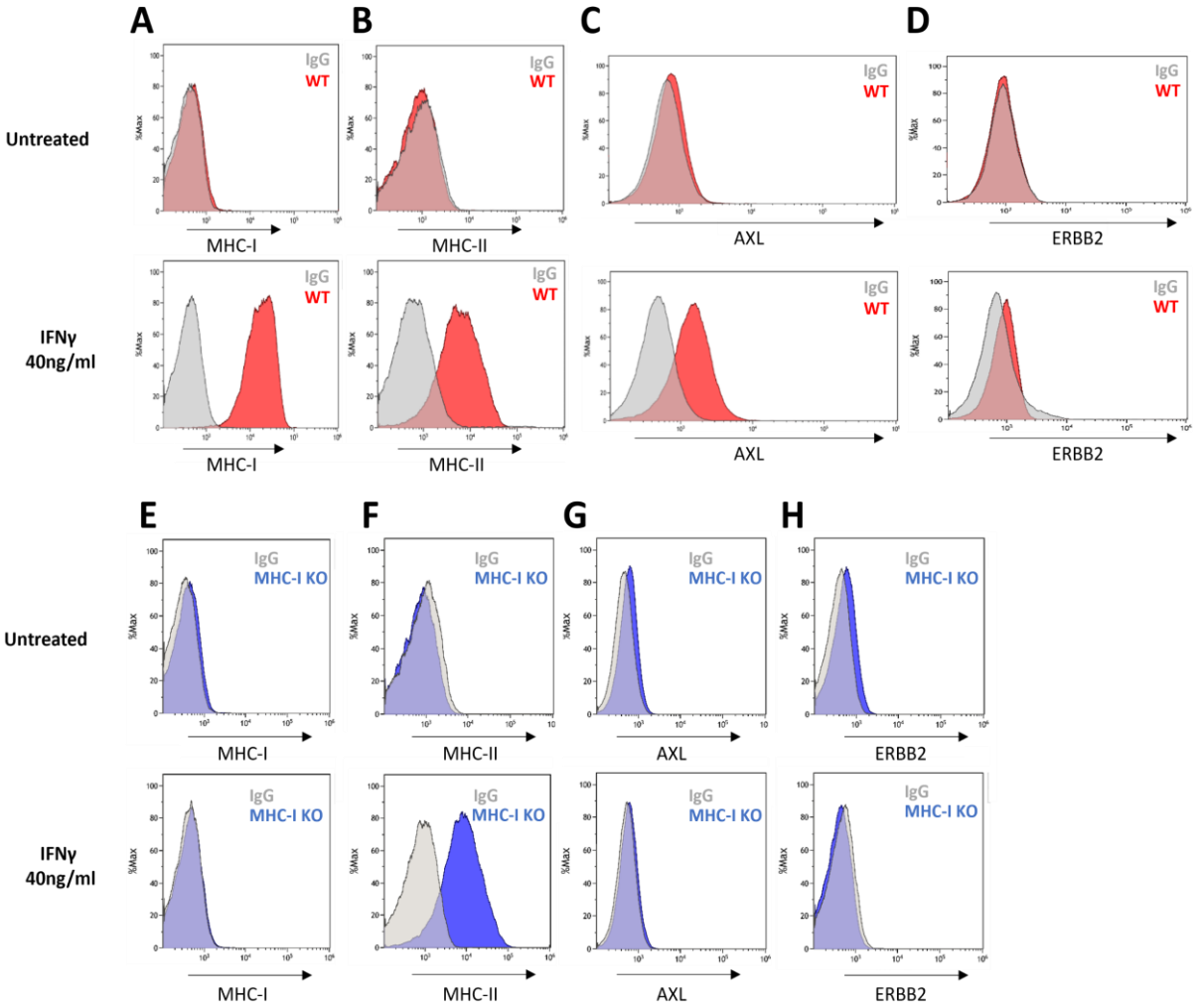

Fig. 24: MHC-I KO upregulates MHC-II under IFNγ stimulation FACS Readout of WT cell line in untreated and IFNγ (40 ng/ml, 24 h) stimulated condition: **(A)** MHC-I, **(B)** MHC-II, (**C)** AXL, **(D)** ERBB2. FACS Readout of MHC-I KO cell line in untreated and IFNγ (40 ng/ml, 24 h) stimulated condition: **(E)** MHC-I, **(F)** MHC-II, **(G)** AXL, **(H)** ERBB2.These experiments were conducted and analyzed by C. Orschel.

4.2.4. MHC-I KO displays an aggressive fast-growing phenotype

To check on the *in vivo* behavior of SCLC cells with depleted MHC-I, the MHC-I KO was injected intravenously into BL6 mice, which have an immunocompetent background. After approximately 30 days the MHC-I KO-injected mice suffered from liver lesions comprising multiple nodules. In contrast, after 76 days, the WT injected mice showed only small, single lesions (Fig. 25A) (*under revision in Nature Communications since 15th January 2025 under review again since 4th August 2025)*.

4.2.5. MHC-I KO liver metastases contain a significantly higher number of granulocytes and macrophages

Analyzing the harvested tumor tissue from the liver revealed that the MHC-I KO tumor cells showed a higher expression of the “don’t eat me”-signal CD47 (Fig. 25B). Via the CD47/SIRPa pathway, CD47 attenuates the anti-tumor reaction of the innate immune system, especially of the macrophages (95). Beside the higher presentation of CD47 on the MHC-I KO tumor cells, a significantly higher infiltration of granulocytes could be found (Fig. 25C). Additionally, there was a tendency towards an increased percentage of macrophages (Fig. 25D). On the other hand, the NK-cells were significantly diminished in the MHC-I KO tumors in comparison to the WT tumors (Fig. 25E). Furthermore, the marker of NK cell functional activity CD107a was decreased in MHC-I KO tumors (Fig. 25F). Regarding the specific immune response, there was a tendency toward a higher CD4 T cell ratio in the WT (Fig. 25G). The relative number of $CD8^+$ T cells showed no significant differences (Fig. 25H). However, there is a trend toward more activated $CD8^+$ T cells in the WT (Fig. 25I).

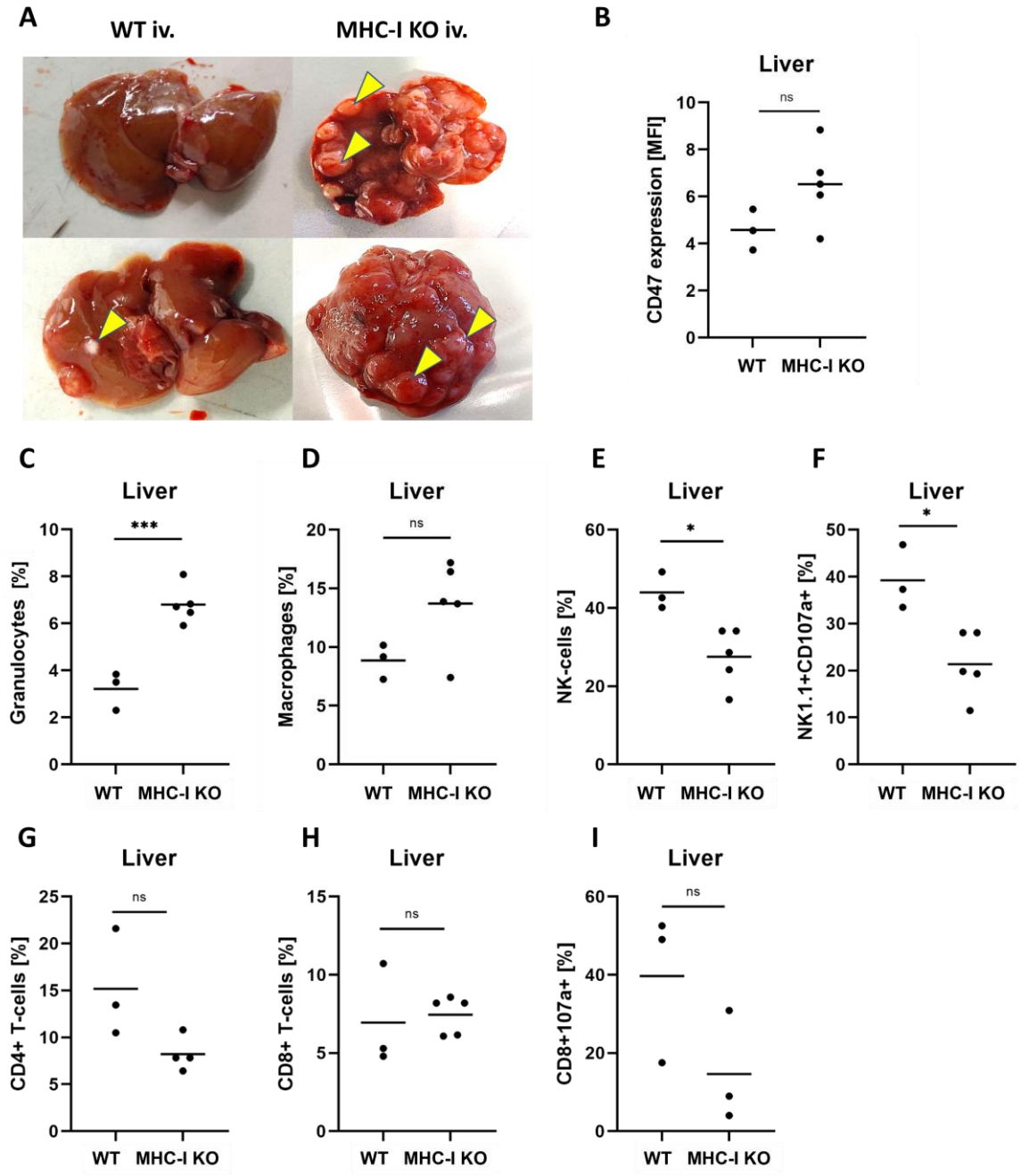

Fig. 25: MHC-I KO liver metastases show a decreased specific immune cell infiltration (A) Representative image of the liver of WT and MHC-I KO intravenously injected mice. **(B-I)** Percentage of immune cell subsets detected by FACS analysis of liver tumor samples. The horizontal lines in dot plots indicate the mean value. * $p < 0.05$, *** $p < 0.001$. The experimental procedures, animal care and analysis were conducted by C. Orschel. This figure contains unpublished data that is adapted from *under revision in Nature Communications since 15th January 2025 under review again since 4th August 2025*.

4.2.6. Decreased T cell infiltration in MHC-I KO pleural effusion

In order to investigate the effect of MHC-I loss also in the context of the lung immune microenvironment, we orthotopically injected WT and MHC-I KO tumor cells. The BL6 mice formed lung tumors with pleural effusion in both cases. FACS analysis revealed that the WT mice generally display a higher immune cell infiltration. Moreover, the WT showed a more specific immune answer with a higher percentage of $CD4^+$ (47.71%) and $CD8^+$ T cells (19.64%) (Fig. 26A). The MHC-I KO exhibited a decreased specific immune cell response with less $CD4^+$ (13.71%) and $CD8^+$ T cells (7.41%) (Fig. 26B).

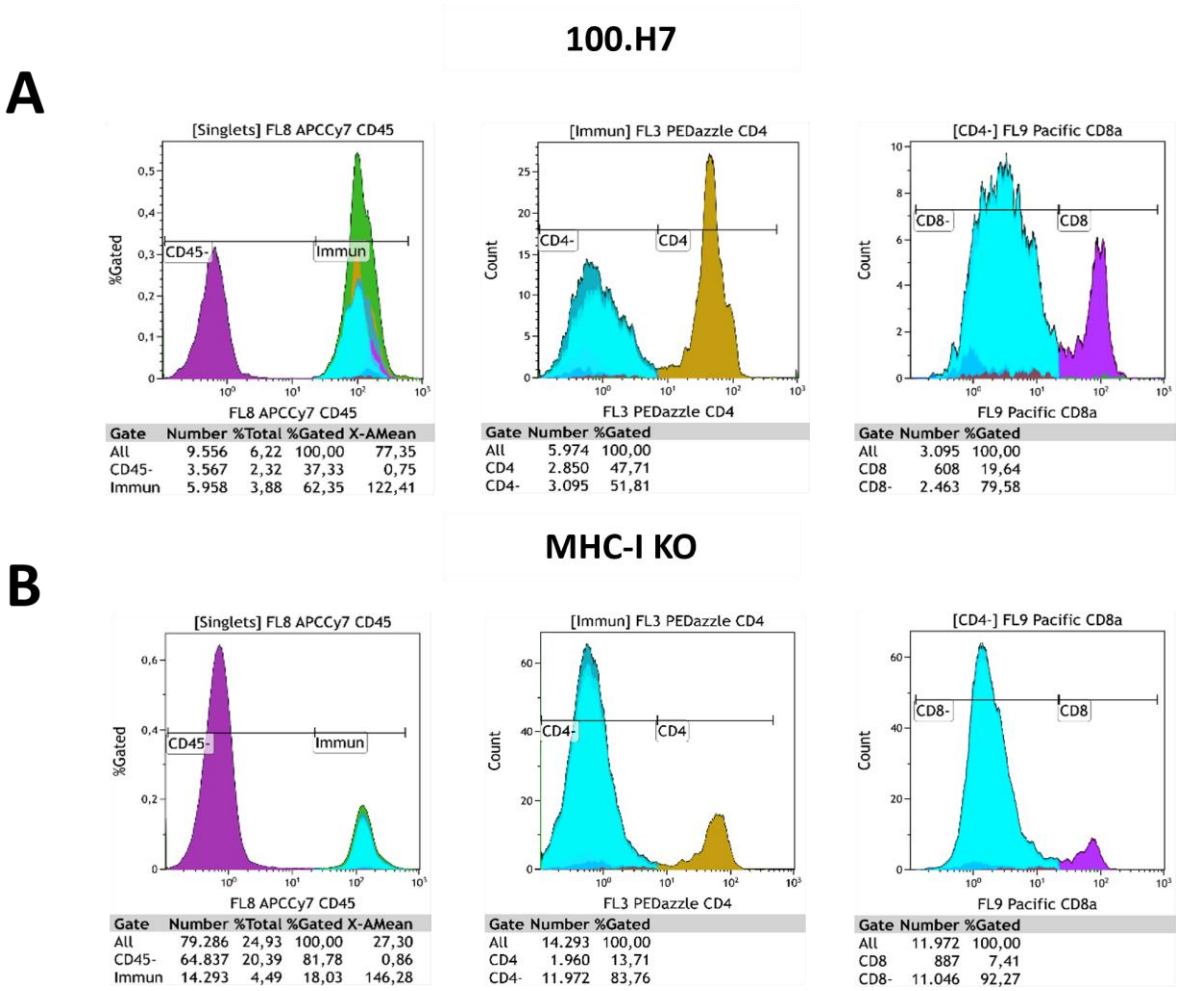

Fig. 26: Lower $CD4^+$, $CD8^+$ T cell infiltration in the pleural effusion of MHC-I KO tumors (A) FACS- Readout of pleural effusion of orthotopically injected WT tumor cells. **(B)** FACS- Readout of pleural effusion of orthotopically injected MHC-I KO tumor cells. Analysis was done by C. Orschel.

4.2.7. MHC-II upregulation in MHC-I KO lung tumors

Orthotopic injection of MHC-I KO tumor cells resulted in lung tumors of massive size. The tumors occupied the entire lung volume after approximately 3 weeks post injection (Fig. 27A). However, the matching liver tissue revealed no large liver metastasis (*under revision in Nature Communications since 15th January 2025 under review again since 4th August 2025)*. Analyzing the tumor tissue, we found no MHC-I expression, as expected (Fig. 27B). However, also in the *in vivo* setting an upregulation of MHC-II can be observed (Fig. 27C).

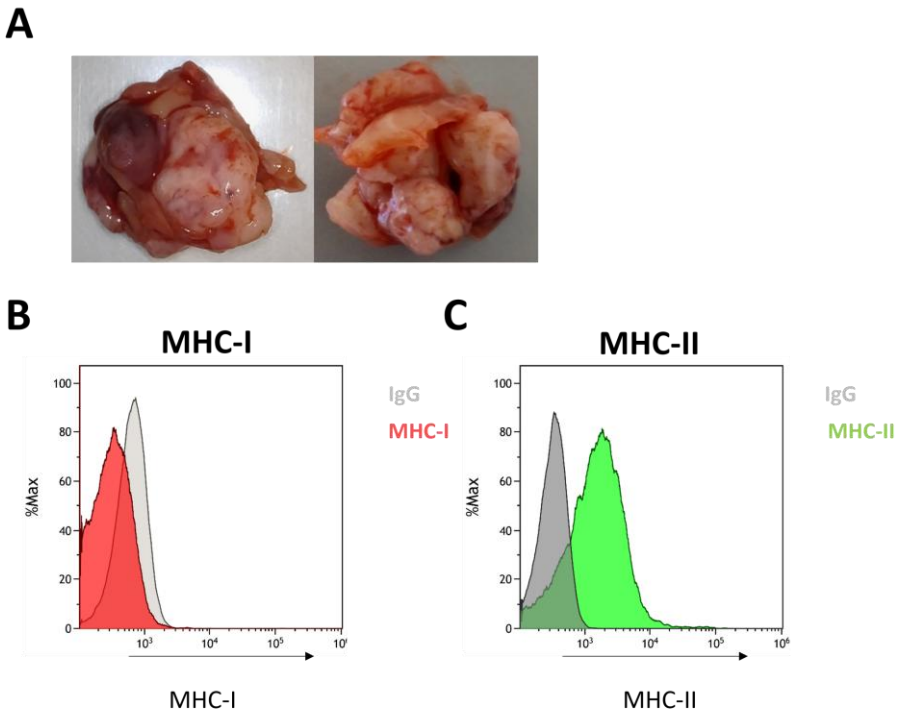

Fig. 27: MHC-II expression in MHC-I KO tumor tissue (A) Large MHC-I KO lung tumor from different perspectives. **(B)** MHC-I expression in MHC-I KO lung tumor with IgG control. **(C)** MHC-II expression in MHC-I KO lung tumor with IgG control measured by FACS. The experimental procedures, animal care and analysis were conducted by C. Orschel. This figure contains unpublished data that is adapted from *under revision in Nature Communications since 15th January 2025 under review again since 4th August 2025*.

4.3. Combined PD-1 and ERBB2 blockade prolongs overall and progression free survival in autochtonous SCLC mouse model

Having ERBB2 identified as a potential regulator of MHC-I and we next sought to investigate therapeutic efficacy of ERBB2 inhibition in combination with immune checkpoint blockade *in vivo*. In our autochthonous mouse model, we established 4 treatment cohorts: vehicle, anti–PD-1 monotherapy, ERBB2 inhibitor monotherapy and combination therapy with anti–PD-1 and ERBB2 inhibitor. We monitored tumor response and resistance using µCT and mouse adapted RECIST criteria ((96). Therapy began after the identification of at least one measurable target lesion with a diameter of ≥1 mm.

Notably, the combined blockade of PD-1 and ERBB2 resulted in significantly improving both overall survival and progression-free survival compared to either monotherapy or control (Fig. 28A, B) (under revision in Nature Communications since 15th January 2025, under review again since 4th August 2025).

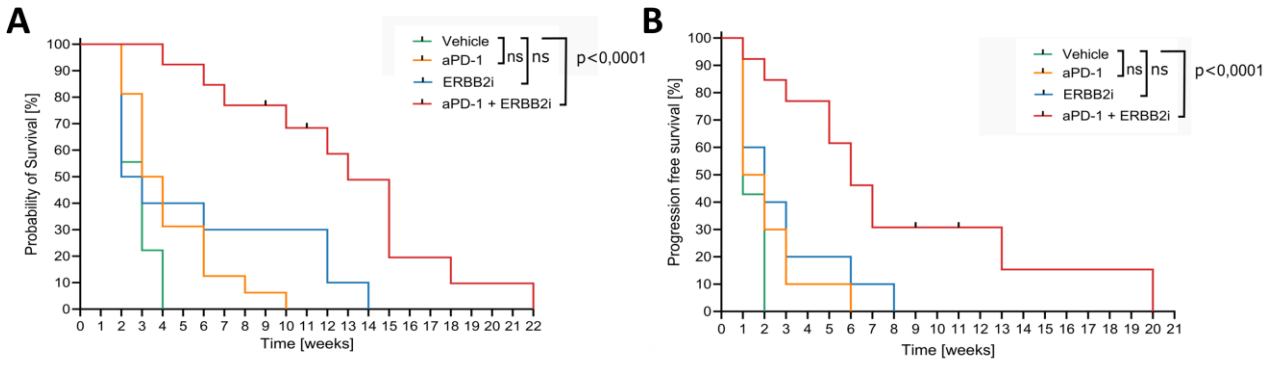

Fig. 28: ERBB2 blockade restores sensitivity to anti–PD-1 therapy and enhances treatment efficacy in autochthonous SCLC mice. (A) Kaplan–Meier curve showing overall survival. **(B)** Kaplan–Meier curve showing progression-free survival (PFS). Data represent survival across the four treatment groups: vehicle (n = 9), anti–PD-1 (n = 16), ERBB2 inhibitor (mubritinib, n = 6), and combination therapy with anti–PD-1 and ERBB2 inhibitor (mubritinib, n = 11). Statistical analysis was performed using the Mantel–Cox test, p values are indicated in the graphs. This figure contains unpublished data that is adapted from *under revision in Nature Communications since 15th January 2025 under review again since 4th August 2025*.

5. Discussion

Regarding the high metastatic potential of SCLC and its life limiting consequences, the purpose of the study was to decipher mechanisms relevant for metastasis formation in SCLC.

Our study provides evidence that CD29 is a key regulator of metastasis in SCLC. In summary, our analysis demonstrated that CD29 KO abrogates angiopoietin-2 and fibronectin stimulated migration in SCLC. Further, our study revealed that after CD29 KO tumor cells do not form liver metastasis after orthotopic injection and do not settle after intravenous injection. This finding indicates that CD29 KO clones lose the capacity to intra- and extravasate and thereby the ability to form metastasis (86).

The second part of our work focused on MHC-I loss, as a common mechanism of immune evasion in cancer. A screening of a unique cohort of matched patient samples identified MHC-I loss in the liver metastases in comparison to primary SCLC. The CRISPR-Cas9 generated B2M KO resulting in MHC-I loss showed fast-growing capacity and created a more aggressive phenotype *in vivo*. Analyzing the immune setting highlighted that the MHC-I KO escapes specific, T cell-mediated immune response. Instead, the innate immune system is activated, but obviously not potent enough to control the SCLC MHC-I KO tumor. Additionally, our findings demonstrate that ERBB2 inhibition in combination with immune checkpoint blockade, significantly prolonged survival in autochtonous SCLC model, supporting its potential to restore MHC-I presentation and warranting further evaluation.

5.1. CD29 in metastasis

5.1.1. CD29 dependent signaling in SCLC and other (solid) cancers

Initial analysis of matched human SCLC liver metastases revealed an upregulation of CD29 in comparison to the primary tumor (86). This leads to the assumption that CD29 high expressing tumor clones in the primary tumor have a selective advantage in leaving the primary site and form metastasis in the liver. Analysis of publicly available RNA-Seq data of patient SCLC tissue and of patient SCLC cell lines revealed a positive correlation of CD29 and vimentin (86). Consistent with this finding, vimentin has been established as a core marker for epithelial-mesenchymal-transition, which initiates the process of metastasis (97) and was found to be upregulated in progressed metastatic disease (98,99). In addition, our metastasis data obtained from a genetically engineered mouse model for SCLC, comparing liver metastasis vs. primary tumors, showed an overexpression of CD29 along with the progression to metastatic disease (86). Also, in the context of breast cancer CD29 plays a role in metastasis formation. Huck and colleagues demonstrated that CD29 deficient tumors display an attenuated capability to form pulmonal metastasis and a general decrease in adhesion signaling (100). In colorectal cancer the expression of CD29 was increased in liver metastasis

and correlated with the histological grading of liver metastasis (101). Similarly, in esophageal squamous cell carcinoma (ESCC), CD29 has been identified as a key driver of metastasis and therapy resistance. Its expression in ESCC tissues showed a strong association with lymph node metastasis (102). Altogether, these results suggest a relevance of CD29 in the context of EMT and for metastatic spread.

The next step was to investigate the mechanism underlying the involvement of CD29 in SCLC metastasis formation. In the scratch assay the CD29-high expressing cell line strongly responded to fibronectin coating by invading the scratch. Fibronectin is a vital component of the ECM and partakes in formation of the premetastatic niche (35). We hypothesized that by attachment to extracellular ligands such as fibronectin the CD29-expressing tumor cells were able to migrate. To elucidate whether CD29 mediates increased migration a knockout was performed. It revealed that under fibronectin stimulation the CD29 knockout abrogates the capacity to overcome the scratch (86). An alternative ligand for CD29 is ANG-2 (90). ANG-2 is classically secreted by endothelial cells (103), but also by macrophages (104) and thereby is potentially also involved in CD29-dependent migration in SCLC. Our experiments indicated that ANG-2 stimulation had similar effects on SCLC migration and invasion as fibronectin, as the CD29KO clones showed decreased invasion and migration through the porous membrane in comparison to the WT under ANG-2 and fibronectin stimulation (86).

Our western blot analysis revealed an increased phosphorylation of FAK and SRC following ANG-2 stimulation (86). The FAK/SRC cascade is known to play an important role in integrin mediated cell adhesion (105) and is therefore likely the underlying mechanism driving the migration-promoting effects of ANG-2 in WT SCLC cells. Concordantly, Vassilopoulos and colleagues also observed decreased migration potential of CD29 CD49f KO breast cancer cells (106). Also hematopoietic stem cells were found to use CD29-dependent mechanisms for migration processes (107). To sum it up, our study shows, that CD29 *in vitro* conceivably fulfills migratory functions and thereby plays a supportive role in SCLC metastasis formation (86).

Next we applied *in vivo* models to investigate metastatic behavior of SCLC in dependence of CD29. In the metastatic cascade the intra- and extravasation process mark important steps in the generation of distant lesions. During intravasation, the tumor cell has to overcome the base membrane and endothelial junction to enter the bloodstream. This portrays the initiation of metastasis formation (108). Also, the process of extravasation is a multistep process, still not fully understood. There are several approaches describing extravasation such as diapedesis or angiopellosis. In brief, the circulating tumor cells attach to the endothelium and transmigrate through the endothelial barrier (109).

We have shown that CD29 is essential or even conditio sine qua non for both processes. Injected locally into the lung by orthotopic injection, CD29 KO SCLC clones were capable of

forming tumors on-site. Despite local tumor formation of the CD29 KO, no metastasis developed in the liver opposing the original nature of the WT (86). This suggests that CD29 is required to leave the primary side and enter the bloodstream. Choosing the most aggressive growing CD29 KO Clone 2, intravenous tumor injection led to no tumor settlement at all (86). These findings lead to the assumption that CD29 is required for the exit from bloodstream. As CD29 is an integrin involved in cell-cell contact formation, the CD29KO tumor cells might lose the function to attach to the endothelial cells. Consistent with our findings CD29 blockade abrogates binding to human umbilical vein endothelial cells *in vitro* by highly invasive human bladder carcinoma tumor cells (110). Taken together, the loss to extravasate aligns with the physiological function of CD29, as it mediates the binding of immune cells to the endothelium (40). In addition, fibronectin is a crucial factor forming the premetastatic niche (35). As fibronectin is a ligand to CD29, the CD29 KO may also lose the ability to attach to the preformed premetastatic niche. This could be a second mainstay of explanation, why the CD29 KO does not form metastasis. Although CD29 seems to be the dominant player in SCLC migration, there might be other players, interacting and potentiating CD29-dependent signaling, which should be addressed in future studies. One of these players influencing CD29-dependent migration might be ADAM9. In RNA-Seq we have identified ADAM9 upregulation after fibronectin and ANG-2 stimulation, along with increased migration capacity in SCLC (86). ADAM9 is a membrane-anchored protein also known as disintegrin and metalloproteinase domain-containing protein 9 (111). Also in other cancer entities such as in melanoma, ADAM9 is expressed by the tumor cell itself and by the surrounding stromal cells (112). The deletion of ADAM9 in melanoma cells led to significant decrease in the formation of lung metastases (112). *In vitro* assays after ADAM9 deletion further showed a reduced transmigration and adhesion behavior towards endothelial cells (112). Furthermore, in pancreatic cancer an overexpression of ADAM9 is associated with quicker tumor progression and poor prognosis (113) as well as increased migration (114). It is of great interest whether CD29 and ADAM9 directly interact to regulate the migration and invasion in SCLC. This will be investigated in follow-up projects using, for example, co-immunoprecipitation and CRISPR-Cas9 KO experiments. As Giebeler and colleagues identified that ADAM9 deletion leads to decreased transmigration (112), future experiments will test whether ADAM9 KO will decrease the migration stimulated by ANG-2 and fibronectin.

5.1.2. Clinical relevance of CD29 targeting in (solid) cancer

As our study has shown the importance of CD29 in metastasis development, the next step is to debate the clinical relevance of our findings. CD29 occupies a universal role in immune processes as the exit of immune cells from the blood system (39,40). Therefore, a general blockade of CD29 would probably lead to unforeseeable effects on the immune system and

could have negative effects on tumor control. For example, the Phase I study of the anti-CD29 monoclonal antibody (mAb) OS2966 was terminated due to safety concerns (NCT04608812) (115).

Our experiments for example have shown that total CD29 depletion on tumor cells also brings along immune effects such as the decrease of dendritic cell infiltration in the tumor. Dendritic cells are vital for activating T cells in anti-tumor response (116). Hence, for therapy approaches it is necessary to focus on certain migration-promoting CD29 ligands as ANG-2 instead of blocking CD29 itself. Our study showed that ANG-2 is a strong attractant for the CD29 WT (86). This fits to previous findings describing ANG-2 as a metastasis promoting factor via effects on the EMT (56). Therefore, an idea for preventing metastatic spread would be the blockade of ANG-2. Testing the immune checkpoint blocker atezolizumab, Horn and colleagues found that liver metastases are a limiting factor in the therapy success (19). So, an anti-ANG-2 targeted therapy could prevent the formation of metastasis and thereby overcome this critical point in therapy success. Indeed BI836880 (aANG-2/aVEGF-A), produced by Boehringer Ingelheim (Germany) is already tested in clinical trials with progressed solid tumors. Two trials combine BI836880 with aPD-1 (ezabenlimab) (NCT03468426, NCT05249426) (117,118). However, one has to keep in mind that the prevention of metastasis would only affect a small patient group, as 85% are already diagnosed in an extensive stage of disease (1).

As the clinical approach should be based on targeting the ligands of CD29, discussing the potential effects of ANG-2 blockade in the tumor micro-milieu is important. Independent of the elaborated CD29-ANG-2 signaling in metastasis formation, ANG-2 is also known to have an influence on the immune tumor microenvironment (119,120). Coffelt and colleagues, for example, described a population of monocytes and macrophages, which express one of the receptors for ANG-2, namely TIE-2. This subgroup of monocytes and macrophages was described to significantly express IL-10 and thereby suppress T cell proliferation. The ratio of CD4 and CD8 shifts towards CD4 cells with T regulatory features. Thereby, ANG-2 contributes to the establishment of an immunosuppressive microenvironment (119).

Our group laid focus on the effects of ANG-2 blockade on the immune milieu. Given the previously described results, a reversal of the immunosuppressive effects would be expected under ANG-2 blockade. Indeed, results of our group displayed an upregulation of IFNγ and IL-2 in the serum of SCLC bearing mice under ANG-2 targeted monotherapy (86). IFNy plays an important role in the activation of the innate immune system (121) and IL-2 in the proliferation of $CD4^+$ T cells (122). Thereby they contribute to an anti-tumor immune response. Moreover, our group revealed that ANG-2 blockade influences the subtypes of tumor associated macrophages and supports the anti-tumorigenic M1-like signature (86). Accordingly, in glioblastoma, a bispecific antibody against VEGFR/ANG2 shifted the tumor macrophage

signature into the M1 profile. The M1 macrophages exerted anti-tumor effects, which led to an increased survival in glioblastoma patients (123).

Therefore, ANG-2 blockade is from different perspectives an interesting approach in the treatment of SCLC. On the one hand, it addresses the CD29-ANG-2 metastasis promoting pathway and on the other hand, our group has also shown its favorable effects on the anti-tumor microenvironment (86,123). Immune checkpoint blockade in combination with chemotherapy was approved for the treatment for SCLC patients in the IMpower133 trial (19). As immune checkpoint blockade has been described not only to enforce T cell mediated anti-tumor immunity but also enhance macrophage mediated tumor cell killing (62) the combination with the M1 signature promoting effects of ANG-2 seems reasonable. Consequently, one should consider adding ANG-2 targeted therapy to established therapy regimens. We hypothesize at that point, that blocking ANG-2/CD29 signaling in a combination with immune checkpoint blockade might improve the outcome in SCLC treatment, which remains to be proven.

5.2. MHC-I loss in (solid) cancer

5.2.1. MHC-I regulatory mechanisms in (solid) cancer

The second part of our research examined the MHC-I loss, which is a common mechanism of therapy resistance across different cancer entities (124–126). Our initial broad screening showed that MHC-I loss particularly can be found in liver metastasis of SCLC patient samples (*under revision in Nature Communications since 15th January 2025 under review again since 4th August 2025*). This leads to the assumption that MHC-I decreased clones in the primary tumor might have an advantage concerning metastasis formation. Analyzing the primary SCLC lung tumor from our autochthonous mouse model, we found two populations of tumor cells with different levels of MHC-I expression. One population showed a reduced MHC-I expression comparable with the MHC-I expression in the liver metastasis. Presumably, this MHC-I reduced colony has an advantage in forming metastasis and settling in the liver. To further evaluate the behavior of MHC-I reduced SCLC clones *in vivo*, we created a B2M knockout resulting in MHC-I loss. The MHC-I KO caused a fast tumor outgrowth with an early death of the mouse (*under revision in Nature Communications since 15th January 2025 under review again since 4th August 2025*). Additionally, we found a predominant activation of the innate immune system and less infiltrating specific immune cells (*under revision in Nature Communications since 15th January 2025 under review again since 4th August 2025*). This is consistent with clinical observations concerning MHC-I loss. In different cancer entities, such as for example melanoma, colorectal, and breast cancer MHC-I loss goes along with worse clinical outcomes (127–129). The MHC-I expression is also a decisive point regarding the response of metastases to immunotherapy. It was described that MHC-I low metastases under

immunotherapy progressed (130). These clinical findings might be due to less recognition by tumor-infiltrating lymphocytes and thereby reduced specific anti-tumor immunity. This is supported by several studies, which have reported that tumor-infiltrating lymphocytes are correlated with MHC-I expression on tumor cells (131,132).

To evaluate the capacity to form metastases the MHC-I KO was injected orthotopically into the lung. However, the matching liver samples just showed single tumor cell nests. These findings resemble the metastatic behavior of the WT (*under revision in Nature Communications since 15th January 2025 under review again since 4th August 2025*). This might indicate that MHC-I loss in the primary tumor does not enhance metastasis formation but locally leads to an aggressive tumor growth. On the other hand, fast local tumor growth of the MHC-I KO led to an early death of the animal (*under revision in Nature Communications since 15th January 2025 under review again since 4th August 2025*). This quick progression could time-related prevent metastatic settlement.

Stimulating the MHC-I KO SCLC cells *in vitro* with IFNγ (40 ng/ml) led to an increased expression of MHC-II. In agreement with this result, it was described in different cancer entities that tumor cells can express MHC-II on their surface (133). Our *in vitro* findings have been confirmed *in vivo*, where we found an increased expression of MHC-II on the SCLC cells, as well. Nevertheless, it seems that the tumor detection by the immune system via MHC-II presentation on tumor cells is not sufficient, since MHC-I KO tumors present as aggressive and rapidly growing lesions. In breast cancer, MHC-II on tumor cells is associated with a better prognosis as well as more infiltrating lymphocytes (134). This observation is likely not transferable to SCLC, where MHC-I seems to be superior to MHC-II regarding anti-tumor immunity.

5.3. Restoring anti-tumor immunity in SCLC

5.3.1. Pharmacological targeting of ERBB2

We aimed to identify targetable pathways regulating MHC-I in SCLC and revealed ERBB2 as potential candidate. The review of Kumagai and colleagues gives a detailed overview of the ERBB2-dependent signaling likely regulating MHC-I expression on tumor cells. As shown in Fig.3 ERBB2 leads via PI3K/AKT and MAPK/ERK downstream signaling to a decreased MHC-I presentation on tumor cells. TBK1 is less phosphorylated, and STING signaling is inhibited. Consequently, IRF3, one of the transcriptional factors of MHC is less activated, which leads to a decreased interferon type I/II signaling and thereby to diminished presentation of MHC-I (70). Indeed, our first trials with the ERBB2 blocker mubritinib in western blots showed a downregulation of phospho-AKT and phospho-ERK (*under revision in Nature Communications since 15th January 2025 under review again since 4th August 2025*). The RAS–RAF–MEK–ERK cascade is a negative regulator of MHC-I presentation and additionally contributes to cell

proliferation and survival of cancer cells (70). Moreover, we observed an enhanced phosphorylation of TBK, which is essential for the MHC-I transcription cascade (*under revision in Nature Communications since 15th January 2025 under review again since 4th August 2025*). Another ERBB-family member, which creates reduced antigenicity, is EGFR. Similar to ERBB2, EGFR downstream signaling pathways (PI3K/AKT, MAPK/ERK) inhibit interferon signaling by downregulating interferon regulatory factor 1. The latter is a transcription factor for MHC-I (70). In the therapy of lung adenocarcinomas, belonging to the group of non-small cell lung cancer (NSCLC), overactivation of EGFR due to the L858R mutation in exon 21 or small deletions in exon 19, is targeted by tyrosine kinase inhibitors (TKIs). Third-generation EGFR-TKIs could achieve a median overall survival of 38.0 after progression under first- or second-generation TKI therapy (135). In SCLC, EGFR mutations and especially the classical L858R mutation in exon 21 or deletions in exon 19 are uncommon (136), and may occur in the context of small cell transitions as acquired resistance mechanisms of lung adenocarcinomas (137,138) and squamous cell carcinomas (137,139). Nevertheless, EGFR targeting mAbs like cetuximab can also target EGFR wild type (140) and might also show effects in SCLC. The same is true for mAbs targeting ERBB2 such as trastuzumab (141). Preclinical models have shown trastuzumab to be effective in chemoresistant SCLC expressing ERBB2 (142). However, irinotecan resistant SCLC cells were refractory to trastuzumab (142). This could be overcome by the antibody-drug conjugate trastuzumab emtansine, which led to inhibition of tumor growth and increased apoptosis (142). Also first case reports reveal favorable effects of combining chemotherapy irinotecan with trastuzumab in SCLC (143). Therefore, targeting ERBB2 might be a potential approach in future SCLC treatment as around 13% of patients express ERBB2 (76).

The next objective is to examine whether ERBB2 blockade leads to increased MHC-I expression on SCLC cells *in vivo* using the genetically engineered SCLC model. The enhanced recognition of SCLC cells by T-lymphocytes upon ERBB2 blockade, consequently, leads to a more efficient killing of tumor cells by the immune system and probably to increased survival. Moreover, growing evidence across different cancer entities indicates that combining immunotherapy with ERBB2-targeted therapy may boost treatment efficacy. The PANACEA trial demonstrated that the combination of trastuzumab and pembrolizumab could overcome trastuzumab resistance by restoring anti-tumor immunity (NCT02129556) (144). Additionally, in a case of squamous cell carcinoma, the combination of the ERBB2 inhibitor lapatinib and Anti-PD-1 antibody nivolumab led to significant tumor regression (145). Also in lung cancer, the combination of ERBB2 blockade with immunotherapy is being actively investigated. A recent clinical trial is assessing the combination of the a PD-1 inhibitor with pyrotinib, a pan-HER tyrosine kinase inhibitor, in patients with advanced NSCLC harboring HER2 mutations (NCT04144569) (146).

Given the limited treatment options for advanced SCLC, our findings that ERBB2 blockade, particularly in combination with immunotherapy, prolongs survival and are promising and could serve as a basis for further evaluation in clinical trials.

5.4. Limitations

Integrins are highly promiscuous ECM receptors forming integrin heterodimers and also interacting with other transmembrane receptors driving oncogenic signaling (39). We focused on the canonical CD29 ligand fibronectin and the pharmaceutically targetable non-canonical ligand ANG-2. We may have overlooked other relevant CD29 ligands contributing to metastasis, since we did not systematically screen for potential CD29 ligand abundance in SCLC. However, we were able to identify CD29 as a key driver in SCLC liver metastasis in relation to other integrins.

Although we observed consistent downregulation of MHC-I in metastatic lesions, we did not systematically assess the epigenetic signature by chromatin accessibility or DNA methylation profiling methods and mutational status of *B2M* or IFNγ response genes such as JAK1, JAK2, STAT1 and IRF1 by next generation sequencing. Epigenetic regulation of MHC-I has been recently described in SCLC (28,29,147) and mutations in B2M and IFNγ response genes are known to contribute to immune evasion in other tumor entities (148,149). Today, we cannot exclude the possibility that epigenetic alterations and genomic mutations are part of the observed MHC-I loss observed in metastasis.

Furthermore, our preclinical evaluation relied on syngeneic mouse models, which may not fully portray human SCLC tumor and the respective tumor microenvironment. In future work, testing the combined therapy regimen in xenograft models using patient-derived tumor could confirm potential therapeutic efficacy and make translation to human more likely.

Finally, our study proposes novel therapeutic strategies combining immune checkpoint blockade and kinase inhibiton. The safety and efficacy of the applied combination using mubritinib and anti-PD-1 remain to be tested in a clinical context. For the reason that mubritinib was also shown to affect the electron tranfer chain (150), investigating further relevant ERBB2 inhibitor such as lapatinib and neratinib on a preclinical basis, would overcome a further limitation of our study to enable a clinical translation with a high probility.

Taken together, our study harbors some limitations highlighting the need for further investigation to translate our findings into effective therapeutic approaches for SCLC patients in the future.

6. Conclusion

In summary, SCLC is still a highly aggressive cancer entity, which lacks favorable treatment options, particularly regarding metastatic spread. Overall, we found CD29 to be a key driver in SCLC metastasis formation. Especially, fibronectin and ANG-2 portray important ligands of the tumor micro-milieu enforcing the tumor cells' migration and invading capacities (86). Therefore, CD29 ligand dependent signaling pathway is a strong mechanism and should be addressed in SCLC therapy. For example, blocking ANG-2 in combination with established therapy regimes might be a promising strategy for future clinical trials.

The second part of our study addressed the loss of MHC-I, frequently observed as a mechanism of immunotherapy resistance, but also relevant for metastasis. We confirmed the devastating consequences of MHC-I loss, which resulted in immune escape and rapid tumor progression. Notably, liver metastases exhibited an increased reduction in MHC-I expression compared to the primary tumor. Based on this finding, we tested the ERBB2 small molecule inhibitor mubritinib, which showed promising results in the western blots initiating an MHC-I regulating signaling cascade (under revision in Nature Communications *since 15th January 2025 under review again since 4th August 2025*). Altogether, our study uncovered two critical signaling mechanisms in SCLC, offering new vulnerabilities within the otherwise unsatisfactory treatment situation of this highly deadly disease.

7. References

1. Saltos A, Shafique M, Chiappori A. Update on the Biology, Management, and Treatment of Small Cell Lung Cancer (SCLC). Front Oncol. 2020 July 16;10:1074.

2. Soomro Z, Youssef M, Yust-Katz S, Jalali A, Patel AJ, Mandel J. Paraneoplastic syndromes in small cell lung cancer. J Thorac Dis. 2020;12(10):6253–63.

3. American cancer society. Lung Cancer Survival Rates | 5-Year Survival Rates for Lung Cancer [Internet]. [cited 2025 Jan 11]. Available from: https://www.cancer.org/cancer/types/lung-cancer/detection-diagnosis-staging/survival-rates.html

4. Ko J, Winslow MM, Sage J. Mechanisms of small cell lung cancer metastasis. EMBO Mol Med. 2021;13(1):13122.

5. Nakazawa K, Kurishima K, Tamura T, Kagohashi K, Ishikawa H, Satoh H, et al. Specific organ metastases and survival in small cell lung cancer. Oncol Lett. 2012;4(4):617–20.

6. Micke P, Faldum A, Metz T, Beeh KM, Bittinger F, Hengstler JG, et al. Staging small cell lung cancer: Veterans Administration Lung Study Group versus International Association for the Study of Lung Cancer--what limits limited disease? Lung Cancer Amst Neth. 2002 Sept;37(3):271–6.

7. Demedts IK, Vermaelen KY, Meerbeeck JP van. Treatment of extensive-stage small cell lung carcinoma: current status and future prospects. Eur Respir J. 2009 Dec 31;35(1):202–15.

8. Chen J, Jiang R, Garces YI, Jatoi A, Stoddard SM, Sun Z, et al. Prognostic factors for limited-stage small cell lung cancer: a study of 284 patients. Lung Cancer Amst Neth. 2010;67(2):221–6.

9. Kim CH, Lee YC, Hung RJ, McNallan SR, Cote ML, Lim WY, et al. Exposure to secondhand tobacco smoke and lung cancer by histological type: a pooled analysis of the International Lung Cancer Consortium (ILCCO. Int J Cancer [Internet]. 2014;135(8). Available from: https://doi.org/10.1002/ijc.28835

10. George J, Lim JS, Jang SJ, Cun Y, Ozretić L, Kong G, et al. Comprehensive genomic profiles of small cell lung cancer. Nature. 2015;524(7563):47–53.

11. Meuwissen R, Linn SC, Linnoila RI, Zevenhoven J, Mooi WJ, Berns A. Induction of small cell lung cancer by somatic inactivation of both TrTP53 and RB1 in a conditional mouse model. Cancer Cell. 2003;4(3):181–9.

12. Lazzari C, Mirabile A, Bulotta A, Viganó MG, Ogliari FR, Ippati S, et al. History of Extensive Disease Small Cell Lung Cancer Treatment: Time to Raise the Bar? Rev Lit Cancers. 2021;13(5):998.

13. Dingemans AC, Früh M, Ardizzoni A, Besse B, Faivre-Finn C, Hendriks LE, et al. Electronic address: clinicalguidelines@esmo.org. Ann Oncol Off J Eur Soc Med Oncol. 2021;32(7):839–53.

14. Jarzebska N, Karetnikova ES, Markov AG, Kasper M, Rodionov RN, Spieth PM. Scarred Lung. An Update on Radiation-Induced Pulmonary Fibrosis. Front Med. 2021;7:585756.

15. Asai N, Ohkuni Y, Kaneko N, Yamaguchi E, Kubo A. Relapsed small cell lung cancer: treatment options and latest developments. Ther Adv Med Oncol. 2014 Mar;6(2):69–82.

16. Johnson BE, Fischer T, Fischer B, Dunlop D, Rischin D, Silberman S, et al. Phase II study of imatinib in patients with small cell lung cancer. Clin Cancer Res Off J Am Assoc Cancer Res. 2003 Dec 1;9(16 Pt 1):5880–7.

17. Moore AM, Einhorn LH, Estes D, Govindan R, Axelson J, Vinson J, et al. Gefitinib in patients with chemo-sensitive and chemo-refractory relapsed small cell cancers: a Hoosier Oncology Group phase II trial. Lung Cancer Amst Neth. 2006 Apr;52(1):93–7.

18. Liu SV, Reck M, Mansfield AS, Mok T, Scherpereel A, Reinmuth N, et al. Updated Overall Survival and PD-L1 Subgroup Analysis of Patients With Extensive-Stage Small-Cell Lung Cancer Treated With Atezolizumab, Carboplatin, and Etoposide (IMpower133. J Clin Oncol Off J Am Soc Clin Oncol. 2021;39(6):619–30.

19. Horn L, Mansfield AS, Szczęsna A, Havel L, Krzakowski M, Hochmair MJ, et al. First-Line Atezolizumab plus Chemotherapy in Extensive-Stage Small-Cell Lung Cancer. N Engl J Med. 2018 Dec 6;379(23):2220–9.

20. Denny SK, Yang D, Chuang CH, Brady JJ, Lim JS, Grüner BM, et al. Nfib Promotes Metastasis through a Widespread Increase in Chromatin Accessibility. Cell. 2016 July 14;166(2):328–42.

21. Ko JH, Lambert KE, Bhattacharya D, Lee MC, Colón CI, Hauser H, et al. Small Cell Lung Cancer Plasticity Enables NFIB-Independent Metastasis. Cancer Res. 2024 Jan 16;84(2):226–40.

22. Ireland AS, Micinski AM, Kastner DW, Guo B, Wait SJ, Spainhower KB, et al. MYC Drives Temporal Evolution of Small Cell Lung Cancer Subtypes by Reprogramming Neuroendocrine Fate. Cancer Cell. 2020 July 13;38(1):60-78.e12.

23. Mollaoglu G, Guthrie MR, Böhm S, Brägelmann J, Can I, Ballieu PM, et al. MYC Drives Progression of Small Cell Lung Cancer to a Variant Neuroendocrine Subtype with Vulnerability to Aurora Kinase Inhibition. Cancer Cell. 2017 Feb 13;31(2):270–85.

24. Kawasaki K, Salehi S, Zhan YA, Chen K, Lee JH, Salataj E, et al. FOXA2 promotes metastatic competence in small cell lung cancer. Nat Commun. 2025 May 26;16(1):4865.

25. Xie M, Vuko M, Rodriguez-Canales J, Zimmermann J, Schick M, O'Brien C, et al. Molecular classification and biomarkers of outcome with immunotherapy in extensive-stage small-cell lung cancer: analyses of the CASPIAN phase 3 study. Mol Cancer. 2024 May 30;23(1):115.

26. Rudin CM, Balli D, Lai WV, Richards AL, Nguyen E, Egger JV, et al. Clinical Benefit From Immunotherapy in Patients With SCLC Is Associated With Tumor Capacity for Antigen Presentation. J Thorac Oncol Off Publ Int Assoc Study Lung Cancer. 2023 Sept;18(9):1222–32.

27. Kim YS, Nabet BY, Cortez BN, Sun NY, Sebastian R, Redon CE, et al. NOTCH1 reverses immune suppression in small cell lung cancer through reactivation of STING. J Clin Invest. 2025 July 8;e185423.

28. Choudhury NJ, Lai WV, Makhnin A, Heller G, Eng J, Li B, et al. A Phase I/II Study of Valemetostat (DS-3201b), an EZH1/2 Inhibitor, in Combination with Irinotecan in Patients

with Recurrent Small-Cell Lung Cancer. Clin Cancer Res Off J Am Assoc Cancer Res. 2024 Sept 3;30(17):3697–703.

29. Hiatt JB, Sandborg H, Garrison SM, Arnold HU, Liao SY, Norton JP, et al. Inhibition of LSD1 with Bomedemstat Sensitizes Small Cell Lung Cancer to Immune Checkpoint Blockade and T-Cell Killing. Clin Cancer Res Off J Am Assoc Cancer Res. 2022 Oct 14;28(20):4551–64.

30. Liotta LA, Kohn EC. Invasion and Metastases. 5th ed. RC B Jr, DW K, RE P, editors. Hamilton (ON: BC Decker; 2000.

31. Zijl F, Krupitza G, Mikulits W. Initial steps of metastasis: cell invasion and endothelial transmigration. Mutat Res. 2011;728(1–2):23–34.

32. Zhou ZH, Ji CD, Xiao HL, Zhao HB, Cui YH, Bian XW. Reorganized Collagen in the Tumor Microenvironment of Gastric Cancer and Its Association with Prognosis. J Cancer. 2017;8(8):1466–76.

33. Moreau JF, Pradeu T, Grignolio A, Nardini C, Castiglione F, Tieri P, et al. The emerging role of ECM crosslinking in T cell mobility as a hallmark of immunosenescence in humans. Ageing Res Rev. 2017;35:322–35.

34. Sung B, Ketova T, Hoshino D. Directional cell movement through tissues is controlled by exosome secretion. Nature Communicationndr7164; 2015.

35. Liu Y, Cao X. Characteristics and Significance of the Pre-metastatic Niche. Cancer Cell. 2016 Nov 14;30(5):668–81.

36. Feldman LE, Shin KC, Natale RB, Todd RF. Beta 1 integrin expression on human small cell lung cancer cells. Cancer Res. 3rd;1991;51(4):1065-70.

37. Wang Z, Wang W, Luo Q, Song G. High matrix stiffness accelerates migration of hepatocellular carcinoma cells through the integrin β1-Plectin-F-actin axis. BMC Biol. 2025 Jan 9;23(1):8.

38. Yuan J, Yuan L, Yang L, Chinnathambi A, Alharbi SA, Huang J, et al. Tinagl1 restores tamoxifen sensitivity and blocks fibronectin-induced EMT by simultaneously blocking the EGFR and β1-integrin/FAK signaling pathways in tamoxifen-resistant breast cancer cells. IUBMB Life. 2025 Jan;77(1):e2940.

39. Hynes RO. Integrins: versatility, modulation, and signaling in cell adhesion. Cell. 1992 Apr 3;69(1):11–25.

40. Langereis JD. Neutrophil integrin affinity regulation in adhesion, migration, and bacterial clearance. Cell Adhes Migr. 2013;7(6):476–81.

41. Desgrosellier JS, Cheresh DA. Integrins in cancer: biological implications and therapeutic opportunities. Nat Rev Cancer. 2010;10(1):9–22.

42. Lawson MH, Cummings NM, Rassl DM, Vowler SL, Wickens M, Howat WJ, et al. Bcl-2 and β1-integrin predict survival in a tissue microarray of small cell lung cancer. Br J Cancer. 2010 Nov;103(11):1710–5.

43. Oshita F, Kameda Y, Hamanaka N, Saito H, Yamada K, Noda K. High expression of integrin beta1 and TP53 is a greater poor prognostic factor than clinical stage in small-cell lung cancer. Am J Clin Oncol. 2004;27(3):215–9.

44. Sethi T, Rintoul RC, Moore SM, MacKinnon AC, Salter D, Choo C, et al. Extracellular matrix proteins protect small cell lung cancer cells against apoptosis: A mechanism for small cell lung cancer growth and drug resistance in vivo. Nat Med. 1999 June;5(6):662–8.

45. Takada Y, Ye X, Simon S. The integrins. Genome Biol. 2007;8(5):215.

46. Lal H, Verma SK, Foster DM, Golden HB, Reneau JC, Watson LE, et al. Integrins and proximal signaling mechanisms in cardiovascular disease. Front Biosci Landmark Ed. 2009;14(6):2307–34.

47. Pankov R, Yamada KM. Fibronectin at a glance. J Cell Sci. 2002;115(Pt 20):3861–3.

48. Shin N, Son GM, Shin DH, Kwon MS, Park BS, Kim HS, et al. Cancer-Associated Fibroblasts and Desmoplastic Reactions Related to Cancer Invasiveness in Patients With Colorectal Cancer. Ann Coloproctology. 2019 Feb;35(1):36–46.

49. Topalovski M, Brekken RA. Matrix control of pancreatic cancer: New insights into fibronectin signaling. Cancer Lett. 2016;381(1):252–8.

50. Sun Y, Zhao C, Ye Y, Wang Z, He Y, Li Y, et al. High expression of fibronectin 1 indicates poor prognosis in gastric cancer. Oncol Lett. 2020;19(1):93–102.

51. Hegele A, Heidenreich A, Kropf J, Knobloch R, Varga Z, Hofmann R, et al. Plasma levels of cellular fibronectin in patients with localized and metastatic renal cell carcinoma. Tumour Biol J Int Soc Oncodevelopmental Biol Med. 2004;25(3):111–6.

52. Saito N, Nishimura H, Kameoka S. Clinical significance of fibronectin expression in colorectal cancer. Mol Med Rep. 2008;1(1):77–81.

53. Hakanpaa L, Sipila T, Leppanen VM, Gautam P, Nurmi H, Jacquemet G, et al. Endothelial destabilization by angiopoietin-2 via integrin β1 activation. Nat Commun. 2015 Jan 30;6(1):5962.

54. Saharinen P, Eklund L, Alitalo K. Therapeutic targeting of the angiopoietin-TIE pathway. Nat Rev Drug Discov. 2017;16(9):635–61.

55. Falcón BL, Hashizume H, Koumoutsakos P, Chou J, Bready JV, Coxon A, et al. Contrasting actions of selective inhibitors of angiopoietin-1 and angiopoietin-2 on the normalization of tumor blood vessels. Am J Pathol. 2009;175(5):2159–70.

56. Dong Z, Chen J, Yang X, Zheng W, Wang L, Fang M, et al. Ang-2promotes lung cancer metastasis by increasing epithelial-mesenchymal transition. Oncotarget. 2018;9(16):12705–17.

57. Chen S, Saeed AFUH, Liu Q, Jiang Q, Xu H, Xiao GG, et al. Macrophages in immunoregulation and therapeutics. Signal Transduct Target Ther. 2023 May 22;8(1):1–35.

58. Ruffell B, Affara NI, Coussens LM. Differential macrophage programming in the tumor microenvironment. Trends Immunol. 2012;33(3):119–26.

59. Zhao X, Qu J, Sun Y, Wang J, Liu X, Wang F, et al. Prognostic significance of tumor-associated macrophages in breast cancer: a meta-analysis of the literature. Oncotarget. 2017;8(18):30576–86.

60. Freeman GJ, Long AJ, Iwai Y, Bourque K, Chernova T, Nishimura H, et al. Engagement of the PD-1 immunoinhibitory receptor by a novel B7 family member leads to negative regulation of lymphocyte activation. J Exp Med. 2000 Oct 2;192(7):1027–34.

61. Zheng Y, Fang YC, Li J. PD-L1 expression levels on tumor cells affect their immunosuppressive activity. Oncol Lett. 2019;18(5):5399–407.

62. Gordon SR, Maute RL, Dulken BW, Hutter G, George BM, McCracken MN, et al. PD-1 expression by tumour-associated macrophages inhibits phagocytosis and tumour immunity. Nature. 2017;545(7655):495–9.

63. Cullen SP, Martin SJ. Fas and TRAIL “death receptors” as initiators of inflammation: Implications for cancer. Semin Cell Dev Biol. 2015;39:26–34.

64. Dunn GP, Old LJ, Schreiber RD. The three Es of cancer immunoediting. Annu Rev Immunol. 2004;22:329–60.

65. Blum JS, Wearsch PA, Cresswell P. Pathways of antigen processing. Annu Rev Immunol. 2013;31:443–73.

66. Thongsin N, Wattanapanitch M. Generation of B2M bi-allelic knockout human induced pluripotent stem cells (MUSIi001-A-1) using a CRISPR/Cas9 system. Stem Cell Res. 2021;56:102551.

67. Dhatchinamoorthy K, Colbert JD, Rock KL. Cancer Immune Evasion Through Loss of MHC Class I Antigen Presentation. Front Immunol. 2021;12:636568.

68. Ugurel S, Spassova I, Wohlfarth J, Drusio C, Cherouny A, Melior A, et al. MHC class-I downregulation in PD-1/PD-L1 inhibitor refractory Merkel cell carcinoma and its potential reversal by histone deacetylase inhibition: a case series. Cancer Immunol Immunother. 2019;68(6):983–90.

69. Zhou F. Molecular mechanisms of IFN-gamma to up-regulate MHC class I antigen processing and presentation. Int Rev Immunol. 2009;28(3–4):239–60.

70. Kumagai S, Koyama S, Nishikawa H. Antitumour immunity regulated by aberrant ERBB family signalling. Nat Rev Cancer. 2021;21(3):181–97.

71. Yarden Y, Sliwkowski MX. Untangling the ErbB signalling network. Nat Rev Mol Cell Biol. 2001;2(2):127–37.

72. Moasser MM. The oncogene HER2: its signaling and transforming functions and its role in human cancer pathogenesis. Oncogene. 2007 Oct;26(45):6469–87.

73. Chandrasekaran S, Sasaki M, Scharer CD, Kissick HT, Patterson DG, Magliocca KR, et al. Phosphoinositide 3-Kinase Signaling Can Modulate MHC Class I and II Expression. Mol Cancer Res MCR. 2019;17(12):2395–409.

74. Figueroa-Magalhães MC, Jelovac D, Connolly R, Wolff AC. Treatment of ERBB2-positive breast cancer. Breast Edinb Scotl. 2014;23(2):128–36.

75. Dirix LY, Takacs I, Jerusalem G, Nikolinakos P, Arkenau HT, Forero-Torres A, et al. Avelumab, an anti-PD-L1 antibody, in patients with locally advanced or metastatic breast cancer: a phase 1b JAVELIN Solid Tumor study. Breast Cancer Res Treat. 2018 Feb;167(3):671–86.

76. Micke P, Hengstler JG, Ros R, Bittinger F, Metz T, Gebhard S, et al. c-erbB-2 expression in small-cell lung cancer is associated with poor prognosis. Int J Cancer. 2001;92(4):474–9.

77. Potti A, Willardson J, Forseen C, Kishor Ganti A, Koch M, Hebert B, et al. Predictive role of HER-2/neu overexpression and clinical features at initial presentation in patients with extensive stage small cell lung carcinoma. Lung Cancer Amst Neth. 2002;36(3):257–61.

78. Minami T, Kijima T, Kohmo S, Arase H, Otani Y, Nagatomo I, et al. Overcoming chemoresistance of small-cell lung cancer through stepwise ERBB2-targeted antibody-dependent cell-mediated cytotoxicity and VEGF-targeted antiangiogenesis. Sci Rep. 2013;3:2669.

79. Wu S, Zhang Q, Zhang F, Meng F, Liu S, Zhou R, et al. HER2 recruits AKT1 to disrupt STING signalling and suppress antiviral defence and antitumour immunity. Nat Cell Biol. 2019 Aug;21(8):1027–40.

80. Mimura K, Shiraishi K, Mueller A, Izawa S, Kua LF, So J, et al. The MAPK pathway is a predominant regulator of HLA-A expression in esophageal and gastric cancer. J Immunol Baltim. 2013;191(12):6261–72.

81. Sapkota B, Hill CE, Pollack BP. Vemurafenib enhances MHC induction in BRAFV600E homozygous melanoma cells. Oncoimmunology. 2013;2(1):22890.

82. Russell W, Burch R. The principles of humane experimental technique. 1959.

83. Nevalainen T, Berge E, Gallix P, Jilge B, Melloni E, Thomann P, et al. FELASA guidelines for education of specialists in laboratory animal science (Category D). Report of the Federation of Laboratory Animal Science Associations Working Group on Education of Specialists (Category D) accepted by the FELASA Board of Management. Lab Anim. 1999 Jan;33(1):1–15.

84. Faul F, Erdfelder E, Lang AG, Buchner A. G*Power 3: a flexible statistical power analysis program for the social, behavioral, and biomedical sciences. Behav Res Methods. 2007 May;39(2):175–91.

85. Meder L, Schuldt P, Thelen M, Schmitt A, Dietlein F, Klein S, et al. Combined VEGF and PD-L1 Blockade Displays Synergistic Treatment Effects in an Autochthonous Mouse Model of Small Cell Lung Cancer. Cancer Res. 2018 Aug 1;78(15):4270–81.

86. Meder L, Orschel CI, Otto CJ, Koker M, Brägelmann J, Ercanoglu MS, et al. Blocking the angiopoietin-2-dependent integrin β-1 signaling axis abrogates small cell lung cancer invasion and metastasis. JCI Insight. 2024 May 22;9(10):e166402.

87. Lamouille S, Xu J, Derynck R. Molecular mechanisms of epithelial–mesenchymal transition. Nat Rev Mol Cell Biol. 2014 Mar;15(3):178–96.

88. George J, Lim JS, Jang SJ, Cun Y, Ozretić L, Kong G, et al. Comprehensive genomic profiles of small cell lung cancer. Nature. 2015 Aug 6;524(7563):47–53.

89. Tlemsani C, Pongor L, Elloumi F, Girard L, Huffman KE, Roper N, et al. SCLC-CellMiner: A Resource for Small Cell Lung Cancer Cell Line Genomics and Pharmacology Based on Genomic Signatures. Cell Rep. 2020 Oct 20;33(3):108296.

90. Hakanpaa L, Sipila T, Leppanen VM, Gautam P, Nurmi H, Jacquemet G, et al. Endothelial destabilization by angiopoietin-2 via integrin β1 activation. Nat Commun. 2015 Jan 30;6:5962.

91. Zhao X, Guan JL. Focal adhesion kinase and its signaling pathways in cell migration and angiogenesis. Adv Drug Deliv Rev. 2011 July 18;63(8):610–5.

92. Shultz LD, Schweitzer PA, Christianson SW, Gott B, Schweitzer IB, Tennent B, et al. Multiple defects in innate and adaptive immunologic function in NOD/LtSz-scid mice. J Immunol Baltim Md 1950. 1995 Jan 1;154(1):180–91.

93. Brea EJ, Oh CY, Manchado E, Budhu S, Gejman RS, Mo G, et al. Kinase Regulation of Human MHC Class I Molecule Expression on Cancer Cells. Cancer Immunol Res. 2016 Nov;4(11):936–47.

94. Axelrod ML, Cook RS, Johnson DB, Balko JM. Biological Consequences of MHC-II Expression by Tumor Cells in Cancer. Clin Cancer Res. 2019 Apr 15;25(8):2392–402.

95. Chao MP, Weissman IL, Majeti R. The CD47-SIRPα pathway in cancer immune evasion and potential therapeutic implications. Curr Opin Immunol. 2012;24(2):225–32.

96. Eisenhauer EA, Therasse P, Bogaerts J, Schwartz LH, Sargent D, Ford R, et al. New response evaluation criteria in solid tumours: revised RECIST guideline (version 1.1). Eur J Cancer Oxf Engl 1990. 2009 Jan;45(2):228–47.

97. Usman S, Waseem NH, Nguyen TKN, Mohsin S, Jamal A, Teh MT, et al. Vimentin Is at the Heart of Epithelial Mesenchymal Transition (EMT) Mediated Metastasis. Cancers. 2021 Oct 5;13(19):4985.

98. Satelli A, Li S. Vimentin in cancer and its potential as a molecular target for cancer therapy. Cell Mol Life Sci CMLS. 2011;68(18):3033–46.

99. Hu L, Lau SH, Tzang CH, Wen JM, Wang W, Xie D, et al. Association of Vimentin overexpression and hepatocellular carcinoma metastasis. Oncogene. 2004;23(1):298–302.

100. Huck L, Pontier SM, Zuo DM, Muller WJ. beta1-integrin is dispensable for the induction of ErbB2 mammary tumors but plays a critical role in the metastatic phase of tumor progression. Proc Natl Acad Sci U S A. 2010 Aug 31;107(35):15559–64.

101. Vassos N, Rau T, Merkel S, Feiersinger F, Geppert CI, Stürzl M, et al. Prognostic value of β1 integrin expression in colorectal liver metastases. Int J Clin Exp Pathol. 2014;7(1):288–300.

102. Xu Z, Zou L, Ma G, Wu X, Huang F, Feng T, et al. Integrin β1 is a critical effector in promoting metastasis and chemo-resistance of esophageal squamous cell carcinoma. Am J Cancer Res. 2017;7(3):531–42.

103. Fiedler U, Scharpfenecker M, Koidl S, Hegen A, Grunow V, Schmidt JM, et al. The Tie-2 ligand angiopoietin-2 is stored in and rapidly released upon stimulation from endothelial cell Weibel-Palade bodies. Blood. 2004 June 1;103(11):4150–6.

104. Coffelt SB, Tal AO, Scholz A, De Palma M, Patel S, Urbich C, et al. Angiopoietin-2 regulates gene expression in TIE2-expressing monocytes and augments their inherent proangiogenic functions. Cancer Res. 2010 July 1;70(13):5270–80.

105. Mitra SK, Schlaepfer DD. Integrin-regulated FAK-Src signaling in normal and cancer cells. Curr Opin Cell Biol. 2006;18(5):516–23.

106. Vassilopoulos A, Chisholm C, Lahusen T, Zheng H, Deng CX. A critical role of CD29 and CD49f in mediating metastasis for cancer-initiating cells isolated from a Brca1-associated mouse model of breast cancer. Oncogene. 2014;33(47):5477–82.

107. Konakahara S, Ohashi K, Mizuno K, Itoh K, Tsuji T. CD29 integrin- and LIMK1/cofilin-mediated actin reorganization regulates the migration of haematopoietic progenitor cells underneath bone marrow stromal cells. Genes Cells Devoted Mol Cell Mech. 2004 Apr;9(4):345–58.

108. Zavyalova MV, Denisov EV, Tashireva LA, Savelieva OE, Kaigorodova EV, Krakhmal NV, et al. Intravasation as a Key Step in Cancer Metastasis. Biochem Biokhimiia. 2019 July;84(7):762–72.

109. Cheng X, Cheng K. Visualizing cancer extravasation: from mechanistic studies to drug development. Cancer Metastasis Rev. 2021 Mar;40(1):71–88.

110. Heyder C, Gloria-Maercker E, Hatzmann W, Niggemann B, Zänker KS, Dittmar T. Role of the beta1-integrin subunit in the adhesion, extravasation and migration of T24 human bladder carcinoma cells. Clin Exp Metastasis. 2005;22(2):99–106.

111. Chou CW, Huang YK, Kuo TT, Liu JP, Sher YP. An Overview of ADAM9: Structure, Activation, and Regulation in Human Diseases. Int J Mol Sci. 2020 Oct 21;21(20):7790.

112. Giebeler N, Schönefuß A, Landsberg J, Tüting T, Mauch C, Zigrino P. Deletion of ADAM-9 in HGF/CDK4 mice impairs melanoma development and metastasis. Oncogene. 2017;36(35):5058–67.

113. Grützmann R, Lüttges J, Sipos B, Ammerpohl O, Dobrowolski F, Alldinger I, et al. ADAM9 expression in pancreatic cancer is associated with tumour type and is a prognostic factor in ductal adenocarcinoma. Br J Cancer. 2004;90(5):1053–8.

114. Mygind KJ, Schwarz J, Sahgal P, Ivaska J, Kveiborg M. Loss of ADAM9 expression impairs β1 integrin endocytosis, focal adhesion formation and cancer cell migration. J Cell Sci. 2018;131(1):205393.

115. National Library of Medicine. Convection-enhanced Delivery of OS2966 for Patients With High-grade Glioma Undergoing a Surgical Resection [Internet]. clinicaltrials.gov; 2023 Aug [cited 2025 Feb 3]. Report No.: NCT04608812. Available from: https://clinicaltrials.gov/study/NCT04608812

116. Broz ML, Binnewies M, Boldajipour B, Nelson AE, Pollack JL, Erle DJ, et al. Dissecting the tumor myeloid compartment reveals rare activating antigen-presenting cells critical for T cell immunity. Cancer Cell. 2014;26(5):638–52.

117. National Library of Medicine. A Study to Test Different Doses of BI 836880 Combined With Ezabenlimab in Patients With Advanced Non-small Cell Lung Cancer Followed by Other Types of Advanced Solid Tumours [Internet]. clinicaltrials.gov; 2024 Dec [cited 2025 Jan 12]. Report No.: NCT03468426. Available from: https://clinicaltrials.gov/study/NCT03468426

118. National Library of Medicine. A Study to Test Whether Different Combinations of BI 765063, Ezabenlimab, Chemotherapy, Cetuximab, and BI 836880 Help People With Head and Neck Cancer or Liver Cancer [Internet]. clinicaltrials.gov; 2025 Jan [cited 2025

Jan 12]. Report No.: NCT05249426. Available from: https://clinicaltrials.gov/study/NCT05249426

119. Coffelt SB, Chen YY, Muthana M, Welford AF, Tal AO, Scholz A, et al. Angiopoietin 2 stimulates TIE2-expressing monocytes to suppress T cell activation and to promote regulatory T cell expansion. J Immunol Baltim Md 1950. 2011 Apr 1;186(7):4183–90.

120. Wu X, Giobbie-Hurder A, Liao X, Connelly C, Connolly EM, Li J, et al. Angiopoietin-2 as a Biomarker and Target for Immune Checkpoint Therapy. Cancer Immunol Res. 2017 Jan;5(1):17–28.

121. Wu C, Xue Y, Wang P, Lin L, Liu Q, Li N, et al. IFN-γ primes macrophage activation by increasing phosphatase and tensin homolog via downregulation of miR-3473b. J Immunol Baltim Md 1950. 2014 Sept 15;193(6):3036–44.

122. Kelly E, Won A, Refaeli Y, Van Parijs L. IL-2 and related cytokines can promote T cell survival by activating AKT. J Immunol Baltim Md 1950. 2002 Jan 15;168(2):597–603.

123. Kloepper J, Riedemann L, Amoozgar Z, Seano G, Susek K, Yu V, et al. Ang-2/VEGF bispecific antibody reprograms macrophages and resident microglia to anti-tumor phenotype and prolongs glioblastoma survival. Proc Natl Acad Sci U S A. 2016 Apr 19;113(16):4476–81.

124. Dhatchinamoorthy K, Colbert JD, Rock KL. Cancer Immune Evasion Through Loss of MHC Class I Antigen Presentation. Front Immunol. 2021;12:636568.

125. Taylor BC, Balko JM. Mechanisms of MHC-I Downregulation and Role in Immunotherapy Response. Front Immunol. 2022;13:844866.

126. Dibbern ME, Bullock TN, Jenkins TM, Duska LR, Stoler MH, Mills AM. Loss of MHC Class I Expression in HPV-associated Cervical and Vulvar Neoplasia: A Potential Mechanism of Resistance to Checkpoint Inhibition. Am J Surg Pathol. 2020 Sept;44(9):1184–91.

127. Kageshita T, Hirai S, Ono T, Hicklin DJ, Ferrone S. Down-regulation of HLA class I antigen-processing molecules in malignant melanoma: association with disease progression. Am J Pathol. 1999;154(3):745–54.

128. Simpson JA, Al-Attar A, Watson NF, Scholefield JH, Ilyas M, Durrant LG. Intratumoral T cell infiltration, MHC class I and STAT1 as biomarkers of good prognosis in colorectal cancer. Gut. 2010;59(7):926–33.

129. Pedersen MH, Hood BL, Beck HC, Conrads TP, Ditzel HJ, Leth-Larsen R. Downregulation of antigen presentation-associated pathway proteins is linked to poor outcome in triple-negative breast cancer patient tumors. Oncoimmunology. 2017;6(5):1305531.

130. Carretero R, Romero JM, Ruiz-Cabello F, Maleno I, Rodriguez F, Camacho FM, et al. Analysis of HLA class I expression in progressing and regressing metastatic melanoma lesions after immunotherapy. Immunogenetics. 2008;60(8):439–47.

131. Rusakiewicz S, Semeraro M, Sarabi M, Desbois M, Locher C, Mendez R, et al. Immune infiltrates are prognostic factors in localized gastrointestinal stromal tumors. Cancer Res. 2013 June 15;73(12):3499–510.

132. Ryschich E, Nötzel T, Hinz U, Autschbach F, Ferguson J, Simon I, et al. Control of T-cell-mediated immune response by HLA class I in human pancreatic carcinoma. Clin Cancer Res Off J Am Assoc Cancer Res. 2005 Jan 15;11(2 Pt 1):498–504.

133. Kambayashi T, Laufer TM. Atypical MHC class II-expressing antigen-presenting cells: can anything replace a dendritic cell? Nat Rev Immunol. 2014;14(11):719–30.

134. Forero A, Li Y, Chen D, Grizzle WE, Updike KL, Merz ND, et al. Expression of the MHC Class II Pathway in Triple-Negative Breast Cancer Tumor Cells Is Associated with a Good Prognosis and Infiltrating Lymphocytes. Cancer Immunol Res. 2016;4(5):390–9.

135. Yu X, Si J, Wei J, Wang Y, Sun Y, Jin J, et al. The effect of EGFR-TKIs on survival in advanced non-small-cell lung cancer with EGFR mutations: A real-world study. Cancer Med. 2023 Mar;12(5):5630–8.

136. Shigematsu H, Lin L, Takahashi T, Nomura M, Suzuki M, Wistuba II, et al. Clinical and biological features associated with epidermal growth factor receptor gene mutations in lung cancers. J Natl Cancer Inst. 2005 Mar 2;97(5):339–46.

137. Meder L, König K, Ozretić L, Schultheis AM, Ueckeroth F, Ade CP, et al. NOTCH, ASCL1, p53 and RB alterations define an alternative pathway driving neuroendocrine and small cell lung carcinomas. Int J Cancer. 2016 Feb 15;138(4):927–38.

138. Yang MH, Yu J, Cai CL, Li W. Small cell lung cancer transformation and tumor heterogeneity after sequential targeted therapy and immunotherapy in EGFR-mutant non-small cell lung cancer: A case report. Front Oncol. 2022;12:1029282.

139. Shen Q, Qu J, Sheng L, Gao Q, Zhou J. Case Report: Transformation From Non-Small Cell Lung Cancer to Small Cell Lung Cancer During Anti-PD-1 Therapy: A Report of Two Cases. Front Oncol. 2021;11:619371.

140. Li S, Schmitz KR, Jeffrey PD, Wiltzius JJW, Kussie P, Ferguson KM. Structural basis for inhibition of the epidermal growth factor receptor by cetuximab. Cancer Cell. 2005 Apr 1;7(4):301–11.

141. Hudis CA. Trastuzumab--mechanism of action and use in clinical practice. N Engl J Med. 2007 July 5;357(1):39–51.

142. Morimura O, Minami T, Kijima T, Koyama S, Otsuka T, Kinehara Y, et al. Trastuzumab emtansine suppresses the growth of HER2-positive small-cell lung cancer in preclinical models. Biochem Biophys Res Commun. 2017 July 8;488(4):596–602.

143. Kinehara Y, Minami T, Kijima T, Hoshino S, Morimura O, Otsuka T, et al. Favorable response to trastuzumab plus irinotecan combination therapy in two patients with HER2-positive relapsed small-cell lung cancer. Lung Cancer. 2015 Mar 1;87(3):321–5.

144. National Library of Medicine. Anti-PD-1 Monoclonal Antibody in Advanced, Trastuzumab-resistant, HER2-positive Breast Cancer (PANACEA) [Internet]. clinicaltrials.gov; 2018 Oct [cited 2025 Feb 3]. Report No.: NCT02129556. Available from: https://clinicaltrials.gov/study/NCT02129556

145. Strickley JD, Spalding AC, Haeberle MT, Brown T, Stevens DA, Jung J. Metastatic squamous cell carcinoma of the skin with clinical response to lapatinib. Exp Hematol Oncol. 2018;7:20.

146. National Library of Medicine. PD-1 Combined With Pyrotinib for Chemotherapy Failure HER2 Insertion Mutation Advanced NSCLC [Internet]. clinicaltrials.gov; 2024 Sept [cited 2025 Feb 5]. Report No.: NCT04144569. Available from: https://clinicaltrials.gov/study/NCT04144569

147. Burr ML, Sparbier CE, Chan KL, Chan YC, Kersbergen A, Lam EYN, et al. An Evolutionarily Conserved Function of Polycomb Silences the MHC Class I Antigen Presentation Pathway and Enables Immune Evasion in Cancer. Cancer Cell. 2019 Oct 14;36(4):385-401.e8.

148. Du W, Frankel TL, Green M, Zou W. IFNγ signaling integrity in colorectal cancer immunity and immunotherapy. Cell Mol Immunol. 2022 Jan;19(1):23–32.

149. Sade-Feldman M, Jiao YJ, Chen JH, Rooney MS, Barzily-Rokni M, Eliane JP, et al. Resistance to checkpoint blockade therapy through inactivation of antigen presentation. Nat Commun. 2017 Oct 26;8(1):1136.

150. Baccelli I, Gareau Y, Lehnertz B, Gingras S, Spinella JF, Corneau S, et al. Mubritinib Targets the Electron Transport Chain Complex I and Reveals the Landscape of OXPHOS Dependency in Acute Myeloid Leukemia. Cancer Cell. 2019 July 8;36(1):84-99.e8.

8. Appendix

8.1. List of figures

8.2. List of tables

8.3. Score sheets

Score Sheet für das Versuchsvorhaben mit dem Titel „Immuntherapie in Kombination mit zielgerichteter Therapie für Bronchialkarzinome in immunkompetenten und humanisierten Mausmodellen“ – Teilversuch 5 (orthotopes Modell)

Die Verantwortlichkeit für die korrekte Aufzeichnung des Versuchsvorhabens und die Überwachung der Tiere liegt beim Versuchsleiter bzw. dessen Stellvertreter.

Beobachter und Anwender:
Diese Personen müssen in den Umgang mit dem Score Sheet und die Protokollierung eingewiesen und über die in der Versuchsgenehmigung festgelegten Kontrollintervalle informiert sein.

☒ Versuchsdurchführende
☒ Tierpflegerisches Personal

A. Körperkonstitution	**Punkte**
Körpergewicht (Bezugsgröße: Ausgangsgewicht bei Versuchsbeginn; Kontrollintervall: wöchentlich)	
Gewichtsreduktion 5-10%	5
Gewichtsreduktion 11-19% bzw. Wirbel und Beckenknochen tastbar (BCS 2)	10
Gewichtsreduktion ≥ 20% bzw. Wirbel und Beckenknochen deutlich sichtbar (BCS 1)	20

B. Allgemeine Kriterien	
Fell/Haut	
Haarausfall (nicht lokal begrenzt)	1
verklebtes Fell	5
verklebte Körperöffnungen mit/ohne verklebtem Fell	10
punktuelle Kratzstellen/Hautverletzungen (oberflächlich, lokal begrenzt, ohne Rötung, ohne Schwellung, trocken und sauber, mit/ohne Kruste) mit/ohne Haarausfall ohne Juckreiz	1
kleine (< 1 cm), krustig-trockene Kratzstellen/Hautverletzungen (oberflächlich, ohne Rötung, ohne Schwellung, trocken und sauber), ohne Juckreiz	3
kleine (< 1 cm), krustig-trockene Kratzstellen/Hautverletzungen (oberflächlich, mit Rötung, Schwellung, trocken und sauber), ohne Juckreiz	5
mittelgradige Kratzstellen/ Hautverletzungen (1-2 cm, oberflächlich, Rötung, Schwellung, Wundheilung gestört/verzögert) mit/ohne Haarausfall ohne Juckreiz	10
Mehrere (2-3), krustige Kratzstellen/Hautverletzungen (1-2 cm, oberflächlich, Rötung, Schwellung, Wundheilung gestört/verzögert); vermehrter Juckreiz	15
massive (>3) und/oder schwerwiegende Kratzwunden/ Hautverletzungen (Rötung, Schwellung, eitriger Ausfluss, keine Wundheilung) mit/ohne Haarausfall, mit/ohne Juckreiz	20
Spontanverhalten inkl. Motorik und Schmerz	
Ataxie (Unregelmäßigkeiten im Gangbild) ohne Lähmungen	5

ausgeprägte Koordinationsstörungen (z.B. Taumeln/Torkeln) mit/ohne Ataxie	10
Parese (unvollständige Lähmung einer oder mehrerer Gliedmaßen)	10
Plegie (vollständige Lähmung einer oder mehrerer Gliedmaßen)	20
gekrümmter Rücken/gekauerte Haltung ohne gesträubtes Fell	10
gekrümmter Rücken/gekauerte Haltung mit gesträubtem Fell	20
intermittierende Stereotypien (z.B. Kreiseln, Hochspringen in einer Käfigecke)	10
ununterbrochene Stereotypien (z.B. Kreiseln, Hochspringen in einer Käfigecke)	20
Apathie mit Reaktion auf Verhaltensprovokation	15
Apathie mit fehlender Reaktion auf Verhaltensprovokation	20
Selbstisolation	20
Automutilation/-aggression	20
Klinischer Befund	
geringgradig betonte, abdominale Atmung	10
deutlich verstärkte, abdominale Atmung*, pathologische Atemgeräusche*, Dyspnoe**, Zyanose *um ggf. das Auftreten einer Dyspnoe zu verhindern **pumpende Atmung mit starker Beteiligung der Bauchmuskulatur, starke Luftnot	20
Rektumprolaps	20
C. Versuchsspezifische Kriterien	
Normaler Stuhl	0
Breiiger Durchfall	5
Flüssiger Durchfall	10
persistierende Durchfälle länger als 2 Tage	20
Infektion der Injektionsstellen	20
Aszites	20
Peritonitis	20

Bewertung	**Punkte**
Keine Belastung	0
Geringe Belastung	1-9
Mittlere Belastung Grad 1	10-14
Mittlere Belastung Grad 2	15-19
Schwere Belastung	≥ 20

Score Sheet für das Versuchsvorhaben mit dem Titel:
Identifizierung von Biomarkern für Resistenz und Ansprechen auf neue Kombinationstherapien mit Immuncheckpointblockade in murinen genetisch veränderten Lungentumormodellen.
Teilversuch 1+3 - RB+p53 abhängig

Die Verantwortlichkeit für die korrekte Aufzeichnung des Versuchsvorhabens und die Überwachung der Tiere liegt beim Versuchsleiter bzw. dessen Stellvertreter.

Beobachter und Anwender:
Diese Personen müssen in den Umgang mit dem Score Sheet und die Protokollierung eingewiesen und über die in der Versuchsgenehmigung festgelegten Kontrollintervalle informiert sein.

☒ Versuchsdurchführende
☒ Tierpflegerisches Personal

A. Allgemeine Kriterien (nicht versuchsspezifisch) *Bezugsgröße: Ausgangssituation zum Start der Adenovirus Applikation* *Beginn: 20 Wochen nach Adenovirus Applikation, zu Beginn der ersten µCT/MRT Messung* *Kontrollintervall: 3x wöchentlich, wenn keine Belastung vorliegt, darüber hinaus Maßnahmen gemäß Score Sheet bei Belastung*	**Punkte**
I. Körpergewicht	
-unbeeinflusst	0
-Änderung < 5%	1
-Gewichtsreduktion 5-10%	5
-Gewichtsreduktion 11-19% bzw. Wirbel und Beckenknochen tastbar	10
-Gewichtsreduktion ≥ 20% bzw. Wirbel und Beckenknochen deutlich sichtbar	20
II. Allgemeinzustand	
-Fell glatt glänzend; Körperöffnungen sauber, Augen klar und glänzend, keine Hautirritation	0
-Fell gesträubt, Fell stumpf und/oder schuppige Haut; punktuelle Kratzstellen/Hautverletzungen (oberflächlich, lokal begrenzt, ohne Rötung, ohne Schwellung, trocken und sauber)	1
- verklebtes Fell und/oder verklebte Körperöffnungen, Augen trüb, gekrümmter Rücken, aufgezogener Leib, Kopfschiefhaltung	10
- mittelgradige Kratzstellen/ Hautverletzungen (oberflächlich, Rötung, Schwellung, Wundheilung gestört/verzögert)	10
- massive bzw. schwerwiegende Kratzwunden/ Hautverletzungen (hochgradige Rötung, Schwellung, eitriger Ausfluss, keine Wundheilung), Abszess; aufgetriebener Leib, Bauch hart/angespannt, Lähmungen	20
III. Spontanverhalten	
-normales, unauffälliges Verhalten	0
-geringe Abweichungen vom Normalverhalten	1
-ungewöhnliches Verhalten, eingeschränkte Motorik oder Hyperkinetik	5
-Selbstisolation, deutlich ausgeprägte Stereotypien (z.B. Kreiseln) und/oder ausgeprägte Koordinationsstörungen (z.B.:	10

Taumeln/Torkeln) und/oder phasenweise Teilnahmslosigkeit mit halb geschlossene Augen	
-Automutilation/-aggression, Apathie (mit ganz geschlossene Augen)	20
IV. Klinischer Befund	
- Atmung normal	0
- schnelle Atmung	5
- geringgradig betonte, abdominale Atmung	10
-deutlich verstärkte, abdominale Atmung* sowie pathologische Atemgeräusche*, Dyspnoe**, Zyanose *um ggf. das Auftreten einer Dyspnoe zu verhindern **pumpende Atmung mit starker Beteiligung der Bauchmuskulatur, starke Luftnot	20
B. Versuchsspezifische Kriterien	
-normaler Stuhl, gesunde Haut	0
-leichter Durchfall	5
-leichter Hautausschlag	5
-auffälliger Durchfall	10
-auffälliger Hautausschlag	10

Bewertung	**Punkte**
Keine Belastung	0
Geringe Belastung	1-9
Mittlere Belastung	10-19
Schwere Belastung	≥ 20

9. Vorabveröffentlichung von Ergebnissen

Diese Arbeit ist teilweise in Anlehnung und Zusammenarbeit mit der Publikation mit dem Titel „Blocking the angiopoietin-2-dependent integrin β-1 signaling axis abrogates small cell lung cancer invasion and metastasis " von Meder et al., 2024 entstanden. Weitere in der Publikation gelistete Mitautoren waren an der Entstehung dieser Arbeit über diesen Weg mittelbar beteiligt. In dieser Arbeit werden Inhalte, die aus der Publikation Meder et al. mit freundlicher Genehmigung übernommen wurden, entsprechend zitiert.

Diese Arbeit ist zusätzlich in Kooperation mit der noch unveröffentlichten Publikation mit dem vorläufigen Titel „ERBB2 signaling drives immune cell evasion and resistance against immunotherapy in small cell lung cancer " von Meder et al. (Ersteinreichung am 13.11.2024 bei „Nature Communications“, in Revision seit dem 15.01.2025, Manuskript NCOMMS-24-74632-T) entstanden. Weitere in der Publikation gelistete Mitautoren waren an der Entstehung dieser Arbeit über diesen Weg mittelbar beteiligt. In dieser Arbeit werden Inhalte, die aus der noch unveröffentlichten Publikation Meder et al. mit freundlicher Genehmigung übernommen wurden, entsprechend zitiert und als *„under revision in Nature Communications since 15th January 2025 under review again since 4th August 2025“* gekennzeichnet. Das schriftliche Einverständnis von Prof. Dr. Lydia Meder über die Vorabveröffentlichung von Teilergebnissen in dieser Arbeit liegt vor.